Investigation on New Structure of Selective Catalyst Reaction Coated Diesel Particulate Filter for Optimising $DeNO_x$

Jun Liang

A Thesis Submitted in Partial Fulfilment of the

Requirements for the Degree of

Doctor of Philosophy

Department of Engineering and Design

Declaration

I hereby declare that this thesis has not been and will not be submitted in whole or in part to another University for the award of any other degree.

Jun Liang

Signature:

July, 2018

Abstract

Selective Catalyst Reduction (SCR) is the most promising technology to reduce NO_x emissions from conventional diesel engines and other lean combustion engines. Traditional aftertreatment system in the majority of diesel vehicles includes a Diesel Oxidation Catalyst (DOC), a Diesel Particulate Filter (DPF) and a Selective Catalytic Reduction (SCR) catalyst.

As emission control by regulations is tightening every year and the demanding for better efficiency, a combination of Selective Catalytic Reduction (SCR) catalyst and Diesel Particulate Filter (DPF) have been researched for several years. The combination catalyst is actually putting an SCR coating on and into DPF's porous walls so that this combination catalyst (SCR coated DPF or SCR-DPF) can be used to filter diesel particulates and reduce NO_x at the same time. The benefit of this combination catalyst system is obvious: the compactness of SCR-DPF reduces the weight, the cost and the complexity of the aftertreatment system; more importantly, it reduces the engine's backpressure losses as one of the catalysts is removed from the aftertreatment system. Despite those benefits, SCR-DPF has some drawbacks. There are studies claiming that the NO_x conversion efficiency of SCR-DPF is lower than traditional SCR catalyst and more challenging to control NO_x conversion process during the regeneration process due to high temperature and so on.

In this research, a new catalyst structure is proposed to solve one of the SCR-DPF limitations. This structure provides large extra surface catalytic area for NO_x conversion and it is free from ash loading effect as the extra surface is located in the outlet channel. And based on the results, for the same NOx conversion rate, the catalyst size can be

reduced to half if using new structure. This is owning to the extra surface area in the new structure.

In this thesis, 3 three-dimensional catalyst models on channel scale, a Flow-Through (FT) catalyst, a Wall-Flow (WF) catalyst and a Wall-Flow catalyst with Fin (WF-Fin) in outlet channel are proposed and built in order to investigate the cause of performance difference between traditional Flow-Through SCR, Wall-Flow SCR and Wall-Flow SCR with fins. The model of Flow-Through SCR is acted as a benchmark since it is built and validated against Olsson's experimental research work. A later model of Wall-Flow type catalyst is modified to Flow-Through SCR model by changing the geometry.

The results from the Flow-Through SCR model follows Olsson's experiment results closely for a wide temperature range under steady and transient conditions, that indicates the successful modelling of the base model. The comparison between WF and WF-Fin model has been made from many different aspects, such as velocity, species composition and reaction rates. The WF-Fin model is focused in the later investigation, the fins bring more active site surface for SCR reactions, but it also has adverse effects to the flow in porous walls if the fin is impermeable as a solid material. The effect of different performance factors requires more studies. But based on the current results, a conclusion can be drawn for the difference between these three types of SCR catalyst, and the possible causes of performance difference are identified.

Acknowledgements

I would like to express my sincere appreciation for the assistance given by many people during my PhD study at the University of Sussex. this project would have been impossible without their help

I would like to thank Dr Weiji Wang, my main supervisor, for his long-term support and encouragement during and after my depression period. I could never accomplish the study without guidance from him.

Also, I would like to thank my previous supervisor Professor Zhijun Peng for giving me the opportunity, bright ideas and great assistance in the early stage of my research.

I need to thank my friends and colleagues whom I meet during the study in Sussex, Dr Li Cheng, Dr Pattarapong Choopanya, Dr Pavlos Dimitriou, Dr Xingnan Zhang and Yeru Shang who is to become doctor very soon, for helping me on academic and non-academic issues during my study.

Last but not least, I’m grateful for the support and encouragement from my family.

Contents

List of Figures

List of Tables

Nomenclature

A	Pre-Exponential Factor
A_s	Surface Area
C_i	Molar Concentration of Species i
d	Channel Width
E	Activation Energy
R	Gas Constant
$\vec{V}$	Velocity
S_m	Source Term
L	Length
M	Molar Mass
$\dot{m}$	Mass Flow Rate
t	Time
ρ	Density
ρ_{site}	Site Density
θ_{NH3}	Catalyst Ammonia Coverage
$NH_3(S)$	NH_3 absorbed on the catalyst Surface

Abbreviations

CFD	Computational Fluid Dynamics
CPSI	Cells Per Square Inch
DPF	Diesel Particulate Filter
FT	Flow Through
NO_x	Nitrogen Oxides: Nitric Oxide (NO) and Nitrogen Dioxide (NO_2)
ppm	Part Per Million
SCR	Selective Catalytic Reduction
SCR-DPF	Selective Catalytic Reduction coated Diesel Particulate Filter
TDI	Turbocharged Direct Injection
WCT	Washcoat Thickness
WF	Wall Flow
WF-Fin	Wall Flow with Fin
WT	Wall Thickness

1. Introduction and Literature Review

Vehicle emission level has been a major international concern in recent decades. The Volkswagen emissions scandal (also known as 'diesel gate') back in 2015 was breaking news for several months. It starts with Volkswagen intentionally manipulated the emissions results from their turbocharged direct injection (TDI) diesel engines by programming emission controls to run only during laboratory emissions testing. This act caused the vehicles to pass emission regulation test easily, but those vehicles emit higher NO_x level in real-world driving. The word 'higher' means 40 times more when compared to their test results [1], and all of those NO_x is emitted into the environment.

NO_x is an abbreviation of nitrogen oxides, which includes nitric oxide (NO) and nitrogen dioxide (NO_2). It is poisonous, highly reactive gases, harmful to the human body directly, also contribute to the formation of acid rain and damage ecosystems. It is produced during engine combustion when there are excess nitrogen and oxygen as higher temperature leads to higher NO_x level. Due to operation characteristics, diesel engine naturally produces higher NO_x output than a petrol engine.

As engine technology developing and automobile manufacturer push their vehicles' efficiency to a higher level, lean burn engines become a popular option. Lean burn engine is delivering an excess of air into the engine to combust with fuel. As a result, more NO_x is formed during the process. Road vehicles contributed more than 20% of the total NO_x emission [2, 3]. And 75% of them comes from diesel and lean-burn petrol engines [4]. Therefore, the control of NO_x emission from diesel and lean-burn engines becomes increasingly necessary.

NO_x reduction technologies, Exhaust Gas Recirculation (EGR) and Selective Catalytic Reduction (SCR) system have been used to reduce NO_x. EGR recirculates exhaust gas back to the engine cylinder. This replaces some of the oxygen coming from intake to reduce peak in-cylinder temperature. Thus NO_x formation is controlled. However, engine add-on method has limited effectiveness to NO_x reduction. Aftertreatment system is a more effective way to meet the future's increasingly stringent emission regulations. The three-way catalyst is used on old petrol engine to reduce NO_x many years ago, but it cannot be used on lean-burn petrol engines as NO_x reduction is inactive due to excess oxygen [5].

Selective Catalytic Reduction (SCR) converter is being fitted on both petrol and diesel engine. SCR system is already used for stationary diesel engines for many years [6], achieving up to 90% NO_x reduction and acceptable ammonia slip. It seems to be the most promising NO_x conversion aftertreatment system when adapting to road vehicles. SCR benefits road vehicles from significant fuel saving compared to other NO_x conversion engine control technologies since it allows the engine is to operate at a maximum efficiency point where usually produce high NO_x [7]. It also shows good durability on road vehicles [6].

When the SCR system is integrated with road vehicles, the NO_x reduction process still the same but many other parts have to be changed. The reason for it is that those stationary engines and boilers are operated mostly at constant load and has no restriction to the size of the catalyst. Whereas car engines are running at variable load and conditions, and the space on a car is much less.

As shown in Figure 1-1, a basis SCR system consists of three major components: reductant storage (component 1), an injection system (component 2) and a catalyst

(component 3). Some advanced SCR system might have additional catalyst or components, like an electrical heater and mixer, to achieve better performance.

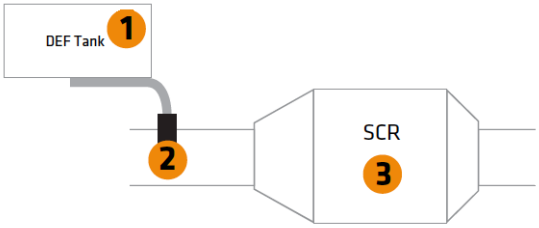

Figure 1-1 Basics SCR system

The SCR control unit receives information, such as engine speed, torque, NO_x concentration, temperature etc. from sensors and then control the injection rate based on its control strategy. Since the reductant is injected into the upstream exhaust gas using an electric pump, it is then evaporated and decomposed into ammonia, and mixed with exhaust gas before enters catalyst. The injection process has to be carefully controlled in case of injecting too much and causes ammonia slip or too little causes low NO_x reduction. When the mixture reaches catalyst, the NO_x conversion happens on the surface of the catalyst.

In current automotive NO_x conversion Technologies, the selective catalytic reduction is a relatively better NO_x control system for lean burn engines. A lot of research and development has been done for automotive SCR systems in recent years. The liquid reductant is dominating the market, but solid reductant is rising. The combination of different coating materials builds a better catalyst. System controls are mainly open loop and NO_x feedback control. Ammonia feedback control and combining closed and open loop control are in development. All of these developments share the same goal: to reduce required catalyst volume while maintaining high selectivity for SCR reaction over the full temperature range and also reach high NO_x reduction at an acceptable ammonia slip.

In this research project, the main topic is regarding the SCR on diesel engines. One of the reasons is that the diesel engines emit higher NO_x compare to the petrol engines. And the other reason is that diesel system has more room for improvement than the petrol system regarding the aftertreatment system. Since there are usually three catalysts used in diesel aftertreatment system: Diesel Oxidation Catalyst (DOC), Diesel Particulate Filter (DPF) and Selective Catalytic Reduction (SCR), the complete system causes higher back pressure, and therefore it affects turbocharge efficiency and fuel efficiency.

SCR-DPF has been a favourite topic when talking about diesel aftertreatment in recent years, and many studies and research projects have been done [8-13]. This SCR-DPF is a combination of SCR and DPF which reduce NO_x from exhaust gas while filter soot at the same time. Since one of the catalysts is eliminated, as Figure 1-2, the benefits of this system are obvious: it reduces back pressure, cost and complexity relative to the conventional system, hence the overall efficiency is improved.

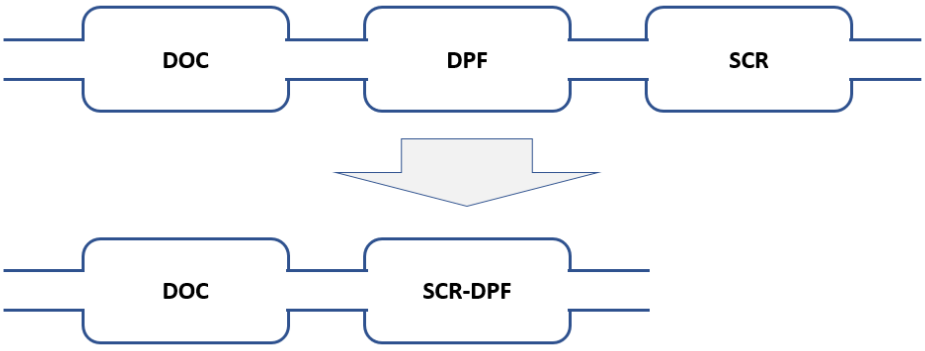

Figure 1-2: Conventional diesel aftertreatment system and the new system

1.1 Performance Factors and Challenges

In general, the limitation of the overall performance of an automotive SCR is from these three groups: reductant delivery, catalyst and control strategy. In the following sections, each of the performance factors and their current position is discussed. Some of these factors are a challenge to the current SCR system.

Urea is widely used in current SCR systems. To further improve the overall performance of an SCR system, this reductant can be replaced by the one with higher ammonia density and easier ammonia releases control. Solid ammonia materials have some advantages which are essential to SCR systems, because of that, it becomes a strong candidate.

The catalyst is to accelerate NO_x conversion over the operating temperature. Traditional single coating material on the catalysts has poor activity either on low temperature or high temperature. They cannot satisfy the complete operating temperature range alone. Recent development has been achieved a good result on this, by mix two different coating materials, could improve activity mostly on low temperature, and only sacrifices very little at high temperature.

One of the design purposes of a control system is to compensate for the faults or limitations from hardware. These limitations can be a time delay of the sensors and cross-sensitivity of the NO_x sensor as NO_x cannot distinguish between NO and NO_2. Also, the unmeasurable ammonia absorption capacity of the catalysts, catalyst age problem etc. Accuracy of compensation model directly affects the overall system performance. The control system plays an important role here.

1.1.1 Reductant Agents

Different reductant has been suggested, such as hydrogen and carbon monoxide [14]. From the view of NO_x conversion efficiency, ammonia attracts more attention, and it is widely used in both stationary plants and automotive SCR systems. Direct use of ammonia gas is the simplest way as it directly reacts with NO_x. However, ammonia gas is difficult to handle in practice, due to safety and the space limitations on vehicles. This makes the direct use of ammonia gas out of consideration. The source of ammonia to use in an automotive application, it is classified into two statuses: liquid and solid.

1.1.2 Liquid Ammonia Source

Liquid ammonia is more commonly used in SCR systems for large stationary applications for more than thirty years [15, 16], and relatively easier to handle to compare with the gas phase. It seems like a good choice for road vehicles. However, safety is still an issue when carrying liquefied ammonia on-road vehicles as it is travelling under high pressure [3], gas leaking is directly dangerous to human and environmental.

Therefore, an alternative reductant on the automotive application is Urea Water Solution (UWS). 32.5% urea by weight water solution is widely used in the current automotive SCR system. It converts to ammonia under appropriate temperature. In comparison, the urea-water solution is non-toxic, easier and safer to handle which make it become a better choice. The known issues are that it is freezing below -12℃, undesired solid deposit build-up and side products are generated when dosing into exhaust gas below 200°C [17]. Slow decomposition of urea may happen in a tank with temperature over 50°C [3], none serious problem is caused since it only releases a small amount of ammonia gas into the tank over

months. Moreover, the undesired deposit may form and accumulate on the inside of the exhaust pipe and injection nozzle.

UWS is a source of ammonia, and it has to be converted to react with NO_x. The conversion relates to the availability of ammonia, and the availability of required amount of ammonia affects NO_x conversion efficiency. Thus, the conversion process becomes an essential factor. The conversion has three steps: evaporation, thermolysis, and hydrolysis [6, 18]

1) Evaporation of water

$$(NH_2)_2CO_{aqueous} \rightarrow (NH_2)_2CO_{solid} + H_2O$$

2) Thermolysis of solid urea

$$(NH_2)_2CO_{solid} \rightarrow NH_{3_{gas}} + HNCO_{gas}$$

3) Hydrolysis of iso-cyanic acid

$$HNCO_{gas} \rightarrow NH_{3_{gas}} + CO_2$$

All three reactions should be completed before entering the catalyst. But the short distance between urea injection point and catalyst only allow short residence time for them. Many researchers investigated the formation process [18-24].

An early investigation of urea thermolysis [23] states urea thermolysis has two decomposition stages: the first stage is ammonia generation and then is ammonia consumption. Melamine complexes are left after the second stage, these products have an adverse effect on catalyst performance, although the second stage can be eliminated by the presence of a catalyst with a good spray system.

A recent study [24] carried out a number of experiments to investigate the evaporation behaviour of suspended UWS droplet over a temperature range from 373 to 873K with an initial diameter of UWS droplets range from 700 to 1450μm. In the experiment, the droplets are evaporating at the stagnant state and dry ambient condition, which is different from real spray systems. Results show evaporation characteristics depends on its ambient temperature; only water evaporates from UWS droplet and no sign of urea gasification below 423K. Clearly, urea gasification was observed after the complete depletion of the liquid component from 473K. The rate of urea gasification is faster than the one in water evaporation at temperature 773K and above. Another observation is that solidified deposit remains at a temperature below 773K and the quantity is reduced with increased temperature; nearly no deposit remained at a temperature above 823K.

A CFD simulation [18] of UWS injection was used to predict ammonia conversion and distribution in a tube. 40 wt.% urea is injected at the axis of a tube. The result shows the main temperature drop and the maximum concentration of water vapour and ammonia happen in the middle of the tube. The highest water vapour concentration very close to the injection point, the highest ammonia concentration is at further downstream, because thermolysis starts after water is complete evaporated, despite mixing starts right after injection. The conversion to ammonia and isocyanic acid (HNCO) increases with rising temperature. The simulation result of converted ammonia shows sufficient agreement with an experimental investigation of Kim et al. [25]. 90% of ammonia conversion is reached at 673K with less than 0.75 second residence time. 20% increase in ammonia conversion compare with the result at 623K. The authors indicated that UWS is unable to evaporate and decompose completely in real condition, the catalyst must have a sufficient capability for the hydrolysis reaction, especially at temperatures below 573 K.

A study [26] points out ‘hydrolysis reaction is negligible at upstream, maximum 50% of ammonia is available at the catalyst inlet. The hydrolysis needs to be catalyzed.’ Other researchers [15, 27] also mentioned that adding a hydrolysis catalyst would have a significant influence on ammonia conversion. Also, ammonia conversion can be improved from sufficiently high temperature and well design of the injection system and pipe geometry [28-32].

1.1.3 Solid Ammonia Materials

Solid ammonia materials were proposed as alternative sources of ammonia many years ago [33]. In recent year, solid ammonia materials have been attracting attention again. In a review of solid ammonia materials [17], many solid ammonia materials provide an equivalent amount of ammonia to urea in one third the volume or one third the mass. The study [3] indicated that for 5kg of ammonia requires approx. 25L (27.4kg) UWS or 8L (9.7kg) AdAmmine which is a solid ammonia material. The differences in weight and volume between liquid and solid materials result in different quantity and size of the necessary reductant to meet the consumption demand.

Apart from the weight and volume, the review [17] investigated into the chemistry of ammonium salts and metal ammines. The result shows the ammonium carbamate, and ammonium carbonate appears to be good candidate for replacing urea as they are readily decomposition, highest ammonia pressure generation, fully decomposition into ammonia gas with no solid residue left, and not water is generated for undesirable reactions. Moreover, metal ammines are studied in the paper [34, 35], the results point out metal ammines offer a clean solution for exhaust aftertreatment application below 80°C.

In both studies [3, 17], Ca-ammine and Sr-ammine lose ammonia at room temperature when vapour pressure lower than one bar. This is a challenge for them to be kept safely in the open air at room temperature.

In the view of chemistry, solid ammonia material is a strong competitor as it has around 3 times ammonia density over UWS at the same volume and releasing ammonia is thermally controlled. Weight and volume reduction would benefit to fuel economy and space saving. The downside is that using solid reductant increases the complexity of the injection system compared with the current one. Moreover, because solid ammonia material is thermally decomposed, it requires extra heating and pressure equipment on board. In short, replacing UWS with solid ammonia material is feasible, but the limitation comes from the storage and injection systems.

1.1.4 Flow Distribution

While meeting high ammonia conversion, an SCR system requires a uniform distribution of ammonia and NO_x in the exhaust gas to maximise NO_x conversion efficiency. Maldistribution mixture gas and poor mixing may cause insufficient NO_x reduction and high ammonia slip.

The flow distribution has to be controlled within the converter, indicated by S. Benjamin [36], maldistributed flow causes emissions to escape from the high flow region, increases pressure loss, lower utilisation of the catalyst volume. Many studies investigated the flow characteristic and their effect on all kinds of catalysts [37] and the references therein. But not only flow distribution affects the system, temperature, ammonia concentration and NO_x concentration distribution also contribute to this effect. Due to the characteristic of system dynamics: nonlinearity and complexity, state distributions vary from upstream to

downstream within the SCR system, ammonia should be distributed to high NO_x concentration region for maximum ammonia utilisation. R. Signalling et al. [38] mentioned the design process for enhanced ammonia distribution in conventional SCR system is illustrated. They pointed out that a high NO_x conversion efficiency SCR system requires excellent ammonia distribution and affected by gas velocity, temperature distributions and other factors. Although the study is based on a conventional SCR system, it shows the importance of state distribution within the catalyst. Moreover, in the experimental study [39] of mobile SCR + CRT system for heavy-duty diesel, the authors state that achieving uniform flow and reductant distribution entering the SCR catalyst is paramount to the emissions performance of urea-SCR systems.

Amount of studies investigated the influence of the distribution and gas flow in SCR system, and it turns out that proper mixing and distribution of ammonia in the exhaust gas and uniform gas velocity through the catalyst are also essential to NO_x conversion performance. A mixer can help to reach better mixing and distribution condition faster.

The higher ammonia conversion rate means available ammonia is closer to the exact required quantity; the ammonia utilization can be maximised. Well control of ammonia formation, distribution and mixture with exhaust gas lead to lower reductant consumption and easier control to ammonia slip.

1.1.5 Catalyst

The catalyst is the most complex subsystems in the SCR, where NO_x conversion takes place, and it catalyses the reactions. In this part, the main influence to NO_x conversion comes from catalyst size and its coating material. Space arrangement on the vehicles and

cost consideration limits catalyst size. Improvement has to be done through the other parts, for example, the types and the active materials.

The first commercial SCR catalysts for the automotive system were extruded honeycomb monoliths with typically TiO_2, V_2O_5 and WO_3 as active component [40, 41]. Currently, both honeycomb extruded and coated monolith catalysts that based on Vanadium or Zeolite are used for the vehicles in Europe market [40-43]. The difference between the active materials is ammonia storage capacity, the activity and oxidation characteristic with various reductants. Thus, many investigations are carried out on the catalysts with different coating materials and containing different active components [2, 44-51].

Kleemann et al. [52] investigated on ammonia absorption behaviour on coated and extruded catalysts, the results show that without the presence of NO, the specific ammonia adsorption capacity of both catalysts is similar. In a typical SCR condition below 400°C, extruded catalyst adsorbs a higher average amount of ammonia than the coated catalyst. But high ammonia adsorption increases response time to changing conditions. Thus it becomes a problem in the control strategy. With the addition of WO_3, ammonia surface coverage is significantly higher, and the high acidity of WO_3 increases the amount of adsorbed ammonia, thus improving the catalytic activity.

Qi et al. [2] compared Fe/ZSM-5 and Cu-ZSM-5 catalysts on similar diesel engine gas exhaust condition. The results show in Figure 1-3, Cu-zeolite catalyst performs better at low temperature, more than 90% NO_x conversion efficiency between 250 and 350°C, then it decreases as temperature climb. Fe/zeolite appears poor NO_x conversion below 350°C, but it reaches over 90% NO_x conversion efficiency from 350°C to 500°C. Taking advantage of both Fe and Cu, high NO_x conversion between 200 and 500°C could be expected by using a combination of these two materials on a catalyst.

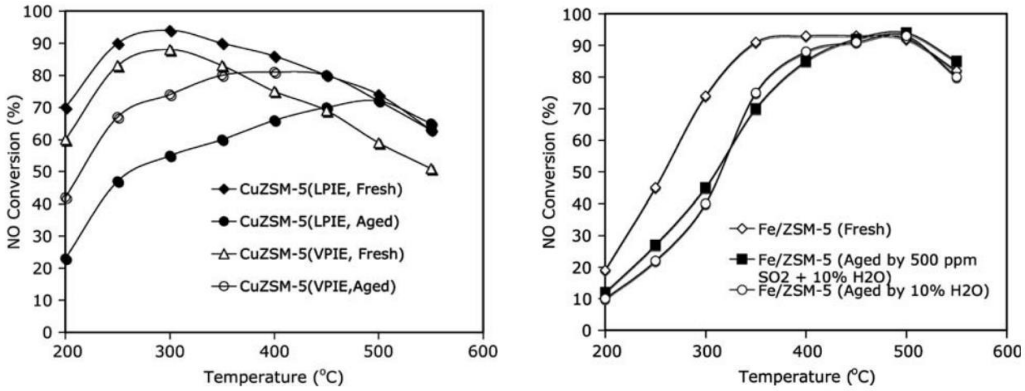

Figure 1-3 NO reduction using Cu-ZSM-5 catalysts (left) and Fe-ZSM-5 catalysts (right) (Qi et al. [2])

Frey, Mert et al. [47] investigated the catalytic activity of Fe ion-based BEA zeolite catalyst, in comparison to iron-containing zeolite catalysts, e.g. ZSM-5 and ZSM-12, and V_2O_5/TiO_2 catalyst, higher activities over broad temperature interval is exhibited. The experiment indicates 3 wt.% Fe-BEA catalyst has slightly higher SCR activity than the other iron loadings.

Stanciulescu et al. [49] performed a number of experiments on the catalyst contain manganese (Mn-). the test catalysts with Mn >1.6% are suitable for AMMONIA-SCR system, and 3.5% Mn exchanged catalyst shows 100% NO_x conversion from 220°C to 450°C Catalysts that combines two active components were tested, such as Cu-Mn, Fe-Mn, Ce-Mn and Ce-Fe, the results (Figure 1-4 and Figure 1-5) prove that adding a second metal to catalyst would more or less affect catalyst's activity and beneficial for the oxidation of NO to NO_2.

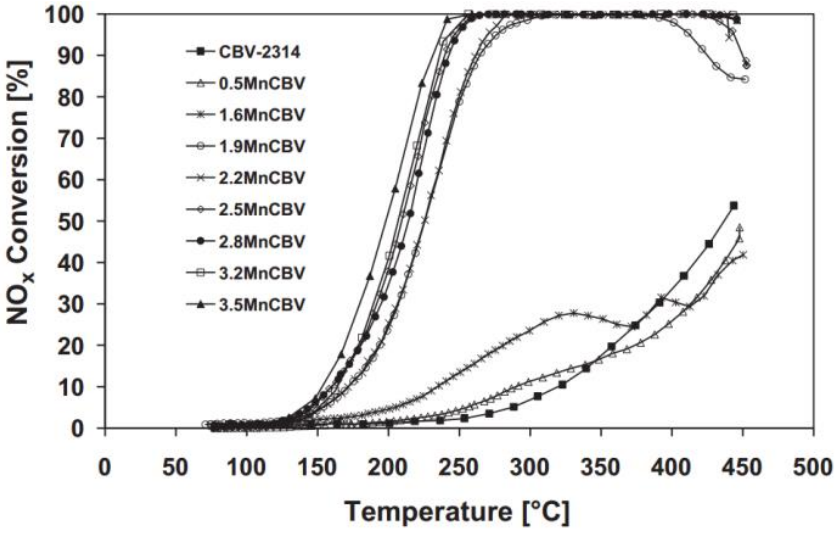

Figure 1-4: effect of the Mn content in Mn-exchanged zeolites on NO_x conversion [49]

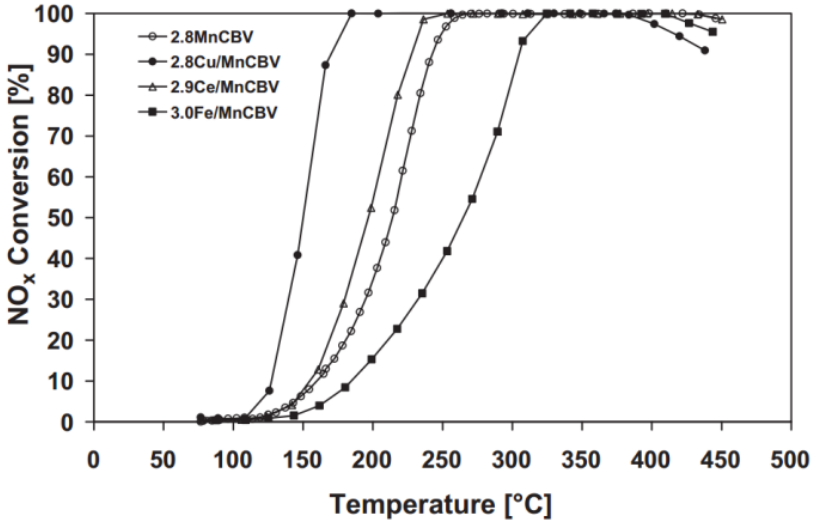

Figure 1-5: effect of the 2nd metal loaded on Mn-exchanged zeolite on NO_x conversion [49]

Krocher and Elsener [45] mounted two different catalysts in series to increase the catalyst's activity and selectivity. Three coated monoliths catalysts, V_2O_5/WO_3-TiO_2, Fe/ZSM-5, and Cu/ZSM-5, were built to four combinations, V_2O_5/WO_3 TiO_2 + Fe/ZSM5 and the reverse order, Fe/ZSM5 + Cu/ZSM5 and V_2O_5/WO_3 TiO_2 + Cu/ZSM5.

No improvement has been shown on the combination of V_2O_5/WO_3 TiO_2, and Fe/ZSM5 compares with the single catalysts. The combination of Fe/ZSM5 and Cu/ZSM5 shows good result, as it takes advantage of Fe/ZSM5 for high temperature and Cu/ZSM5 for low temperature, 50% NO_x conversion rate can be reached at around 220°C, peak conversion rate closes to 98% between 400°C and 500°C. High NO_x conversion rate (>90%) is maintained up to 600°C. The last combination group only shows slight improvement at low temperature than V_2O_5/WO_3 TiO_2 alone.

Another experiment on a combination of Fe- and Cu- zeolite catalysts were done by Metkar et al. [50], three configurations: sequential brick, mixed washcoat and dual layer, were examined. Cu-zeolite catalyst placed in front of Fe-zeolite in series at equal loading does not improve NO_x conversion performance, but better performance shows in reversed order. And the combination of 33% Fe and 67% Cu has the best overall NO_x conversion over a wide temperature range. NO_x conversion on mixed washcoat catalyst is similar to the average of individual Fe-only and Cu-only catalysts. In the dual-layer test, total washcoat loading is 24-25%. Coating Cu-zeolite layer on the top of the Fe-zeolite layer improves low-temperature conversion, but high-temperature conversion is decreased, as seen in Figure 1-6 below. Since the reactants always encounter the top layer first, where Cu-ZSM-5 has high activity at low temperature. Thus, this catalyst has improvement at low temperature. But at a temperature over 400°C, ammonia is consumed by oxidation in the top layer; it leads to a lack of ammonia for complete NO_x conversion.

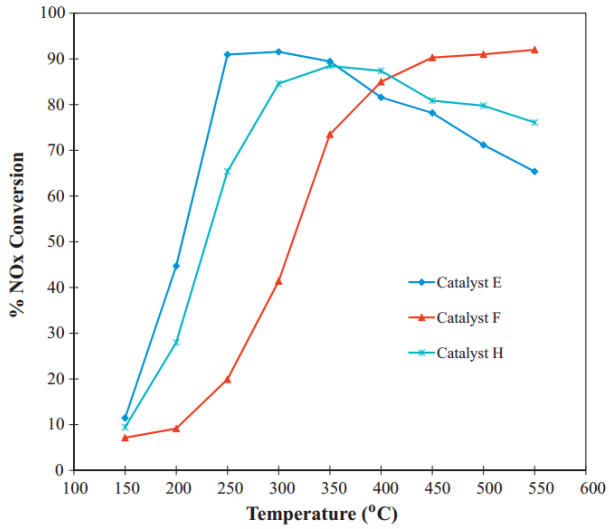

Figure 1-6: Steady State NO_x Conversions

E: 25% Cu-Zeolite, F: 24% Fe-Zeolite, H: 13%Cu-Z on 12% Fe-Z [50]

When using Fe- layer, on the top, NO_x conversion is enhanced. The results, Figure 1-7 show that decreases the fraction of Fe-ZSM-5 from 12 wt.% to 8 wt.% (increase Cu-ZSM-5 12 wt.% to 16 wt.%) keep increasing low-temperature NO_x conversion but slightly reduce high-temperature conversion. Because of the decrease of Fe-ZSM-5 loading, ammonia is penetrating to the underlying layer and gets oxidized. As total washcoat is further increased to 30 wt.%, a further enhancement at low temperature is shown on higher loading and thinner Fe-ZSM-5 top layer, more importantly, the conversion at a high temperature nearly unchanged.

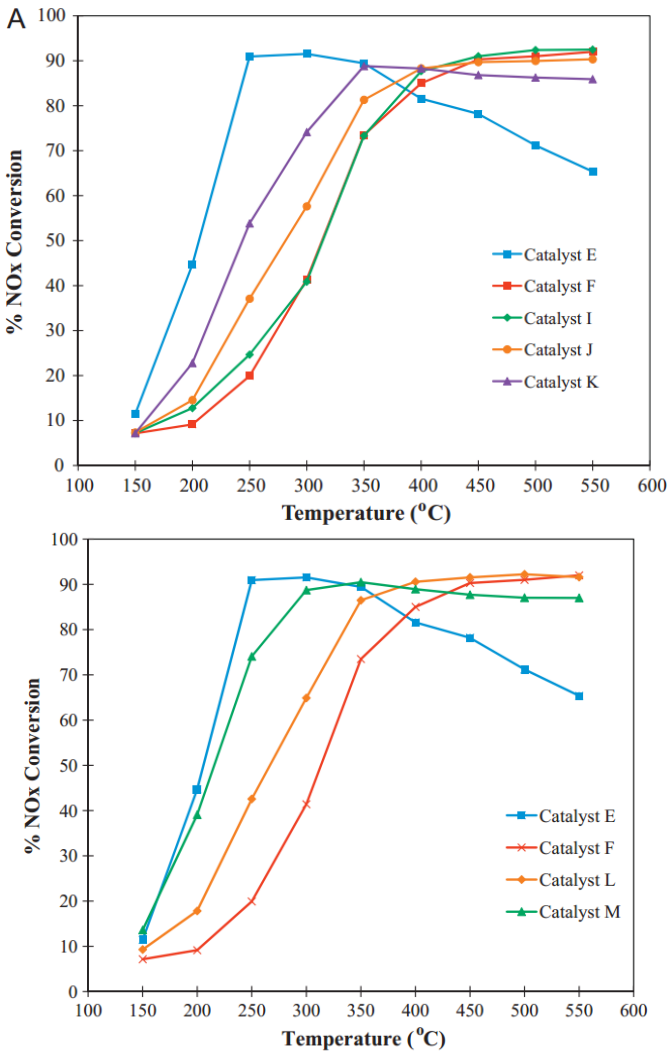

Figure 1-7: Steady State NO_x Conversion
(I: 16% Fe- on 8% Cu-, J: 12% Fe- on 12% Cu-, K: 8% Fe- on 16% Cu-, L: 15% Fe- on 15% Cu-, M: 10% Fe- on 20% Cu-) [50]

1.1.6 Ammonia Adsorption Capacity

Once ammonia reaches the catalyst, it is adsorbed on the catalyst surface and reacts with NO_x. Adsorption capacity mainly depends on temperature. The coating material inside the SCR catalysts has lower ammonia storage capacity at high temperature [6, 26, 53]. Therefore, when the storage is fully loaded at low temperature, a certain amount of ammonia will be released during temperature rise. It causes extra ammonia slip. Besides temperature, the capacity of ammonia storage is also decided by the material. In the experiments done by A. Grossale et al. [40], iron-exchanged zeolite catalyst adsorbs up

to 0.75 mmol/g_{cat} at 50°C. The capacity is reduced to 0.4 mmol/g_{cat} at 200°C. Commercial vanadium-based SCR catalyst is characterized as lower ammonia storage capacity, around 0.35 mmol/g_{cat} at 50°C and down to about 0.15 mmol/g_{cat} at 200°C [54].

The overall performance of a catalyst is decided by its type, material, cell density, catalyst volume etc. From a large number of experiments, it can be seen that the active component has the most impact on NO_x conversion. The single coating material is challenging to meet the NO_x conversion requirement in the future, and a combination of different active components would enhance NO_x conversion over a wide temperature range.

1.1.7 System Control

Since the accuracy of ammonia injection has an excellent impact on NO_x conversion efficiency, a proper reducing agent dosage for all operating condition is essential. Most current SCR systems have a feedback control that allows the system to collect information from the sensors and makes a decision to give a suitable response to the system. Because of the technologies of the sensors and unpredictable driving behaviours, the wrong decision could be made by the controller. A well-known sensor problem is the cross sensitivity of the NO_x sensor; incorrect feedback directly leads to abnormal response. Therefore, correction models (or compensation models) are employed. The correction models consider all necessary parameters to provide reliable feedback, or to predict the state of a subsystem.

Heieh and Wang have developed several correction models. An extended Kalman filter is proposed to estimate actual NO_x concentration after catalyst, ammonia cross sensitivity factor and design ammonia cross sensitivity error elimination [55], the model shows well

prediction on the simulation based on FTP75. An extended Kalman filter is also used in the design of the ammonia coverage ratio and ammonia storage capacity estimations [56].

An alternative approach is using an ammonia sensor to overcome this limitation [57]. The authors examined an ammonia sensor with adaptive surface coverage/ammonia slip control strategy in an engine test cell. Through comparison between ammonia and NO_x sensor-based control strategy, the proposed ammonia sensor-based control shows robustness against disturbances during transient and real-life, and high NO_x conversion (around 90%) is maintained while lowering ammonia slip. The investigation also proves that this ammonia sensor shows independent to total pressure effect, no significant flow-rate dependence in the speed range of 2.46 m/s to 43.04 m/s. Moreover, the cross interference of NO, HC, CO and N_2O were not observed, cross-sensitivity with H_2O and O_2 is acceptable. SO_2 interference effect has to be compensated by low sulfur fuel.

Devarakonda et al. conducted a simulation based on ammonia sensor feedback [58], a four-state control-oriented lumped parameter model is used. The analysis shows the strategy based on a NO_x sensor performed slightly better than the ammonia sensor-based strategy. The authors point out model-based SCR control systems with an ammonia sensor can be implemented in real time.

An open-loop control strategy is able to reduce up to 80% NO_x, but future emission regulation limits the use of open-loop control. More robustness and effective control strategy are required.

Willems et al. [26] studied SCR control requirements for the future and compared three different control strategies: open loop map based, NO_x sensor based and adaptive surface coverage/ammonia slip control. They point out open loop control strategy requires lots of calibration effort to achieve optimal performance over the driving cycles, but difficult to

handle with variable transient conditions. NO_x sensor-based control has a better result, as urea correction model and cross-sensitivity model is added. This control is only able to compensate for slowly changing effects. Adaptive surface coverage/ammonia slip control shows the highest NO_x conversion rate and the best ammonia slip control. The combination of open loop surface coverage control and closed loop ammonia slip control offers robustness and adaptation capabilities.

Shost et al. [59] performed a simulation study on the ammonia-based closed-loop control system on a heavy-duty FTP cycle to meet the NO_x emission requirement and ammonia slip targets. The report pointed out several advantages of the system, allowing the update of model storage factor to compensate for other degradation factors, the ability to improve ammonia slip per volume SCR. A study [60] indicates a better NO_x conversion control system could reduce SCR catalyst volume by 22%, as well as ammonia slip. A model-based control system employing an embedded real-time SCR chemistry model and an ammonia sensor is presented in paper [61], the use of ammonia sensor provides fast response and high sensitivity for meeting ammonia slip target. It also indicated that using of ammonia sensor has the ability to detect degradation of the SCR system.

Many studies have pointed out the advantages of using the ammonia sensor; however, in some cases, NO_x sensor-based control strategies outperform the one with ammonia sensor slightly. It is because current control models are mainly developed for NO_x sensor-based system. Since the ammonia sensor is new, development on ammonia sensor-based control strategies is relatively less than NO_x sensor-based control. But ammonia sensor is a strong candidate for SCR control applications.

1.1.8 System Limitations and Possible Solutions

While meeting future emission standard, the general goal is to maintain high NO_x conversion over full temperature, also minimise ammonia slip. To archive the goal, there are many limitations that need to be solved.

Starting from the reductant, firstly, it has to be non-toxic and stable due to the consideration for the people and environment; secondly, it can convert to ammonia quickly, which is to fit the transient driving conditions. AdBlue takes three steps to complete convert to ammonia that would slow the whole NO_x conversion process. And it is difficult to be fully converted before it reaches the SCR catalyst. Using a hydrolysis catalyst helps on this problem, the study of hydrolysis catalyst is required. The investigation should be carried out regarding catalyst size and activity of isocyanic acid (HNCO) over various catalysts.

A solid reductant has higher ammonia density compare with AdBlue. Ammonia conversion is controlled be heat only, thus released ammonia is easily predicted. Installation of additional heating equipment, safely heating the reductant and injecting ammonia gas are the problems. A possible solution is to design a new storage system and an injection system. Dynamics thermal decomposition control system is also essential. It has to meet unpredictable driving behaviours and to minimise undesired ammonia release. And addition equipment brings extra power consumption should be considered. Attention is needed on the solid materials' selection. The use of solid reductant potentially solves the other problems during ammonia formation from liquid ammonia sources: slow ammonia conversion, deposit formation.

The flow distribution affects SCR performance. To prevent emissions escape from the high flow region, or the ammonia is injected too low NO_x concentration flow region, a

flow mixer helps it and achieves well flow distribution. As the dosing system decides injection pressure, droplet size, distribution and spray pattern [62] control the injection, thereby would control evaporation and ammonia distribution. A proper design of the injectors and pipes also improves the effect. The key to this problem is using CFD simulation as it can simulate the mixing and distribution of the reductant in the exhaust system when designing various injectors and proper geometry of upstream pipes.

With regards to the limitations on the catalyst, one is deficient activity at a temperature lower than 200°C, and the other one is ammonia storage capacity which is temperature dependence. The combination of two active components shows enhancement on overall NO_x conversion. However, there is room for improvement at the low-temperature activity, components ratio, combination and preparation method require further investigation. The catalyst ageing also needs attention. Due to the characteristics of ammonia storage, it can cause undesired ammonia slip during temperature rise. In order to minimise undesirable ammonia release from catalyst desorption, the dynamic capacity of ammonia storage has to be carefully considered and controlled. A compensation model can help on this issue, but the difficulty is that ammonia storage can only be estimated rather than measured. There are two ways to control ammonia slip, and one is to reduce the dosage of ammonia, which compromises between ammonia slip and slightly lower NO_x conversion. And the other one is using an ammonia catalyst to oxidise unreacted ammonia.

In the control system, the closed-loop control strategy is necessary. However, cross-sensitivity of the NO_x sensor is an issue, as most systems still use NO_x sensor, despite more and more investigations and studies base on ammonia sensor. A better control model based on the NO_x and ammonia sensor and tailpipe NO_x prediction method is necessary. Since most of the current control model are feed-forward or linearized feedback models [28], any nonlinear control model would be helpful to the development.

In general, this chapter can be summarized as follows. Ideal reductant for the SCR system is something easy to control, fast conversion, left no deposit during the conversion process. The solid reductant is a potential candidate but requires a redesign of reductant storage and conversion system. If liquid reductant is continually used, extra hydrolysis catalyst and ammonia catalyst can maximise the ammonia conversion process and control ammonia slip. One of the challenges to SCR catalysts is NO_x conversion efficiency at low temperature. Combining Fe-(10%) and Cu-(20%) brings the advantage of each material and offers better overall performance, but durability and ageing issue is unknown.

Another challenge is the control strategy, because of model compensation, e.g. sensor's cross-sensitivity, injection delay and unmeasurable ammonia storage, only to a certain level. Proper control requires accurate models, also needs to taking consideration of the unpredictable driving and nonlinearity of the SCR dynamics. This is the problematic part of the control system.

1.2 Literature Review

The objective of this study is to investigate the performance of SCR-DPF by using computational fluid dynamics. Several performance studies of SCR-DPF for passenger and commercial vehicles have been carried out in recent years. [8, 10, 13, 63-67]

There are two ways to investigate the performance on SCR-DPF, one is experimental measurement, and the other one is numerical modelling. Experimental measurement requires test rig setup and monitoring equipment. It is a costly and time-consuming way. Whereas numerical modelling is more affordable in terms of timing and cost. Despite the fact that numerical modelling can never reach an exact solution to a problem. The degree

of accuracy is based on numerical models. However, there is clearly the advantage of using numerical modelling. It is able to simulate all kind of operation condition, even one beyond extreme conditions. And monitor the result and data in a location that is impossible to do in reality. So, most of the researchers using numerical modelling to simulation the case before going into the experiment, but some of the data and parameters in modelling require the experimental result to support.

Mojghan et al. [8] have done an experiment and comparison between two aftertreatment configuration systems, DOC+CSF+SCR and DOC+SCR-DPF+SCR. For the same engine operation condition, the SCR-DPF system shows significant higher NO_x reduction than CSF system under steady state and heavy-duty FTP driving cycle. The performance during the passive regeneration process was also evaluated, SCR-DPF plus appropriate NO_x control strategy has promising potential for passive regeneration.

Sadeghi et al. [68] has investigated the effect of channel geometry on the SCR catalyst and compared the simulation result from different models. CFD model of 1-D, 2-D and 3-D simulation are used and compared, the detailed study of different channel geometries was using 3-D simulation. Four different channel geometries, circular, hexagonal, square and triangular were studied using single channel modelling. Only NO conversion and NH_3 oxidation are considered in the kinetics model. And all those channels have the same residence time of gas and the amount of catalyst despite the difference in shape.

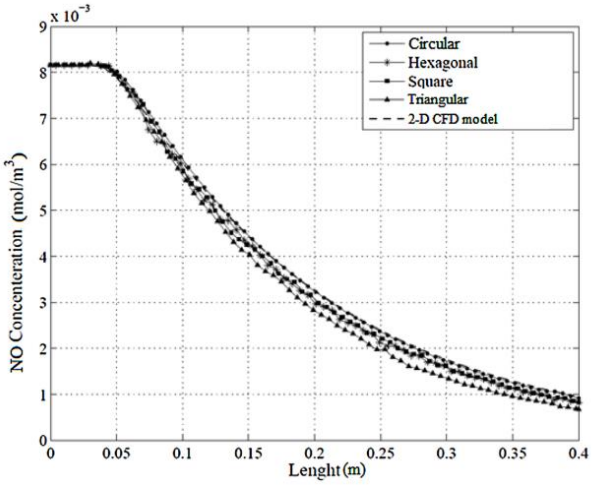

Figure 1-8: NO_x concentration along the channel for different channel geometries [68]

As their simulation results show, Figure 1-8, all 4 geometries have a very similar result; NO is consumed along the channel and reach the maximum level at the end of the channels. NO reduction in the triangular channel is slightly more significant than the others. They also plotted a figure of pressure drop, conversion rate against the number of faces of the channels, as in Figure 1-9, N is the number of faces. The result shows both pressure and conversion rate drop as the number of faces increase. It means the reaction rate is strongly affected by diffusion in the washcoat in the corner of a noncircular channel [68].

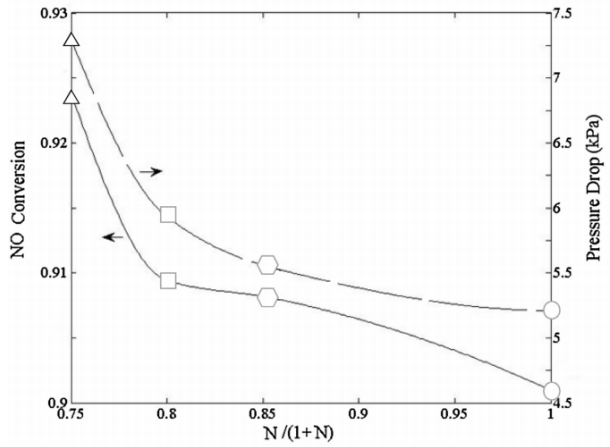

Figure 1-9: Pressure drop and conversion as a function of the number of faces [68]

Mladenov et al. have investigated into transport and chemistry in the channel flow of different geometries. [69] 18 different numerical models are studied and compared, based on three channel geometries, circular, square and square with rounded corners. Their focus is on the modelling of mass transfer rather than the performance comparison of different channel geometries. The authors point out in the conclusions, 2D and 3D Naiver-Stokes models with few assumptions provide the most accurate solution, but they are also much more computationally expensive. Boundary-layer approach ignores axial diffusion and still offers excellent result with much lower computation time. And the plug flow model is further simplified from boundary-layer mode by neglecting both radial and axial diffusion terms, it is able to predict the conversion of gas-phase species much faster than the others. Mass transfer coefficient is able to improve the accuracy of the plug-flow solution, but it highly relies on empirical correlations. In terms of diffusion modelling inside porous media, simple effectiveness factor washcoat model is computationally inexpensive with questionable universal validity. Detailed reaction-diffusion models have provided the most accurate solution, and they are the most computationally expensive model.

Timothy et al. [10] developed and validated a one-dimensional model for the SCR-DPF catalyst. The kinetics used in the model was developed for flow-through Cu-zeolite or Fe-zeolite monolith catalysts, together with a physical model of a coated DPF. A total number of SCR reaction in this model is 9, as listed in the below figure.

$$NH_{3(g)} \rightleftharpoons NH_{3(ads)}$$

$$4NH_{3(ads)} + 4NO + O_2 \rightarrow 4N_2 + 6H_2O$$

$$2NH_{3(ads)} + NO + NO_2 \rightarrow 2N_2 + 3H_2O$$

$$2NH_{3(ads)} + 2NO_2 \rightarrow N_2 + 3H_2O + N_2O$$

$$4NH_{3(ads)} + 3NO_2 \rightarrow 3½N_2 + 6H_2O$$

$$4NH_{3(ads)} + 3O_2 \rightarrow 2N_2 + 6H_2O$$

$$4NH_{3(ads)} + 5O_2 \rightarrow 4NO + 6H_2O$$

$$NO_2 \rightleftharpoons NO + ½O_2$$

$$2NH_{3(ads)} + 3NO_2 \rightarrow 3NO + N_2 + 3H_2O$$

Figure 1-10: Reaction Scheme in Timothy et al.'s Model [10]

Two additional reactions are: NH_3 oxidation reaction forming NO and reduction of NO_2 to NO by NH_3. These two reactions are less usual than the others. Thus other researchers remove these two reactions when they cite this model in their recent work. Upon validation of their model against experimental engine data, the model is capable of predicting the species and conversion of NO, NO_2, NH_3 and N_2O, also the effects associated with NH_3 storage and desorption. Diffusion in radial and axial direction are also included. And then, an investigation of soot effect on SCR-DPF is performed based on this model, and the result shows the existence of soot on the SCR-DPF have no significant impact on NO_x conversion, while SCR activity (NO_x reduction) is predicted to significantly retard the rate of soot removal by oxidation with NO_2. [10]

1.3 Research Aims and Objectives

The ultimate goal of research on SCR system for the automotive application is to achieve maximum NO_x conversion over a wide temperature range while keeping ammonia slip at

a minimum level, as well as reducing the cost, weight and size of a complete aftertreatment system.

One way to simplify current aftertreatment configuration in lean combustion system is to combine SCR and DPF into a single unit. The benefits of the combination catalyst are lower cost, weight and size, but the performance is difficult to control as this combination unit has two tasks: NO_x conversion and diesel particulate filtration.

There are two major problems with this combined catalyst. The first is temperature conflict. NO_x conversion requires a dedicated temperature range between 300°C and 500°C, the reaction rate is limited at low temperature, and undesired reaction consumes reductant agent if the temperature is too high. Whereas, the temperature during the regeneration process of diesel particulate filtration is 600°C. there needs to be a compromise between NO_x conversion rate and diesel particulate filtration. The second problem is the ash left in the inlet channel after the regeneration process. In the inlet channel, the catalytic surface material that intends for NO_x conversion is slowly covered by the ash. As a result, the overall surface area is lower, and the NO_x conversion rate is then reduced.

The ideal in this research provides a solution to the second problem by the mean of increasing catalytic surface area in the outlet channel. In this way, the surface catalytic area is free from the ash. The NOx conversion rate is then much less affected by ash loading.

In details, this research will focus on the investigation of the combination catalyst. Two catalyst model will be compared: SCR-DPF model, and SCR-DPF with extra fins in the outlet channel. In order to complete this task, the first step is to model and verify a flow-through type selective reduction catalyst, then apply the model into wall flow type

catalysts, one of them is normal SCR coating on DPF, and the other one has extra fins in the outlet channel. Commercial software package ANSYS FLUENT is used in the simulation of the flow and conversion processes. The characteristics of both wall flow type catalysts (WF and WF-Fin) will be investigated. A set of inlet velocities and temperatures are used to exams the system performance and any positive or negative effect on NO_x reduction and possible causes and improvement to be discussed. All three types of catalyst model are compared from different aspects, advantage and disadvantage of WF and WF-Fin and possible optimizations are discussed.

1.4 Thesis Layout

This thesis is organised in seven chapters and summarised as followed,

Chapter 1: The performance factors and limitations are introduced and discussed. Research aims and objectives are also given and end with a thesis outline.

Chapter 2: Chemical reactions and mathematical formulas of the model is presented.

Chapter 3: essential boundary conditions, numerical aspects of the models are calculated and discussed. Mesh independent, time step studies and converge criteria are also presented in this chapter.

Chapter 4: Provides information on step by step rate parameter calibration and validation of the proposed model.

Chapter 5 and chapter 6: Presents the results of WF SCR model and WF-Fin SCR model under steady-state condition. And they are then followed by performance comparison.

Chapter 7: Conclusion to this thesis, the discussion and recommendation of the future work of the proposed catalyst structure is made.

2. Methodology and Model Development

This chapter is to explain the research method and procedure. The objective of this research is to study the performance of finned wall flow type selective reduction catalyst for road vehicles. The plan is to build a flow-through type catalyst using commercial CFD software ANSYS FLUENT. Once the flow-through type catalyst model is verified then convert it into a wall flow type catalyst model and wall flow type with the fin in the outlet channel model. These 3 models are then going through several performance tests under different operation conditions, and their results are then compared.

The first step is to develop a general computation fluid dynamics model for the SCR system, and then determine the computation domains. Physical data of a flow-through type catalyst and other parameters are collected from other researchers' experimental work.

Then, a flow domain is built in ANSYS FLUENT based on collected dimensions and parameters. SCR rate parameters from Olsson's experiment [70] is used here to initiate first simulation results, mesh independent study and time step size study for transient problems. The purpose of mesh independence and time step size study is aiming to eliminate any possible numerical error caused by inappropriate meshing or time step size.

When mesh refinement is done, the following step is to reproduce those experimental result using a flow-through type model. Since there are many unknown factors and parameters of the catalyst, several assumptions are made. And because of that, the reaction rate from their work cannot be used directly in this CFD model. Otherwise, it leads to a different result. The catalytic reaction rate is precise to catalyst material and formulation, and the rate is based on serval conditions, e.g. catalyst mass, volume and

surface area. In most case, the global reaction rate is used, despite it is affected by different conditions, like an ageing issue and channel roughness. In most cases, the global reaction rate measured from one catalyst sample might differ from the other one unless the catalysts are manufactured carefully using the same material, formulation and method. Due to this reason, the result of the simulation can be affected by those conditions and parameters in the assumption. In order to compensate for those unknown factors due to the assumption, global reaction needs to be calibrated before applying to the final model. Thus, the reaction rate in the reference paper is used to initiate the first result, and then a simple trial and error method is used for reaction rate calibration. When the model has a similar result to the experimental one, this model can be considered as validated.

Once the model is validated, the channel length is cut from 30mm to 10mm in order to reduce computation expanse. Since the length is one-third compared to the previous case, overall performance is expected to reduce to one-third which should be the same as the first 10mm section of the full-length model (30mm). however, any performance difference between these two models is calculated and plotted. The comparison results between full-scale and reduced-model are presented in chapter 4.2.

It is followed by extending the flow-through model to wall flow type catalyst model, with and without fins. At this point, there are three 10mm models: flow-through type, wall flow type without fins and wall flow type with fins. In recent years, there are many types of research on SCR coated diesel particulate filter, that is wall flow type SCR. Therefore, in the later stage of this study mainly focus on the wall flow type catalyst with fin added into outlet channels. This kind of catalyst provides more surface area for SCR reactions. In terms of NO conversion rate, it is expected to perform better than the one without fins. Other performance factors and characteristics are compared to the other two.

2.1 General SCR Chemical Reactions

The SCR system is used to reduce NO_x. In a typical SCR system, there are 7 chemical reactions as follows:

Ammonia adsorption	$NH_3+S_{washcoat} \rightarrow NH_3(S)$	R_{ad}
Ammonia desorption	$NH_3(S) \rightarrow NH_3+S_{washcoat}$	R_{de}
Overall Ammonia ad/desorption can be presented as:	$NH_3+S_{washcoat} \leftarrow\rightarrow NH_3(S)$	R_{01}
Ammonia oxidation	$4NH_3(S)+3O_2 \rightarrow 2N_2+6H_2O+S$	R_{02}
Nitrogen oxide oxidation	$NO+\frac{1}{2}O_2 \leftarrow\rightarrow NO_2$	R_{03}
Standard SCR	$4NH_3(S)+4NO+O_2 \rightarrow 4N_2+6H_2O+S$	R_{04}
Fast SCR	$2NH_3(S)+NO+NO_2 \rightarrow 2N_2+3H_2O+S$	R_{05}
Slow SCR	$4NH_3(S)+3NO_2 \rightarrow 3.5N_2+6H_2O+S$	R_{06}
Nitrous oxide formation	$NH_3(S)+ 2NO_2 \rightarrow N_2+ N_2O+ 3H_2O+S$	R_{07}

When the mixture of ammonia and exhaust gas flows into a catalyst, ammonia is firstly adsorbed on the catalyst coating, and then the reaction occurs when NO_x contacts adsorbed ammonia. In a steady state condition, ammonia ad/desorption might be neglected, but it is essential to have a correct reaction rate for the adsorption and desorption process, as the following reactions are related.

Generally, the reaction rates of the above chemical reactions are [70-72]

Ammonia ad/desorption		
Adsorption	$R_{ad} = A_{ad} e^{-\frac{E}{RT}} C_{NH3}(1-\theta_{NH3})$	(E2-1)
Desorption	$R_{de} = A_{de} e^{-\frac{E}{RT}} \theta_{NH3}$	(E2-2)
Overall Ad/Desorption	$R_1 = A_{ad} e^{-\frac{E}{RT}} C_{NH3}(1-\theta_{NH3}) - A_{de} e^{-\frac{E}{T}} \theta_{NH3}$	(E2-3)
Ammonia Oxidation	$R_2 = A e^{-\frac{E}{RT}} C_{NH3} C_{O_2}$	(E2-4)
Nitrogen Oxide Oxidation	$R_3 = A e^{-\frac{E}{RT}} C_{NO} C_{O_2}$	(E2-5)
Standard SCR	$R_4 = A e^{-\frac{E_{NO}}{RT}} C_{NO} C_{NH_3}$	(E2-6)
Fast SCR	$R_5 = A e^{-\frac{E}{RT}} C_{NO} C_{NO2} C_{NH3}$	(E2-7)
Slow SCR	$R_6 = A e^{-\frac{E}{RT}} C_{NO2} C_{NH3}$	(E2-8)
Nitrous Oxide Formation	$R_7 = A e^{-\frac{E}{RT}} C_{N_2} C_{NH3}$	(E2-9)

2.2 CFD Governing Equations

Below are the basic physical models of fluid flow.

2.2.1 Conservation of Mass

Conservation of mass equation is also called the continuity equation. The general form of the time-dependent mass conservation equation can be written as

$$\frac{\partial \rho}{\partial t} + \nabla(\rho \vec{V}) = S_m \quad \text{(E2-10)}$$

Where ρ is the mixture density, t is time, $\vec{V}$ is velocity, and source term S_m is the generation or consumption rate of mass to the continuous phase, for example, due to desorption or absorption of the mixture in catalyst washcoat.

For 3D axisymmetric channel flow, the mass conservation is given by

$$\frac{\partial \rho}{\partial t} + \frac{\partial \rho u}{\partial x} + \frac{\partial \rho v}{\partial y} + \frac{\partial \rho w}{\partial z} = S_m \quad \text{(E2-11)}$$

where u, v and w are the velocities in x, y, and z-direction. For steady flow, $\frac{\partial \rho}{\partial t}$ term becomes 0.

2.2.2 Conservation of Momentum

The velocity field is governed by conservation of momentum

$$\frac{\partial \rho \vec{V}}{\partial t} + \nabla\left(\rho \vec{V}\vec{V}\right) = -\nabla P + \nabla \bar{\bar{\tau}} + \rho \vec{g} + \vec{F} \quad \text{(E2-12)}$$

Where p is the static pressure, $\bar{\bar{\tau}}$ is the stress tensor, $\rho \vec{g}$ is the gravitational body force, and $\vec{F}$ is external body force, model-dependent source terms, like porous-media source, also included.

Due to the porous media in wall flow type catalyst, resistance increases considerably; there is momentum lost and pressure drop rise in this region.

2.2.3 Conservation of Species

$$\frac{\partial (\rho Y_i)}{\partial t} + \nabla\left(\vec{V} \rho Y_i\right) = -\nabla \vec{J_J} + R_i + S_i \quad \text{(E2-13)}$$

Fluent mass transport for species takes convection-diffusion production and consumption of related species into account.

where R_i and Y_i is the reaction rate and mass fraction of each species i in the mixture. And S_i is the rate of creation by addition from the dispersed phase plus any user-defined sources.

Regarding the diffusion of the species in the channels, Fick's law is used. It describes the relationship between the diffusive flux of species i, the surface area, concentration difference and thickness of the membrane under the assumption of steady state.

In equation E2-14, $\vec{J_J}$ is mass diffusion flux term, which include diffusion due to concentration and temperature gradients. That is modelled as follow,

$$\vec{J_\imath} = -\rho D_{i,m} \nabla Y_i - \frac{D_{T,i} \nabla T}{T} \quad \text{(E2-14)}$$

where $D_{i,m}$ is mass diffusion coefficient for the species i, and $D_{T,i}$ is thermal diffusion coefficient. Since the temperature is assumed uniform across the entire domain, the thermal diffusion term can be dropped.

In order to convert species concentration between molar concentration and molar fraction, equation E2-15 is used,

$$c_{s,i} = \frac{P}{RT} x_{s,i} \quad \text{(E2-15)}$$

Where $c_{s,i}$ is molar concentration of the gas specie i, P is pressure, R is gas constant, T is temperature and $x_{s,i}$ is molar fraction of the gas species i.

2.2.4 Conservation of Energy

Even though the temperature inside catalyst is assumed evenly distributed, heat transfer is still an essential factor as all SCR reactions are temperature-dependent. Enabling the energy equation gives a more accurate result in temperature distribution and reaction rates.

$$\frac{\partial}{\partial t}(\rho E) + \nabla\left[\vec{V}(\rho \mathrm{E} + \mathrm{p})\right] = \nabla[\mathrm{k_{eff}} \nabla \mathrm{T} - \sum_j h_j \vec{J_J} + (\bar{\bar{\tau}}_{eff}\, \vec{V})] + S_h \quad \text{(E2-16)}$$

where ρ is density, p is static pressure, E is specific total energy, k_{eff} is effective conductivity, $\bar{\bar{\tau}}_{eff}$ is stress tensor calculated from effective viscosity.

Effective terms are used when there is moving fluid which can cause fluctuation of thermal value, fluctuation caused by or combination of many different material layers, it is the mean thermal value of such system or combination.

The first three terms on the right-hand side represent energy transfer due to conduction, species diffusion, and viscous dissipation, respectively. Source term S_h includes additional heat due to other heat mechanisms, chemical reactions for example. Sensible enthalpy h in incompressible flow is defined as

$$h = \sum_j Y_j h_j + \frac{p}{\rho} \tag{E2-17}$$

enthalpy of species j is

$$h_j = \int_{T_{ref}}^{T} c_{p,j} dT \tag{E2-18}$$

where reference temperature T_{ref} is 25°C.

2.3 Model Scale Choice

Generally, there are four model scales to catalyst modelling: washcoat modelling, single channel modelling, multichannel modelling and entire catalyst modelling [73]. Different model scale servers' different purpose. Washcoat scale focus on catalyst layer and reactions characteristic, like effectiveness factor and catalyst reaction improvement, can be done based on this scale. single channel scale can be used to study the characteristic of the complete catalyst if it is based on an appropriate assumption, for example, all channels are identical and behave exactly the same and uniform inlet conditions. Since a single channel is one size up from washcoat scale, sometimes the catalyst layer can be

included in a single channel to study the interaction between fluid phase, washcoat and whole catalyst. For more accuracy result, the entire catalyst model scale is required, as this model scale eliminates many assumptions compared to the single channel scale. This model scale allows non-uniform inlet conditions, block channels, deactivated catalyst layer and rough channel shape or dimensions. the multichannel scale can be treated as a simplified version of entire catalyst scale, a number of representative channels can be used to address the different situation in a different location, this can be non-uniform inlet temperature or species distribution. Multichannel scale unable to cover every aspect of a catalyst, but it can provide better insight into the whole catalyst when compared to single channel scale without increase computation expense dramatically.

Due to the limitation of computer performance in this research project, the entire catalyst scale is not under consideration. Washcoat scale is more about local nature and parameters. Therefore, it is not fit for this research purpose. Channel scale is the only option for this project, it is relatively less computation expense, and it is able to represent the entire catalyst with reasonable accuracy.

Single channel scale modelling is the most suitable model scale for the purpose of this study.

2.4 Computation Domains

In this study, three computation domains are used. First one, as in the figure below, is a single channel in flow-through type catalyst, d means channel width. Washcoat is excluded from the domain because it is assumed that no limitation of mass transfer in the washcoat. For the purpose of reducing computational expense, only a quarter of the

channel is simulated (the dark grey area in Figure 2-1). In this domain, full-length 30mm is used as it is used in validation and rate calibration.

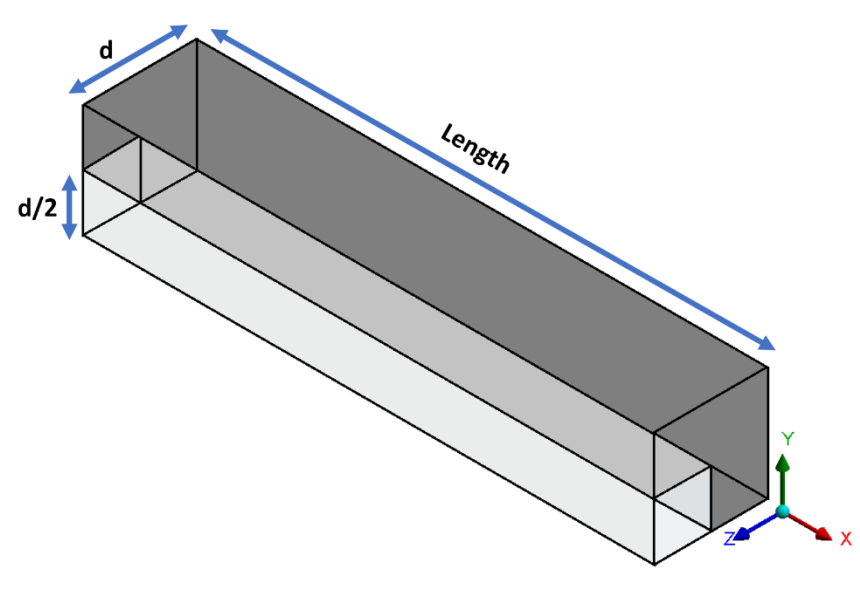

Figure 2-1: Flow Domain 1 single channel in flow-through type catalyst

After model validation, those data and models are applied to a new flow domain for wall flow type catalyst study. The changes in the new flow domain are: one-quarter channel changes to 4 quarter channels and the channel wall becomes a porous media for gas to pass through. As shown in Figure 2-2, that is two pairs of wall flow type catalyst (bottom). In the figure top left is a complete wall flow system that contains an inlet channel, an outlet channel and a wall. The wall is actually porous media, where surface reaction happens.

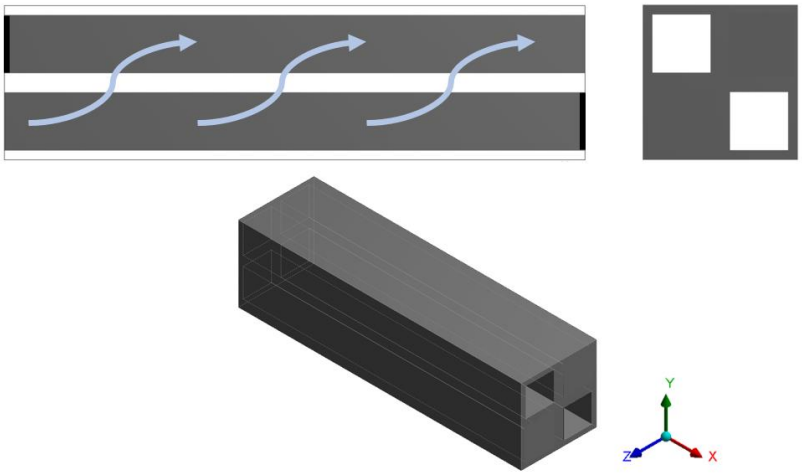

Figure 2-2: two pairs of wall flow type catalyst

The light grey area in the next figure is the flow domain for wall flow type catalyst simulation. Since the catalyst wall is porous media and allows flow to go through, SCR reactions also happen in this area, computation increase dramatically if all 4 channels are simulated. Therefore, only the centre part is simulated, box in by dash line, to keep computation expense low.

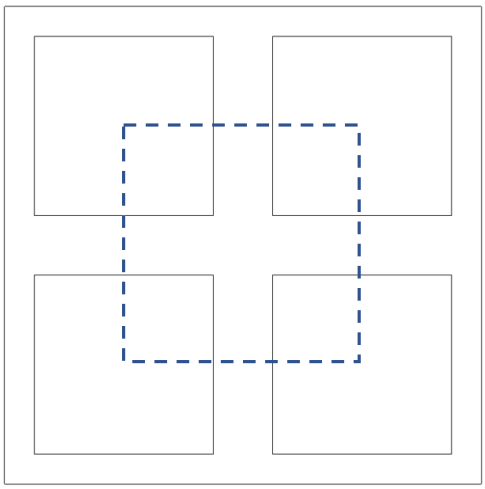

Figure 2-3: Complete Cross-Section View of Two Pairs WF catalyst

In the case of WF-Fin model, Figure 1-1Figure 2-4 shows the complete view of WF-Fin catalyst, and the fins are located in outlet channels.

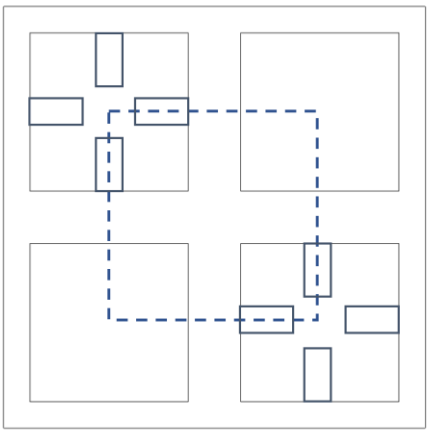

Figure 2-4: Complete Section View of Two Pairs WF-Fin catalyst

Again, for the purpose of reducing computational expanse, only the centre part is selected as the flow domain. Since the fins act as solid material and no heat transfer is modelled, the fins are cut out from flow domain for further reduction of computation expanse, as in Figure 2-5. Top left and bottom right are outlet channels while top right and bottom left are inlet channels.

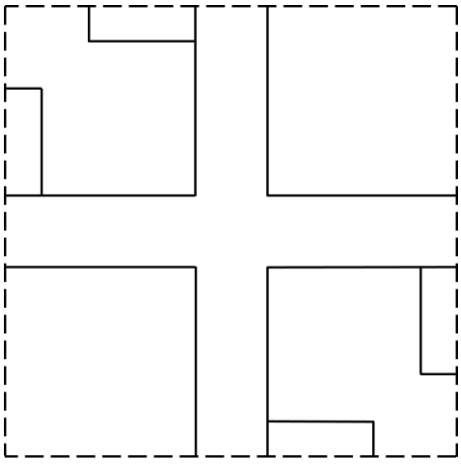

Figure 2-5: Front View of The Flow Domain for WF-Fin model

Figure 2-6 shows the actual flow domain for WF-Fin modelling. Two highlight channels, the top one is the outlet channel, and the bottom one is the inlet channel.

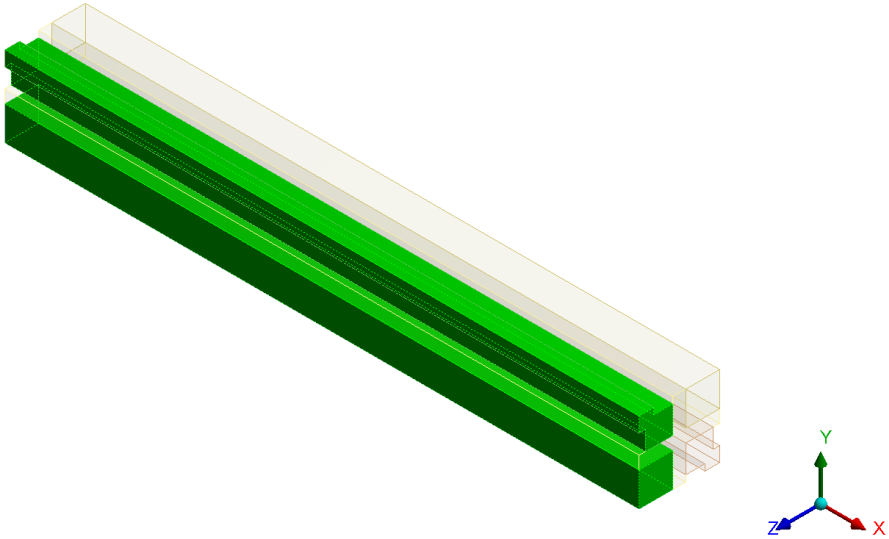

Figure 2-6: Fluid Domain for WF-Fin Model

2.5 Assumptions

Due to the limitation of computing power and the complex nature of reality, some assumptions have to be made. Assumptions lower the difficulty of modelling and simulation, reduce the complexity of the problem and running the system under the desired condition, but they also bring inaccuracy if a case is oversimplified. Below it is the assumptions for later works:

- All channels are identical, behaves exactly the same
- Inlet mixture gas is well mixed and distributed
- Uniform distribution of catalytic material
- Uniform temperature across the channel
- The flow is incompressible
- Ideal gas law is applied
- Constant mass diffusivity is used
- Zero heat loss from the catalyst

2.6 Summary

This chapter is mainly regarding methodology and model development. General chemical reactions of an SCR system, the conservation equations of mass, momentum, species transport and energy for this particular case are presented. Single channel scale model and computation domain were discussed, and a reasonable explanation was given for each of the choices. There are several assumptions of the flow were made.

3. Boundary Conditions and Numerical Methods

In the study performed by Olsson et al. [70], some data of that sample catalyst and conditions are unknown or unpublished, for example, wall thickness and channel width. Therefore, the calculation of varies parameters, physical data and boundary conditions are presented here. This chapter is divided into 3 sections, physical data of the sample catalyst, boundary conditions and numerical methods.

3.1 Physical Data

Since SCR reactions rate used in this work is adapted from Olsson's work[70], the same physical data, listed below in Table 1, of the sample SCR catalyst is used in this flow-through SCR simulation in order to do validation of the complete model.

	Value
Length	30 mm
Diameter	22 mm
Number of Channels	188
Cell Density	400 CPSI
Site Density	200 mol-site/m^3

Table 1: Simulated Flow-Through SCR catalyst characteristics

Assumptions

There are assumptions made in simulation work is listed in the previous section, and here are the assumptions made about the physical dimensions of the catalyst. Washcoat

thickness is assumed as 1mil (0.0254mm) and uniformly distributed on the channels inner wall. Wall thickness is set to be 6mil (0.1524mm). Therefore, channels width is 42mil (1.0668mm). Overall, all channels are assumed to have the same physical characteristics and behave essentially the same.

The reference catalyst sample, shown in Figure 3-1, is a 22mm diameter, 30mm length cylinder. It contains 188 channels with a cell density of 400 cells per square inch.

CFD modelling of a complete catalyst requires a considerable amount of computing power. In order to reduce computation time, a single channel is modelled for the validation process.

Flow through SCR catalysts use ceramic monolith or metallic monoliths coated with active catalytic materials. In the case here is to simulate exhaust gas flow through a square channel SCR catalyst. The catalyst sample used in the study of Louise O et al. is a 30mm long and 22mm diameter square channel Cu-ZSM coated SCR catalyst, shown in the figure below.

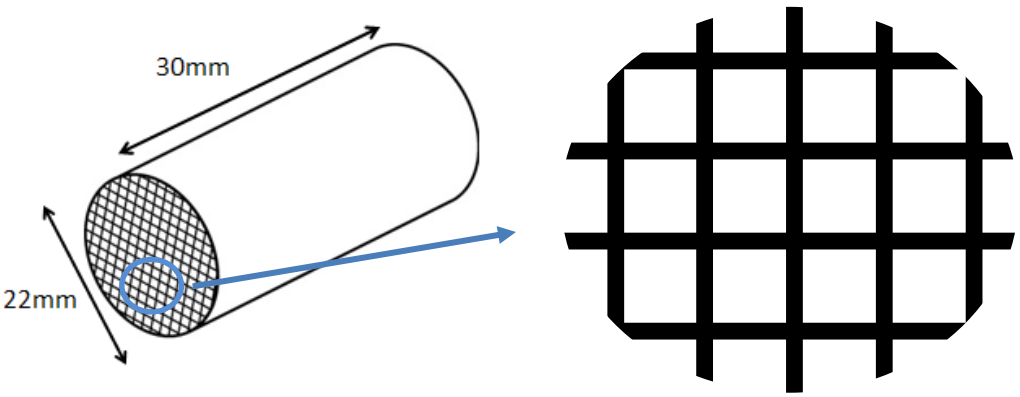

Figure 3-1: Sample Catalyst Dimensions

Calculation of wall thickness and the channel width is straightforward by using cell density. Since cell density is 400 CPSI, the area taken by a single channel can be obtained from

$$\frac{total\ area}{number\ of\ channels} = \frac{1\ \text{square inch}}{400\ channel} = 0.0025\frac{in^2}{channel}$$

therefore, the side length of this channel is

$$\sqrt{0.0025} = 0.05\ inch = 1.27\ mm$$

Figure 3-2 is the front view of zoom in the catalyst, and the dashed line indicates a complete square channel area. the side length of this square, represented by Ls, includes channel width (d), two washcoat thickness (WCT) and wall thickness (WT*2). Thus,

$$L_s = 1.27\ mm = d + \delta_{wall} + 2 * \delta_{washcoat}$$

Where d is channel width, δ_{wall} is wall thickness, δ_{washcoat} is washcoat thickness.

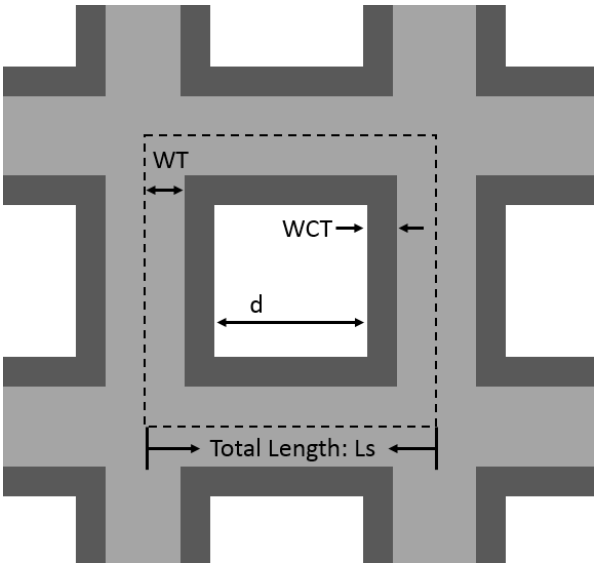

Figure 3-2: Zoom-in Catalyst (Front)

Since washcoat thickness is unknown, assumptions are made for washcoat thickness and wall thickness.

As catalyst technology developed, the cell density of a catalyst reaches up to 900 CPSI, and the wall thickness can be as thin as 2mil. However, for the automotive purpose, most

of the catalysts still using 400 to 600 CPSI, and wall thickness varies from about 4mil (flow-through type, e.g. SCR and three-way catalyst) to 12mil (wall flow type, e.g. diesel particulate filter). Catalysts with cell density between 200 and 600 CPSI, wall thickness from 12mil to 6mil are very common. In this simulation work, initial wall thickness (δ_{wall}) is assumed as 6mil and washcoat thickness ($\delta_{washcoat}$) is 1mil. Therefore, the total wall thickness is 8mil (0.2032mm). Then, Channel width (d) can be obtained from

$$d = 50 - \delta_{wall} - 2 * \delta_{washcoat} = 50 - 6 - 2 = 42\ mil = 1.0668\ mm$$

Site Density

In the reference, the sample catalyst is 22mm in diameter, 30mm length, with 188 channels. Channel width is 1.0668mm in this study. Thus, the total catalytic surface for flow-through type catalyst can be calculated from below,

$$A_{cat} = 4dL * 188 = 1.0668 * 30 * 4 * 188 = 24067.008\ mm^2$$

Which is $0.024067008\ m^2$

And catalyst volume

$$V_{cat} = \frac{\pi D^2 L}{4} = \frac{\pi * 22^2 * 30}{4} = 11403.98\ mm^3$$

Base on the value given by the authors, $200\ mol\ sites/m^3$ for the sample catalyst, the total amount of ammonia that the site can absorb (the maximum capacity of the sample catalyst) is

$$200 * (1.140398 * 10^{-5}) = 2.280796 * 10^{-3}\ mol$$

Mole-site per area (site density) can be obtained as

$$\rho_{site} = \frac{2.280796 * 10^{-3}}{0.024067008} = 0.09477 \frac{mol}{m^2}$$

Surface-to-Volume Ratio

The surface-to-volume ratio is required in FLUENT when using porous media. In this case, here is the assumption for the porous media,

- All holes are identical and in a cylinder shape,
- Diameter is 0.05mm
- Evenly distributed across the wall surface
- All perpendicular to the wall surface
- The porosity of porous media is 50%

wall surface area on the inlet and outlet channel is

$$A_{channel} = 2 * 4 * dL * 50\% = 128.016\, mm^2$$

The total surface area in porous media is calculated from the number of cylinder pores.

The maximum number of the cylinder on a wall is

$$\frac{dL * 50\%}{\pi r^2} = 8149.75 \approx 8150$$

Thus, the surface area of all cylinder pores in one inlet channel (4 walls) is calculated from

$$A_{pore} = 2\pi r * (\delta_{wall} + 2 * \delta_{washcoat}) * 8150 * 4 = 1040.546\, mm^2$$

The surface-to-volume ratio is then

$$\frac{\left(A_{pore} + A_{channel}\right) * \left(\frac{188}{2}\right)}{V_{cat} - 188 * d^2 * L} = \frac{109844.828}{4985.309} = 22.03371 \text{ mm}^{-1}$$

Summary of Physical Data

All calculation of boundary conditions and physical data were shown in the above sections. These data are then used in later sections and studies. The following table is to summarise all the data and parameters to be used

Name	Value	Unit
Channel Width	1.0668	mm
Channel Length	30	mm
Wall Thickness	0.1524	mm
Washcoat Thickness	0.0254	mm
Inlet Velocity	0.27264	m/s
Site Density	0.9477	mol/m2
Surface to Volume Ratio (Porous Media)	22033	1/m
Temperature	100 – 500	°C

Table 2: Physical Dimensions and Boundary Conditions

3.2 Boundary Conditions

Several boundary conditions are discussed in this section.

Inlet Velocity

Since the channels are the only consideration of the flow domain, therefore velocity at channels inlet should be calculated for boundary condition. Mixture gas flow rate from upstream is maintained at constant 3500ml/min, Velocity at the channels' inlet can be obtained using the below equation

$$v_{inlet} = \dot{V}/A$$

where $\dot{V}$ is volumetric flow rate, A is the cross-section area of all the channels, which is calculated from

$$A = 188 * d^2 = 188 * 1.0668^2 * 10^{-6} = 2.139557 * 10^{-4}\ m^2$$

Thus, inlet velocity is

$$v_{inlet} = \frac{\dot{V}}{A} = \frac{0.0035}{2.139557 * 10^{-4}} * \frac{1}{60} = 0.27264\ m/s$$

Reynolds Number

The Reynolds Number (Re) is a dimensionless parameter which indicates if a flow is a laminar, transient or turbulent. To classify

- Laminar Flow: Re < 2300
- Transition Flow: 2300 < Re < 4000
- Turbulent Flow: Re > 4000

Reynolds Number is calculated from

$$Re = \frac{\rho u L}{\mu}$$

Where ρ is the density of the fluid, u is the fluid velocity, L is a hydraulic diameter and μ is the dynamic viscosity of the fluid. For a square pipe, the hydraulic diameter is the width of the pipe.

Based on the above equation and the dimensions, the Reynolds number for FT type catalyst is between 30 and 100 and for WF type catalyst is between 60 and 200. The flow is classified as laminar flow.

Inlet Gas Composition

The volume flow rate of the mixture gas at the inlet is set to 3500ml/min while the gas composition is varied on the purpose of each simulation case, for example, the gas composition in reaction rate validations cases are different from each other and also different from later simulation cases. This is to make sure there are no side reactions during the validation process.

However, when comparing the 3 models, FT, WF and WF-Fin, side by side the same gas composition and the concentration are used. In this case, there are two conditions are considered, as listed in the below table.

Composition	Concentrations	
	Case 1	Case 2
NH3	500 (ppm)	1000 (ppm)
NO	500 (ppm)	500 (ppm)
H2O	8%	8%
Ar	Balanced	Balanced

Table 3: Inlet Gas Composition and Concentrations

Heat Transfer

Regarding heat transfer of the model, it is assumed that the temperature of the inlet gas is the same as the catalyst and the temperature is uniform inside the catalyst. Therefore, there is no heat loss from channel to nearby channel, and the heat loss to the surrounding environment is outside the consideration in this case.

3.3 Numerical Methods

Numerical modelling is not only about solving governing equations, calculating flow properties and boundary conditions, but also the way those governing equations are solved, that is solving algorithms. Solving algorithms, more or less, decides if the calculation goes smoothly toward convergence and an error pop up at some point. Three numerical aspects: fluent solver and settings, mesh and time step size are discussed in this chapter.

3.3.1 Solver and Settings

In general, all flow problems have the same physical laws but slightly different governing equations, using a different way to solve those governing equations or to calculate fluid properties can affect result convergence and even cause an error. Those are the solving algorithms in FLUENT. One solver can handle one case very well but cause instability in the other case; each solver has a different characteristic to flow problems. Faster convergence, shorter computation time and better stability and accuracy can be benefited from using suitable solvers and its settings for the flow problem. Flow inside the channels

of a catalyst is considered as a laminar flow. Therefore all solver and settings are chosen based on the characteristic of flow conditions.

3.3.2 Segregated and Coupled Solver

FLUENT has two numerical methods, segregated and coupled. The segregated solver is the default setting, and it is the solver to be used in this study. Both methods solve the governing equations for the conservation of mass, momentum, energy and chemical species using control volume technique. The governing equations are solved sequentially in segregated solver whereas in coupled solver solves the equations simultaneously. As governing equations are solved one by one, computation time is faster and less memory is used.

The procedure of segregated solver is as follow,

1. Update fluid properties from the current solution (or initialized solution)
2. Solve momentum equations
3. Solve pressure correction that derived from the continuity equation, linearize momentum equations and update the variables.
4. Solve energy, species and other equations

Due to the nonlinearity of the coupled governing equations, iteratively calculation must be carried out until the solution reaches convergence.

3.3.3 Discretization

Regarding discretization schemes, using an appropriate scheme can reduce instability, minimise residuals and get to convergence solution faster. In this research project, second-order upwind is used for momentum, species and energy in spatial discretization due to its higher-order accuracy and stability [74]. In the transient simulation, first order implicit is used because it is unconditionally stable with respect to time step [74].

3.3.4 Species and Chemistry Solver

In terms of species and chemical reactions, FLUENT is solving conservation equations of convection, diffusion and reaction sources of each species. Volumetric and wall surface reactions are activated for the chemical reactions in the fluid phase and on the wall surface.

Since there are only 9 simple chemical reactions, the explicit source is used in chemistry solver, that is direct use of chemistry source terms in the species transport equations. As the recommendation by FLUENT's manual, this solver is not suitable for stiff or complex chemistry. In the converse of this, using stiff chemistry solver for this situation leads to inaccuracy results in a transient state as it requires extremely small time-step-size. This error is demonstrated in a later section.

The turbulence-chemistry interaction model is not used in this study as chemical source terms are computed using general reaction rate expression without any effects of turbulent fluctuations.

3.3.5 Pressure-Velocity Coupling

As in a steady incompressible flow, density is a constant; the pressure is independent of density. Therefore, the pressure term is dropped from the continuity and momentum equation, and there is no other equation for the pressure field. A special algorithm is introduced to link velocity and pressure. This algorithm reformates continuity equation to derive an additional term for pressure condition. Then, the resulting fields will satisfy the continuity equation. This linkage between velocity and pressure is called pressure-velocity coupling, and it has many different pressure correction schemes.

The most basic and widely used scheme is SIMPLE (Semi-Implicit-Method-for-Pressure-Linked-Equations), proposed by Patankar in 1980 [75]. This scheme acts as pressure correction in step 3, the procedure of segregated solver in section 6.1.1. the procedure is kept repeating until convergence.

SIMPLEC is one of the variations of SIMPLE, C stands for consistent. According to FLUENT's manual, because of the increased under-relaxation, many problems will benefit from the use of SIMPLEC. This acts as convergence acceleration for simple laminar problems and improves stability for complicated problems.

3.3.6 Grid Independent

In a CFD simulation study, the governing equations are unable to solve a whole computational flow domain directly otherwise resulting in a significant error, unless it is a straightforward case; for example, simple geometry, uniform boundary conditions with zero change to the flow. Therefore, one large flow domain is divided into numbers of cells. As the cells' size is reduced, the boundary condition of those cell is more uniform,

and the difference between inlet and outlet conditions of the cells is getting smaller, and the difference between adjacent cells is also getting smaller, all of these help on reducing the computation errors.

Mesh quality plays a significant part in the accuracy and stability of the numerical computation, two indicators to check if the mesh quality is good or bad are the orthogonal quality and the aspect ratio.

Orthogonal quality is calculating from below two equations for each face i of a given cell.

- the normalized dot product of the area vector of a face and a vector from the centroid of the cell the centroid of that face [74]

$$\frac{\overrightarrow{A_i}\,\overrightarrow{f_i}}{\left|\overrightarrow{A_i}\,\overrightarrow{f_i}\right|}$$

- the normalized dot product of the area vector and a vector from the centroid of the cell to the centroid of the adjacent cell that shares that face [74]

$$\frac{\overrightarrow{A_i}\,\overrightarrow{C_i}}{\left|\overrightarrow{A_i}\,\overrightarrow{C_i}\right|}$$

The minimum value from the calculation of all the faces is defined as orthogonal quality, 0 means the worst cell quality, and 1 means the best cell quality.

And the aspect ratio is a measure of the stretching of a cell. It is a ratio of the maximum value to the minimum value of any distances between the cell centroid and face centroids, and the distances between the cell centroid and nodes. Mesh element distribution and smoothness also affect the accuracy of the numerical solution.

General speaking, providing mesh quality is excellent, reducing cell size (more cells) leads to the more accurate result, and a better solution is possible when the cell size is halved compared to the previous case. However, an exact solution is impossible as there

are always other errors exist in the system: modelling errors, discretization errors and iteration errors. There is not a universal solution for the size of the mesh; it is different from case to case. It is impractical to apply tiny mesh size to all cases. The first problem is hardware, despite the fact that computer technology has rapidly developed in the past decade, not many individuals or groups can afford to pay for such a powerful machine. Secondly, when the flow problem is getting complicated, there are lots of equations to be solved, infinitely increasing the number of cells will increase computation time, even with a super powerful computer. At the end of the day, the errors still exist despite the fact that they might be very small. Taking computer power, computation time and project goal into account, there has to be a compromise between the accuracy of the results and the number of cells.

Mesh independent study is a necessary step in this kind of simulation study. The process of mesh independent study is to initial a mesh as a starter and keep refining it at a constant factor (halved the cell size) until the results show no further improvement.

In this section, two cases are considered; one flows through type catalyst, and the other one is wall flow type with the added fin in the outlet channel. The reason is that the geometry is slightly different after adding fins into the outlet channel, previous mesh for flow through type catalyst might be inappropriate on the fins' edge and surface.

In order to reduce computation time, only quarter of a channel is used to run the simulation, as shown in Figure 2-1. Porous media washcoat is dropped, because the assumption of mass-transport has no limitations in the wash-coat, the process of ammonia adsorption and desorption is set to the surface wall.

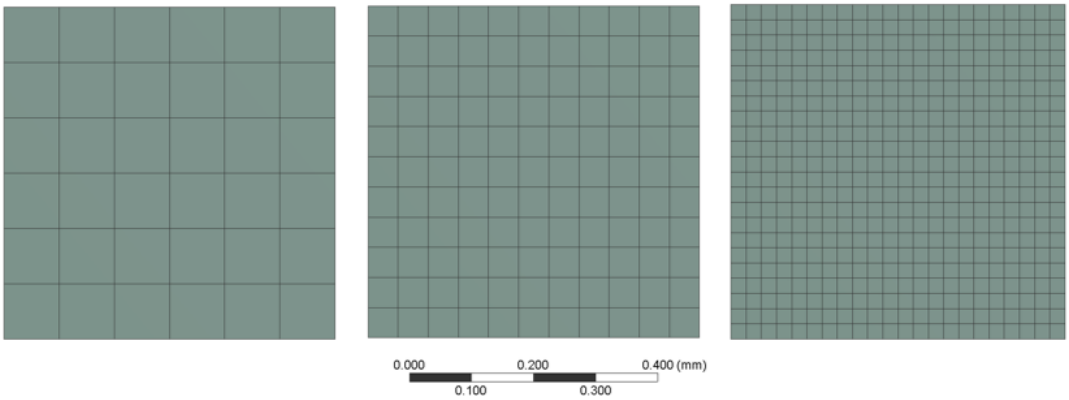

Figure 3-3: Mesh Case 1, 2 and 3 (from left to right), outlet view

This figure shows the outlet of the flow channel; it is the mesh changes in the transverse direction. The left one is first mesh, it has cell size 0.1mm*0.1mm and in the second mesh (middle) the cell size is reduced by half, 0.05mm*0.05mm, hence higher mesh density. And in the third mesh (right), cell size is reduced by another half to 0.025mm*0.025mm. in this way, from initial mesh case 1 to case 3, the number of nodes and elements are increased at nearly the same value, 3.6times to 4 times.

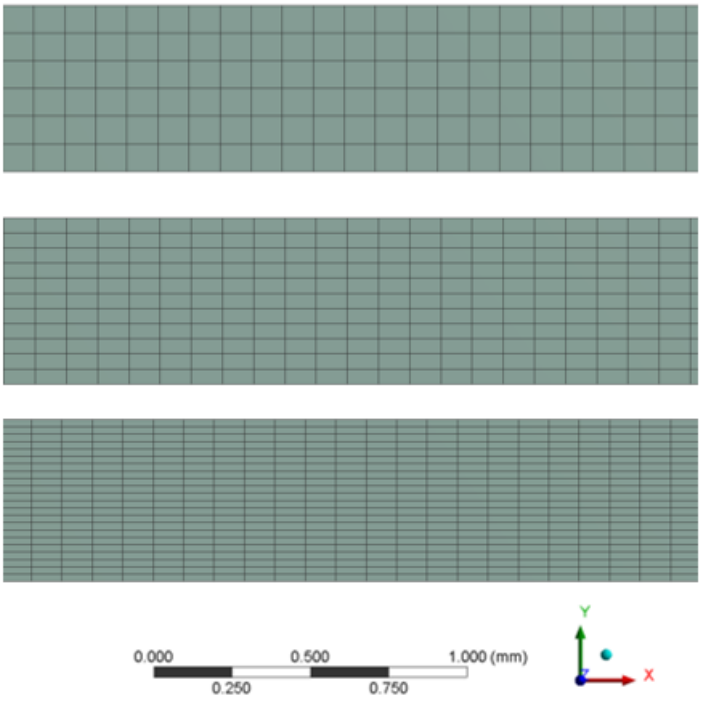

Figure 3-4: Mesh Cases 1, 2 and 3 (from top to bottom), channel side view

Since the shape of this geometry is a long thin tube, and the flow is laminar, there is no strong flow variation along the tube. Therefore, in a longitudinal direction mesh size can be set at a fixed value, 0.1mm, as shown in above Figure 3-4.

The term mesh aspect ratio is used here; it relates to the degree that mesh elements are stretched. It is the ratio of maximum to minimum integration point surface areas in the elements [74]. When mesh size in the transverse direction is refined to half of the previous case, aspect ratio increases from 1.12 to 2.06 and then 4.03 which is still very low. When the flow is aligned along stretched control volume, and no strong variation shows in the flow, the acceptable range for aspect ratio in ANSYS is less than 1000 if running double precision.

Mesh refinement statistics in Table 4 shows the details data of each mesh case, L is the mesh size in the longitudinal direction, and side means mesh size in the transverse direction. One of the primary mesh quality measure is skewness, how close a face/cell compare to the ideal case. Skewness value is range from 0 to 1 and 0 means better skewness. Orthogonal quality is another measure. The values of these two quality factors tend to close to (or equal to) its best value in the structured mesh.

	case 1	case 2	case 3
L (mm)	0.1	0.1	0.1
Side (mm)	0.1	0.05	0.025
Nodes	14749	43344	159229
Elements	10800	36300	145200
Aspect Ratio (min/avg)	1.12/1.12	2.06/2.06	4.03/4.03
Skewness (avg)	1.31E-10	1.31E-10	1.31E-10
Orthogonal Quality (avg)	1	1	1

Table 4: Mesh Refinement Statistics

For result monitor, 3 lines are added into the flow domain for result monitoring purpose, as shown in the below figure, the yellow surfaces are symmetry surface, green surfaces are defined as reaction wall. the first line is named ‘L-line-C’; it is used to monitor the data at the centre of the channel along the length of the axis. The second line is ‘V-line-2’; it is set between symmetry surface and reaction wall and 2mm away from the inlet to capture data variation across the channel. The third line is ‘V-line-wall’, it is also 2mm away from the inlet, but it lays on the wall to monitor surface reactions.

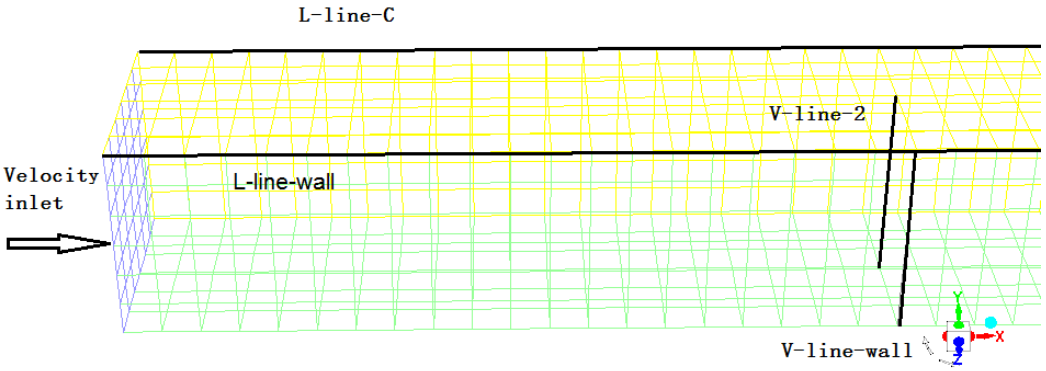

Figure 3-5: Flow-Through type Catalyst Channel Mesh (at the inlet)

Since it is reacting flow, ammonia mole fraction level is the first parameter to be examined. This Following figure shows the ammonia levels are identical in those 3 cases along the centre line of the channel. That means mesh refinement has no effect on the species in bulk flow at the middle of the channel.

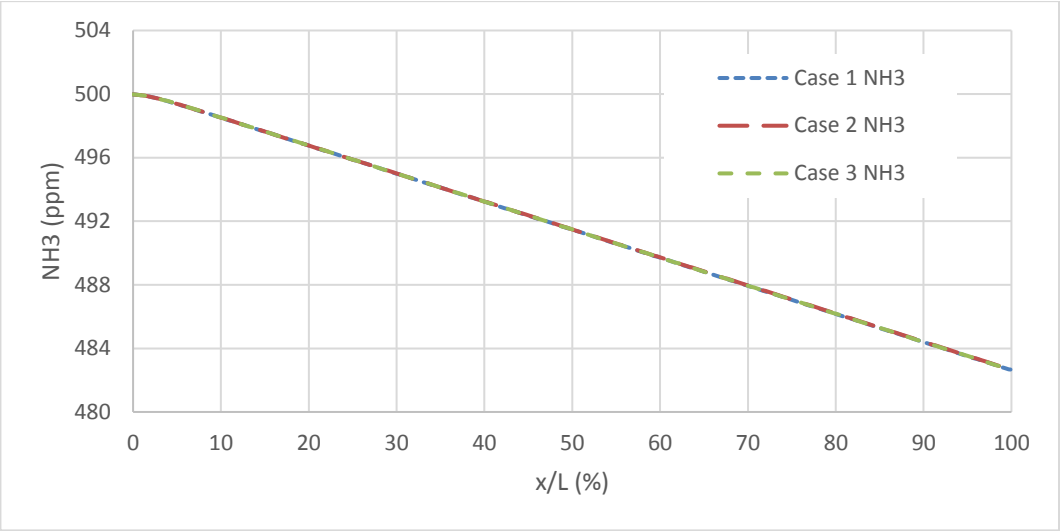

Figure 3-6: Ammonia Concentration on L-line-C

Ammonia coverage ratio and reaction rate show the same result between 3 mesh refinement cases. Figure 3-7 shows ammonia coverage ratio and ammonia desorption rate on L-line-wall. The ammonia coverage ratio is the ratio between the amount of ammonia adsorbed on the surface material, and the maximum capacity of the surface material can absorb (or called site storage), and this ratio is decreasing as temperature increase due to material's characteristics. Ammonia desorption rate is the rate that the surface material release absorbed ammonia back to the gas phase. All 3 cases have the same ammonia coverage ratio and desorption rate from the beginning of the channel to the end. It is difficult to see the difference in the figure because they are almost identical to each other. This means refined meshes show no improvement to ammonia coverage ratio; the initial mesh case is good enough to capture the adsorption and desorption of ammonia on the surface.

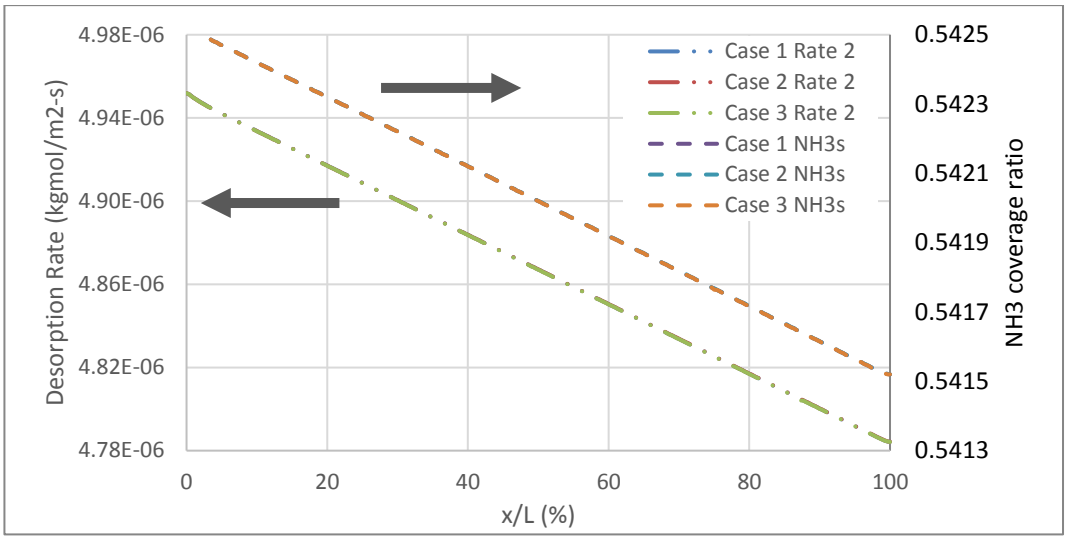

Figure 3-7: Desorption Rate and Ammonia Coverage Ratio on L-line-wall

Figure 3-8 shows the velocity value on the central line of the channel (L-line-c) from the inlet to the outlet, there is not much different at the inlet as the flow is developing, but there is slightly different when velocity becomes stable. When measuring the velocity at the outlet channel, there is 2.25% and 0.73% improvement when compare case 2 to case 1 and case 3 to case 2 respectively.

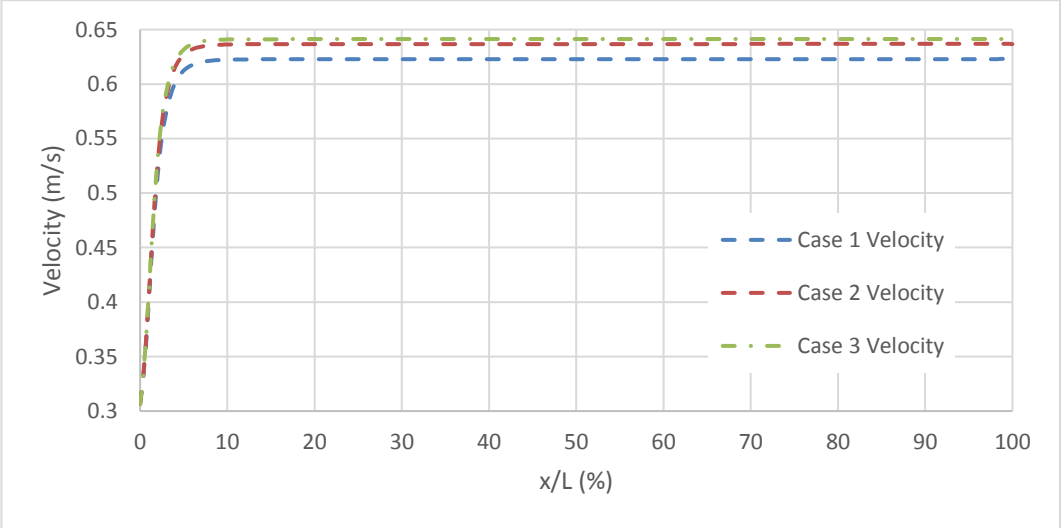

Figure 3-8: Velocity on L-line-c

In the transverse direction, V-line-2 and V-line-wall are used to monitor the parameters in the flow and on the wall. In Figure 3-9 and Figure 3-10, Y-axis (y/L) is the length of

the width of the channel in percentage, monitor lines V-line-2 and V-line-wall are perpendicular to XZ panel. 0% is at the bottom of the flow domain, and 100% is on the top side of the flow domain.

Figure 3-9 shows the difference in velocity at V-line-2, the most significant difference is in the centre of the channel, as the mesh is refined, there is 1.96% and 1.01% difference. On the other part of this line, the difference is minimal.

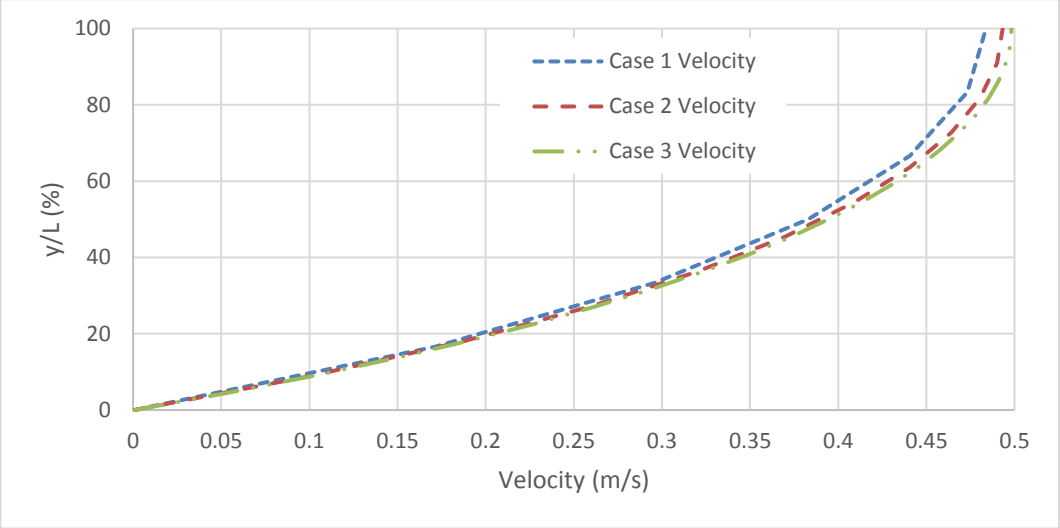

Figure 3-9: Velocity on V-line-2

Ammonia desorption rate is monitored on V-line-wall, as shown in Figure 3-10, the difference between coarse mesh and fine mesh is from the edge of the reaction wall, which is in the corners. However, the difference here is less than -0.01%, at this level of error, it can be ignored.

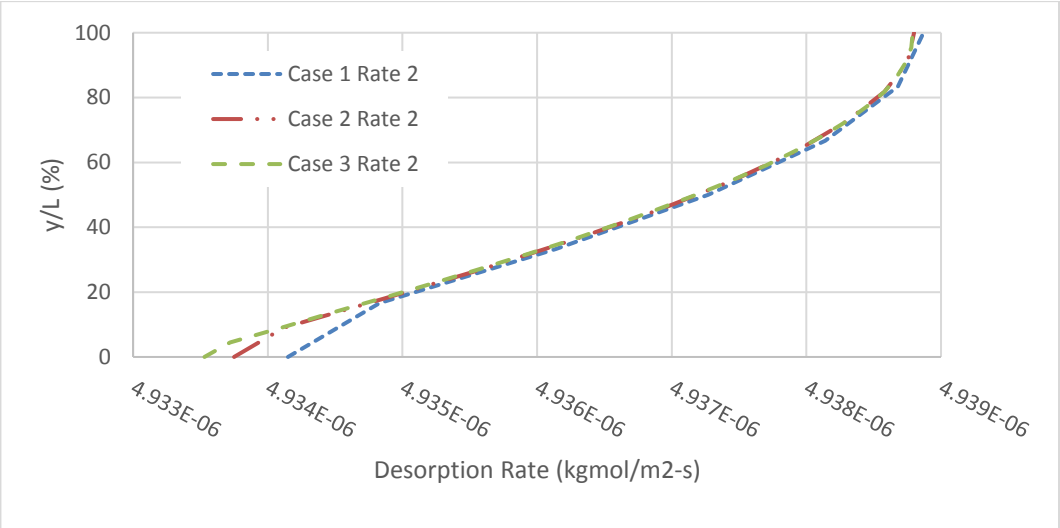

Figure 3-10: Desorption Rate on V-line-wall

All the error difference of that the monitored parameter are listed in Table 5. As the mesh is refined nearly 4 times than the previous case, there is not much improvement in the results. Most considerable improvement is from the velocity at the centre of the channel, 3% change when increase mesh number by almost 14 times. Therefore, mesh case 1 is used in the next simulation for the best compromise between accuracy and computation time.

	Units	Case 1	Case 2	Case 3
Velocity @ L-line-C	m/s	0.62275	0.63677	0.64143
Improvement	%		2.25	0.73
Velocity @ V-line-2	m/s	0.48382	0.49332	0.49833
Improvement	%		1.96	1.01
Rate 2 @ V-line-wall	mol/m2-s	0.0049342	0.0049338	0.0049335
Improvement	%		-0.008	-0.004

Table 5: Result Changes During Mesh Refinement

3.3.7 Time Step Size

Ammonia adsorption and desorption not only involves the reaction rate of ad/desorption and temperature but also site storage and time. The coverage of ammonia in the surface site storage is crucial as the SCR reaction rate dependents on the ammonia coverage because the ammonia coverage ratio reflects the amount of available ammonia for the SCR reactions. Characteristic of ammonia ad/desorption process can only be represented using transient state simulation as the site storage takes time to fill up with ammonia, overall adsorption and desorption rate decide the length of this time and the overall SCR reaction rates.

The time step size is a factor to be carefully considered when running a transient state simulation. A large time step size decrease computation time, but less accuracy during sudden change of flow condition and temperature, whereas small time step size gives more accurate result but lead to longer computation time. Same as all other simulation studies, a compromise has to be made between computation time and accuracy.

When setting up the coverage-dependent reaction rate, FLUENT's GUI setting automatically rounds the number to 1 decimal place. For example, when entering the number -1.77E+08, the system rounds it to -1.8E+08. Therefore, coverage dependent constant cannot be an exact number from the calculation.

Before obtaining an initial result with the original value, the first step here is to select a suitable time step size. In this subsection, the ammonia ad/desorption process is selected for time step size study as it can reflect the time step size effect more clearly than other reactions and with much less computation expanse. All reaction rates used in this subsection is the original values from Olsson's experiment [70]. All the boundary conditions are set to the same, the only difference is inlet temperature, and gas

composition profile is slightly different from the one in the reference work. Inlet ammonia of 500ppm is only maintained for 20mins, whereas it is 80 minutes in the original work; and initial temperature of 150°C is kept only for first 40mins before it rises 10°C per minutes, on the contrary in the reference work it was kept for 100mins. The total length of this shorted process is 75min, as shown in Figure 3-11, compared to original work which is 175min. These changes have zero effect on the behaviours of ammonia ad/desorption. Because they are in a steady period, site storage is full, and no more ad/desorption happens, there is no change in the system. The critical part is temperature rise at 10°C per minute which remains the same in the short version. The benefit is a less computational expense in terms of time scale.

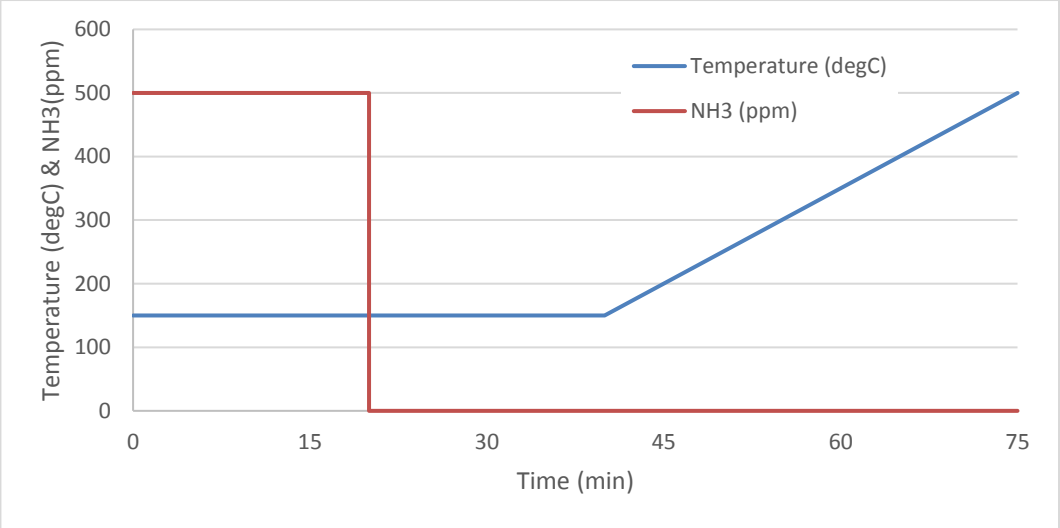

Figure 3-11: Inlet boundary condition for time step size study

Figure 3-12 shows the results of ammonia ad/desorption process with 0.2s, 0.1s, 0.05s time step size. This is a demonstration of inaccuracy result caused by using stiff chemistry solver when there is not turbulent fluctuation effect.

Smaller time step size certainly improves the accuracy of the ammonia level at the outlet during temperature rise period (between 40min and 75min). And this improvement is large when the time step size is changed from 0.2s to 0.1s and from 0.1s to 0.05s.

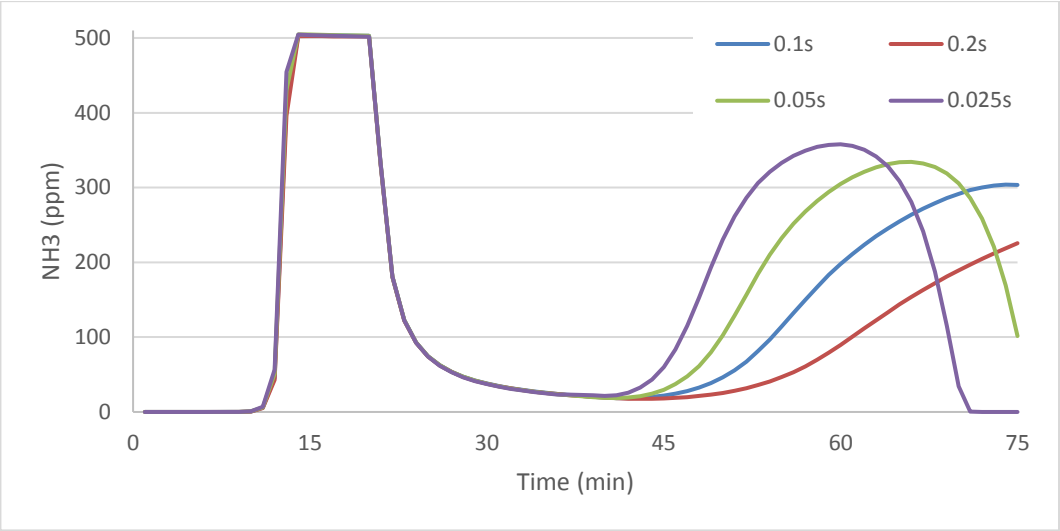

Figure 3-12: Ammonia ad/desorption result with varies time step sizes

Whereas in the first 40 min, it is a different situation. There is hardly any difference between these time step sizes. The only difference during this period is around 13min to 15min, that is because ammonia storage is nearly full, ammonia desorption about to reach its maximum rate. Desorption reaction rate at this point reaches a maximum, it is then reflected from the result, but the difference between them is small and can be neglected. This other possibility that causes this difference is because the results are recorded at the 60s interval, and the turning point happens to sets in the 60s gap, the result is, therefore, looks unsmooth.

For the first 40min, there is only one change in the boundary condition, that is 500ppm ammonia is shut off at 20th minute. apart from that, there is no change in temperature and gas composition; the result proves any of those time step sizes can handle this change well as their result is almost identical to each other. On the other hand, in temperature rise period, it is hard to say if the 0.025s time step is able to produce a satisfying result, but any time step larger than 0.025s certainly unable to handle the temperature change. 10°C increment per minute is 0.1667 °C per second, much smaller time step is required for this case.

The computer is i7-4790k 4.0GHz CPU with 16Gb ram, running this model with 0.05s time step size takes about 5 days and 0.025s time step size requires more than 2 weeks to compute, not to mention this model only contains 2 surface reactions, ammonia ad/desorption, and 5 species. Whereas in a full SCR model, there are 8 surface reactions and 10 species., one of the strategies to overcome this problem is to use large time step for the first 40min and then use a small time step size for temperature increase period; this helps to reduce computation expense by almost half. In Figure 3-13, light blue dash line is the result of mix use of the different time step size, the 0.2s time step is used for 0-39mins and from 39min to the end is 0.0125s, the result is taken at the 12s interval.

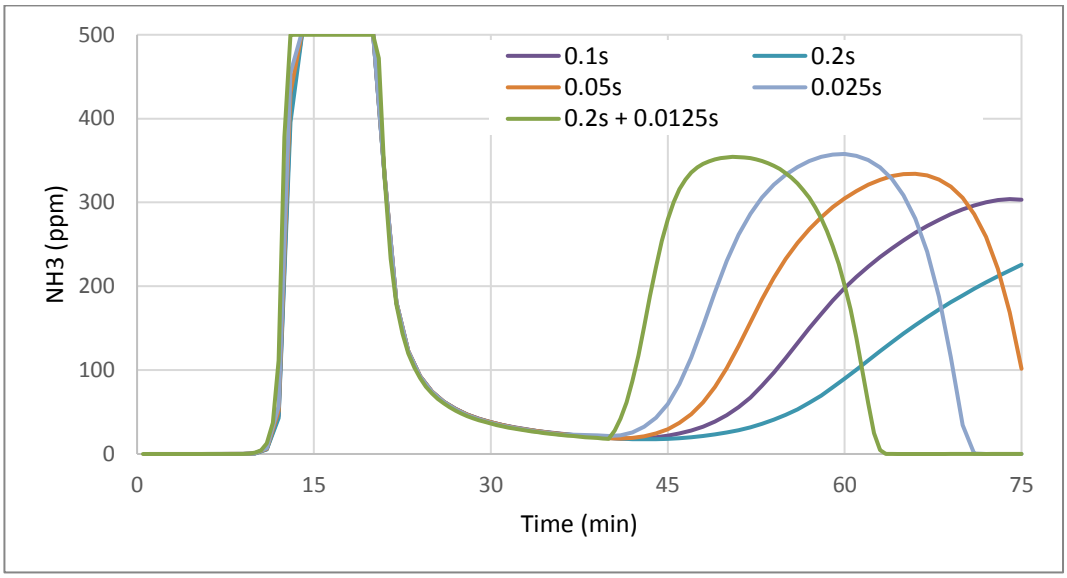

Figure 3-13: Mix Use of Time Step Sizes (0.2s for 0-40min and 0.0125s for the rest)

When comparing this result to the previous result of other time step sizes, there is a further improvement during the temperature rise period.

In the case here, although there is not turbulent fluctuation effect, stiff chemistry solver can still be used, and the accuracy depends on the time step size. The smaller time step size can provide better accuracy, whereas large time step size can be used when using none chemistry solver which makes explicit use of chemistry source terms in the species

transport equations [76]. Due to the computer performance, none chemistry solver is used for the later of this study, because it is more efficient and has the capacity of handling much larger time step when directly use finite-rate kinetics.

3.3.8 Converge Criteria

In CFD analysis, it solves the governing equations iteratively. During the calculation, the solution is different from one iteration to another, and as calculation goes on the solution is approaching the final solution or exact solution in theory. This stage is called solution converged. Since the solution keeps changing during iteration, therefore it is essential to make sure the solution has converged. In this study, two criteria are used for assessing solution convergence.

First one is residual values that directly quantify the error in the solution. This is one of the most fundamental measures to assess solution convergence. After discretization of the conservation equations, an algebraic expression of general variable Ø at cell P can be represented as [[74]]

$$a_p \emptyset_p = \sum_{nb} a_{nb} \emptyset_{nb} + b \qquad \text{(E 3-1)}$$

Here a_p is the center coefficient for cell P and a_{nb} are the influence coefficients for the cell around cell P, b is the constant part of the source term S_c in $S = S_c + S_p \emptyset$.

As defined by ANSYS FLUENT, for pressure-based solver the residual $R^{\emptyset}$ is the imbalance in equation (E 6-1) summed over all the computational cells, and it is referred to as unscaled residual

$$R^{\emptyset} = \sum_{cell\ P} \left| \sum_{nb} a_{nb} \emptyset_{nb} + b - a_p \emptyset_p \right| \qquad \text{(E 3-2)}$$

Since there is no scaling is applied in the above equation, it is difficult to judge convergence by examining this residual value. However, adding global scaling and local scaling factors into the equation makes it become scaled residual which is a more appropriate indicator to judge convergence for most problems. Scaled residual is the error between the solution from this iteration to the last one. In theory, it decreases to zero as the exact solution is converged. But this is not the case in practice, as the final solution is approaching scaled residuals decay to a small value and finally level out.

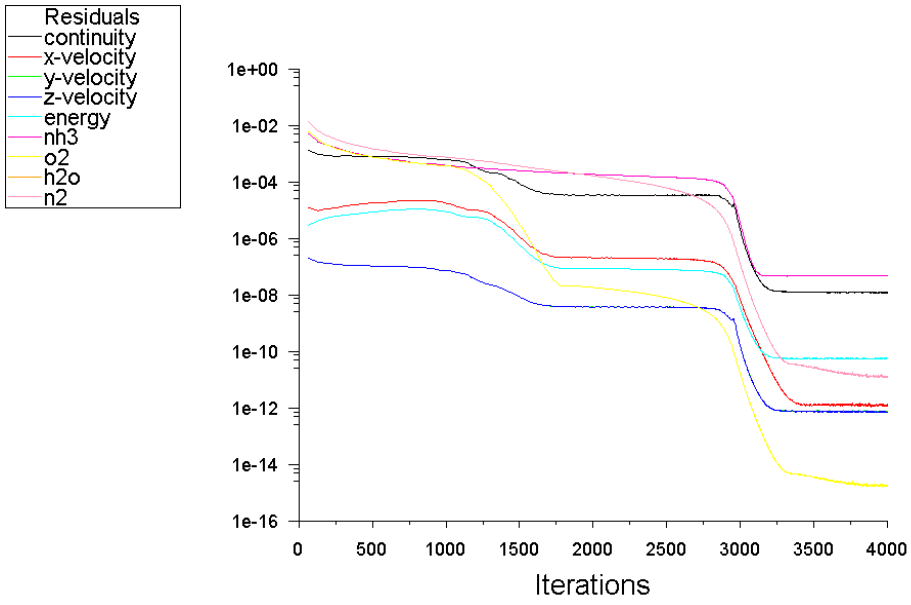

Figure 3-14: Residuals History in NH_3 Oxidation Modelling

Figure 3-14 is a global scaled residual history from ammonia oxidation modelling. All residuals trend decreases from the first iteration to 1500 iterations. After 1750 iterations, all the residuals are stable for almost 1000 iterations. And then they sharply drop and become stable from 3300 iterations.

In order to understand this residual figure, the ammonia adsorption process needs to be understood first. The overall adsorption is equal to adsorption rate minus desorption rate,

as in equation E2-3. Adsorption and desorption rates change with the state of site coverage. Thus, there are two stages in this process,

Stage 1, adsorbing: adsorption > (desorption + consumption)

Stage 2, fully adsorbed: adsorption = (desorption + consumption)

In Figure 3-14, iteration 1750 to 3000 reflects stage 1 of the adsorption process. This is the period where the site coverage is slowly filling up with ammonia while all other flow variables and species are steady. This is false stable as the site coverage is not monitored. After 3000 iterations, there is a further decrease for all residuals, and then it enters the stable stage after 3300 iterations. This means the system has reached stage 2 of the adsorption process and the site coverage ratio reaches the maximum level. From this point on, all flow variables, species and site coverage ratio are in steady state.

Residual value is one of the criteria, but it is not guaranteed to work for all problems. Therefore, monitoring quantities of interest is another criterion. All those quantities should be constant when a solution is converged.

Figure 3-15: The Average Velocity Value on the Outlet Panel

In this modelling case, 4 values are monitored: average velocity values and ammonia level at outlet panel and ammonia coverage and reaction rate on reaction walls. As shown in Figure 3-15, velocity is the average of vertex value on outlet panel. The velocity is converged after 3000 iterations, and the changes before that it is because iterative computation and solution are not stable.

Whereas in Figure 3-16, it is ammonia mole fraction at channel outlet, it is also calculated using the average of the vertex on the outlet panel. ammonia level maintains at 0 in first 2500 iterations; this is not a converged solution; it is ammonia adsorption process. Once all washcoat is entirely filled by ammonia, any excessive ammonia goes to outlet directly if there is no reaction to consume ammonia, either from gas bulk or washcoat. The increase of ammonia level from 2500 iteration indicates washcoat is saturated. In this context, full filled and saturated means at some point where adsorption rate equal to desorption rate, any amount of ammonia is absorbed by washcoat, the same amount of ammonia is desorbed from it.

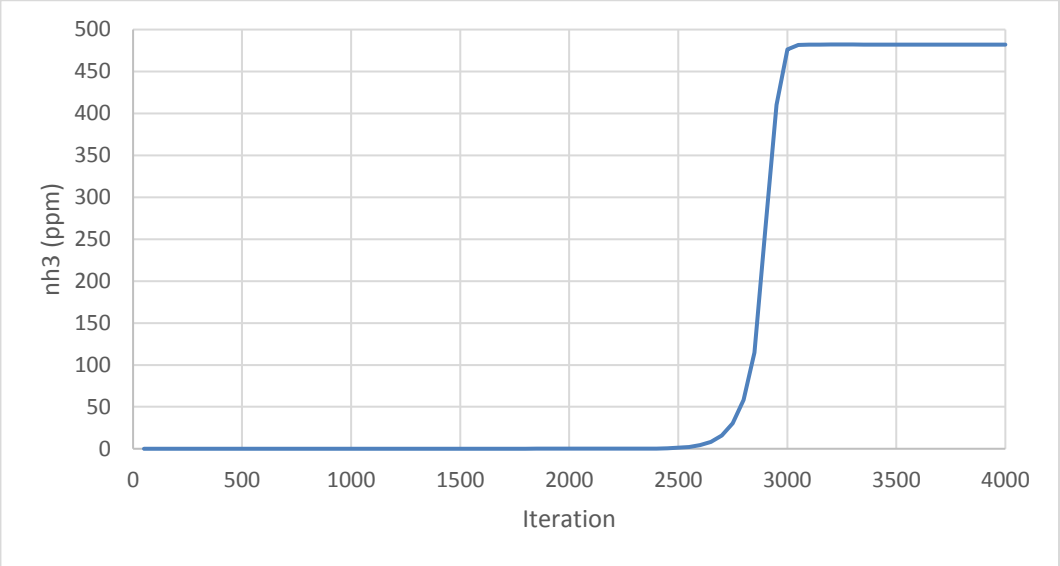

Figure 3-16: Outlet Ammonia Level

To prove this, ammonia coverage, represented by $NH_3(S)$, is plotted against iteration in Figure 3-17. This value is calculated from the average of the surface vertex on both reaction walls. This is one of the most interest quantities as it affects other SCR reaction rates, thus the overall performance of the SCR system. During the ammonia coverage raise period, computation is fighting to find a converged solution, cause that little fluctuation. After 1500 iterations, there is a level out period in residuals (Figure 3-14) because the velocity profile becomes much stable and almost reach converge solution. But on the species side, ammonia still filling up washcoat storage, ammonia coverage is changing. When ammonia coverage ratio reaches its maximum point, after 3000 iterations, the solution is converged, outlet velocity and ammonia level become constant, the coverage ratio maintains a constant level.

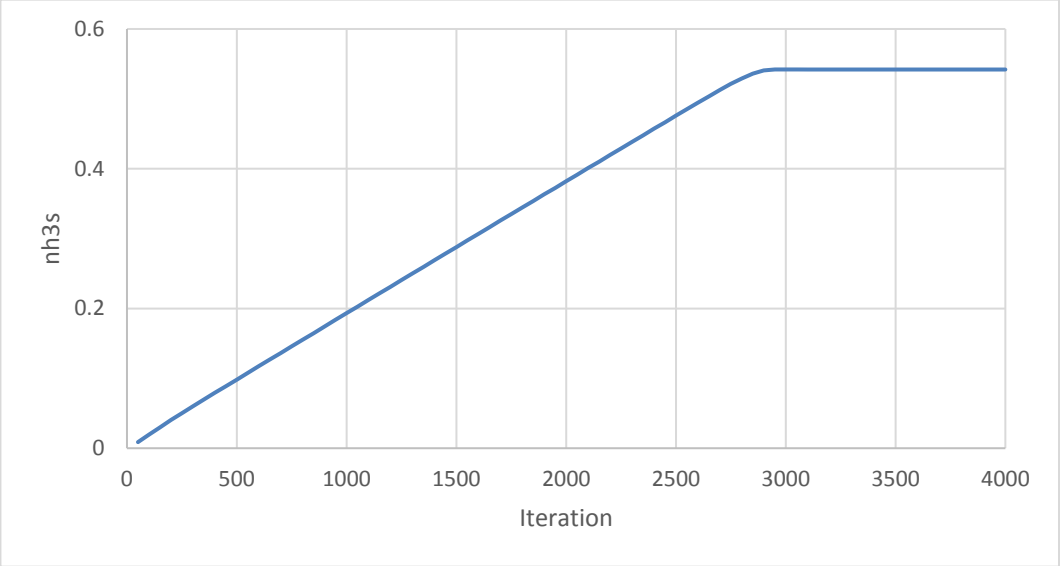

Figure 3-17: NH_3 Coverage on Reaction Wall

This is a prove that residual alone is not strong evidence for converge solution in every case. That makes quantities of interest is another important criterion.

Overall, there are four criteria to determine if the case is converged: residuals history of the iterations, the average velocity value from outlet panel, the ammonia level from the

outlet and the ammonia coverage on the reaction wall. The case is considered converged when all of these monitor data reach steady condition.

3.4 Summary

Essential boundary conditions of the flow and physical dimensions of the sample catalyst were discussed and calculated in this chapter. The selection of numerical solvers and settings were discussed and selected accordingly.

An example was given when choosing chemistry solver; using the most suitable solver is essential. In this case, stiff chemistry solver can provide an accurate result if the time step size is small enough. So, choosing suitable solver means to choose the balance between accuracy and computation time.

4. Model Validation

It is difficult to reproduce the original experimental result in simulation work, especially in the case when some important values are unknown or subject to the condition status of critical factors. Those reaction rates measured from their experiment is unique to certain conditions and materials. Even with a known velocity, temperature, site-density etc. etc., there still are unknown parameters, such as channel wall resistance, if all catalysis material active or only part of it is active. Thus, some assumption is made during numerical model building, and then by adjusting a few values to produce a similar result to an experimental one.

This section is to represent the calibration work for the SCR reaction model and validation of each reaction.

4.1 Rate Parameter Calibration

In this subsection, rate parameters of SCR reactions are adjusted in FLUENT in order to reproduce similar result compare to reference work. The original reaction rates from reference's work are used to initiate the first result; then each value is then adjusted accordingly to match the simulation outcome to experimental data. All original rates that are used to produce initial results are listed in Table 6 below.

	Pre-Exponential Factor	E_a (kJ/mol)
NH_3 Adsorption	0.93	0
NH_3 Desorption	1e11	181.5
NH_3 Oxidation	1.2e11	162.4
standard SCR NO+O2	2.3e8	84.9
Fast SCR NO+NO2+O2	1.9e12	85.1
Slow SCR NO_2	1.1e7	72.3
NO Oxidation	80	48
N2O formation	36000	43.3

Table 6: Rate Parameters in Olsson's Experiment[70]

4.1.1 Ammonia Adsorption and Desorption

Inlet temperature and composition of the mixture gas condition used in ammonia ad/desorption test is shown in Figure 4-1. In the first 80mins, mixture gas contains 0.0005% (500ppm) mole fraction of ammonia, after that inlet mixture gas is replaced by an inert gas, Argon, for the rest of 100 minutes. The initial temperature is maintained at 150°C for 140min; then it starts to increase at 10 °C/min rate, it reaches 500 °C at the end of the test (175mins). This is a full length of ad/desorption test in comparing to the short version of this in Figure 3-11 from the last section. In the period of adsorption, there is not much difference between 20 and 80 minutes as long as the adsorbed ammonia on the site surface reaches a constant level.

After the cut off of ammonia supply, inlet mixture gas is replaced with Argon gas. There are 60 minutes cool down period in the full-length ad/desorption test, compared to 20 minutes in the short version. In other words, it is 60 minutes natural desorption of

ammonia from the surface site compares to 20 minutes. At the time that temperature starts to rise, this full version provides a more accurate value of adsorbed ammonia on the site surface than the short version when validating the result with the reference work [70].

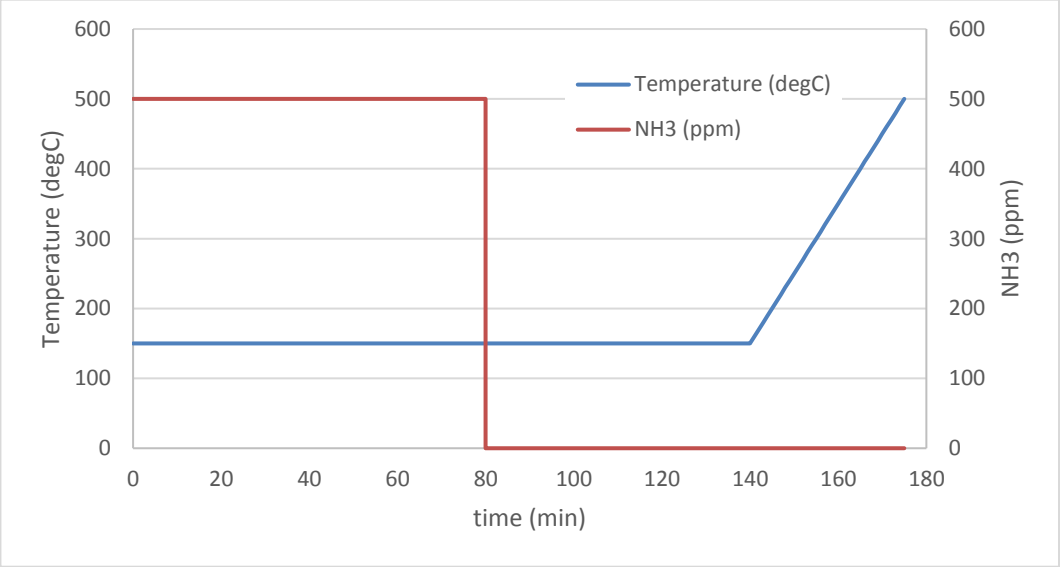

Figure 4-1: Inlet Mixture Gas Temperature and NH_3 Condition

The following plot, Figure 4-2, is the validation of ammonia adsorption and desorption process and the results of 4 reaction rates is shown. the original rate is used directly from the reference work without any modifications; this rate value provides good agreement at 150°C during ammonia adsorption process and natural desorption from 80 to 140 minutes. As soon as temperature rise, outlet ammonia concentration increases rapidly. Despite the dramatical ammonia level as temperature goes up, the gradient of this increase is slightly larger than the one with experimental data. That is an indication of desorption rate is over sensitive to temperature change. Therefore, a slower reaction rate with less sensitive to temperature change is needed for ammonia desorption process.

Thus, three more simulations were run with slower reaction rates. Rate 1, 2 and 3 are modified from original values since activation energy (E) relates to the temperature sensitivity of a reaction, this value stays unchanged, only pre-exponential factor value is

reduced (K). Pre-exponential value is 1.0E+09, 1.0E+08 and 1.0E+07 for rate 1, 2 and 3 respectively.

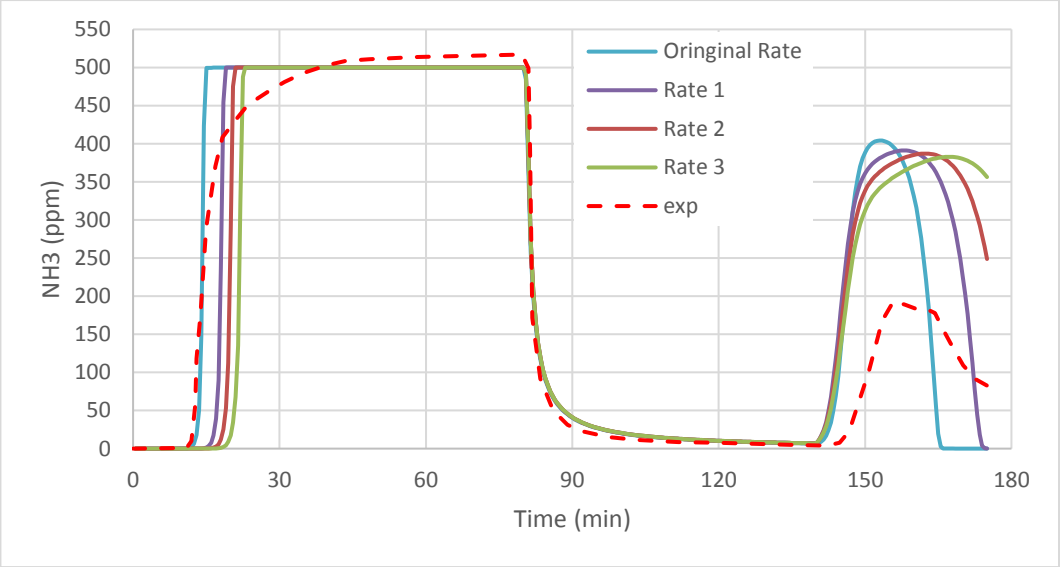

Figure 4-2: Validation of Ad/desorption Results with Various Reaction Rates

The modified rates require a longer time to reach the maximum level of absorbed ammonia on-site surface in the absorption period. But during the last 40 minutes of the simulation, rate 2 shows a very similar tendency of ammonia release compares to experimental data. Once the rate is decided, the total amount of adsorbed ammonia is controlled by site storage of the surface material. Based on the calculation, this value is 0.0000945 kgmol/m2 in the experiment, but when using this value in simulation model with reaction rate 2, the catalyst takes 21 minutes to reach fully absorbed condition, and the released ammonia level is nearly 400ppm during temperature rise. In comparison to the case that fully absorbed condition is reached in 12 minutes and 200ppm ammonia release during a temperature rise, the difference is nearly twice. The goal here is to match simulation result to experimental result, a good agreement is achieved by using half of the site storage value from the experiment, as shown in Figure 4-3.

In general, this result meets early expectation: the time take to reach the fully-absorbed condition in 12 minutes, peak ammonia release during temperature rise is reduced to 220ppm.

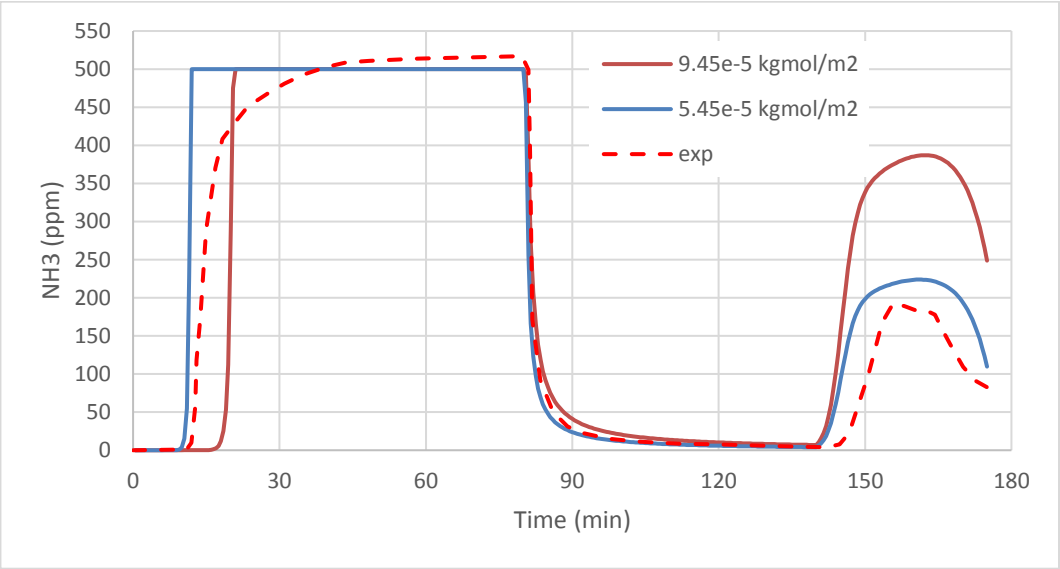

Figure 4-3: Validation of Ad/desorption Results with Different Site Density

However, there are two discrepancies in this figure. The first one is the difference between simulation result and experimental data in absorption period, 10 to 30 minutes, overall adsorption rate decreases with ammonia site density, so in the experiment outlet ammonia level reaches 500ppm slowly, it takes more than 20minutes rather than 1.5 minutes in the simulation. This discrepancy is caused by an improper value setting of coverage dependent activation energy. The value measured from their work cannot be used directly in simulation modelling and the value changes due to various assumptions.

The second discrepancy is about the temperature rise. The rising starts at 140min in simulation and outlet ammonia level almost instantly response to temperature change whereas in the reference experiment outlet response at 3 minutes later. The assumption of uniform and well distribution of temperature in the simulation model and slow response of the catalyst in the experiment are the primary cause of this discrepancy.

Either way, modified reaction rates and site density values provide a reasonable result and match with experiment data well.

4.1.2 Ammonia Oxidation

In the ammonia oxidation process, ammonia is aborted into catalyst first, and then it reacts with oxygen. As the rate of ammonia ab/desorption is determined, this subsection is to calibrate the ammonia oxidation reaction rate. The chemical equation of absorbed ammonia reacts with oxygen is shown here,

$$4NH_3(S)+3O_2 \rightarrow 2N_2+6H_2O+S$$

In ammonia oxidation validation, steady-state simulation is used to reduce computation time. Inlet temperature condition starts at 100°C, and then it increases to 400°C at 50°C increment. The composition of the inlet mixture gas is 500ppm of NH_3, 8% O2, 5% H2O and Argon gas. After all the boundary conditions are set, the initial result is shown in Figure 4-4.

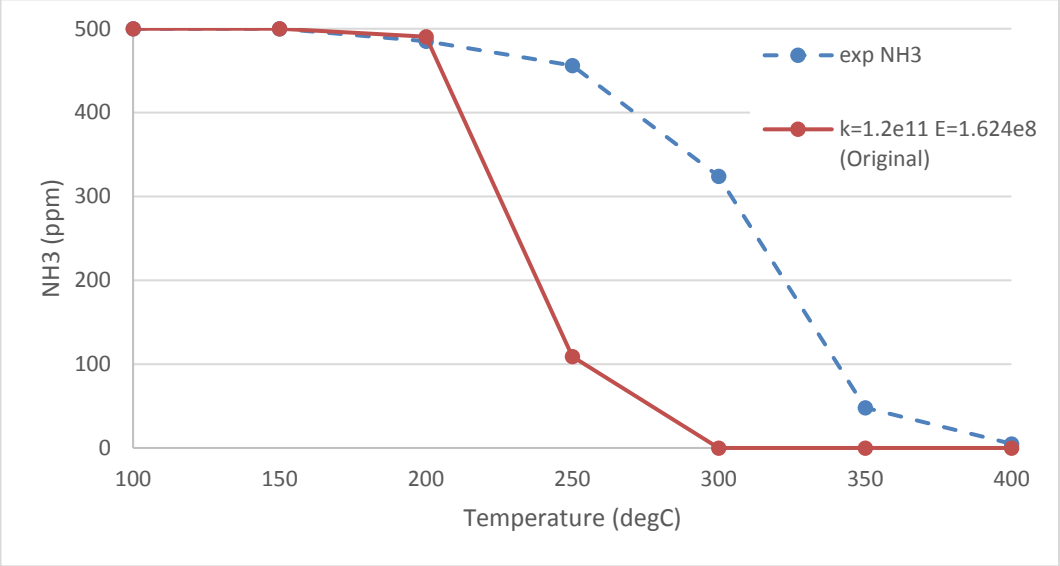

Figure 4-4: initial result for NH_3 oxidation, outlet NH_3 level VS temperature

The brown dots in the figure are initial results from using the original reaction rate in reference work[70]. In comparing to Olsson's experimental data[70], the initial result shows pretty good agreement below 200°C, and at a temperature higher than 200°C simulation result and experimental result have a significant difference, apparently reaction rate of ammonia oxidation in the simulation model is much faster than the one in experimental, or much more sensitive.

The simulation results at 200°C to 300°C indicates original reaction rate has huge responses to a temperature change above 200°C, and outlet ammonia level at 150°C and 200°C is a slightly higher value than experimental data. In order to increase ammonia concentration at the outlet, reaction rate needs to be reduced. Change activation energy values can change the response of a reaction to temperature changes as the required energy in the reaction is changed. Thus, the first step is to change activation energy and match the trend of outlet ammonia to a similar level as an experimental result.

Here is the procedure to follow, adjust activation energy first, monitor ammonia concentration at the outlet, the pre-exponential factor can be adjusted once outlet ammonia level has a similar trend as an experimental result in response to temperature change, the value of activation energy need is lowered to have a faster reaction rate at low temperature, and also lower pre-exponential factor value reduces temperature response between 150, 200 and 250°C. By lowing activation energy, simulation result at 200°C should be lower.

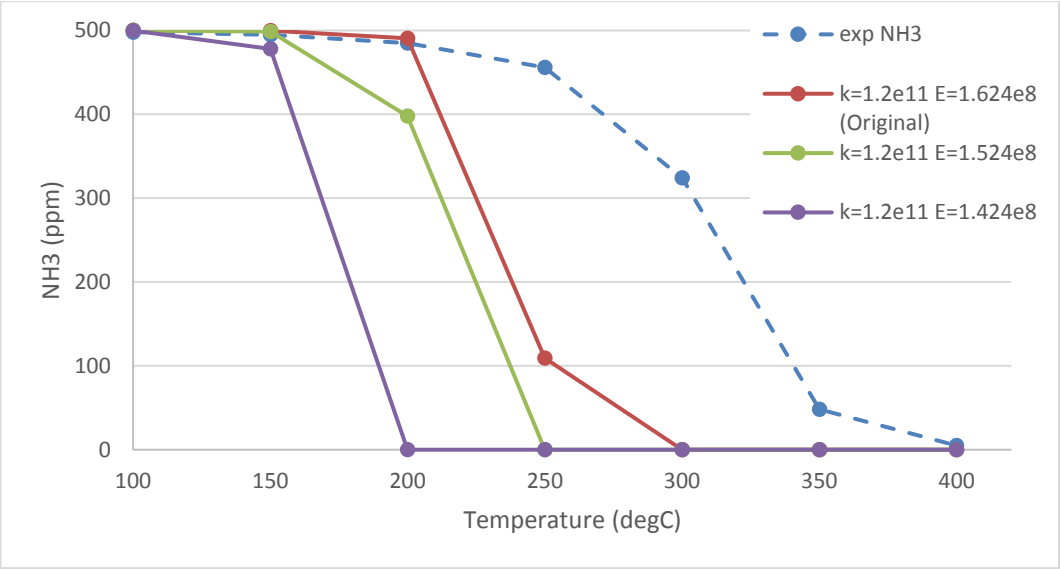

Figure 4-5: Demonstration of Outlet NH3 Level from Activation Energy Change

The results of outlet ammonia after using lower activation energy for ammonia oxidation reaction is shown in Figure 4-5. It proves the expectation of the relationship between the activation energy and simulation result at low temperature (from 150 to 250°C) is correct. The next step is to reduce the pre-exponential factor value (K).

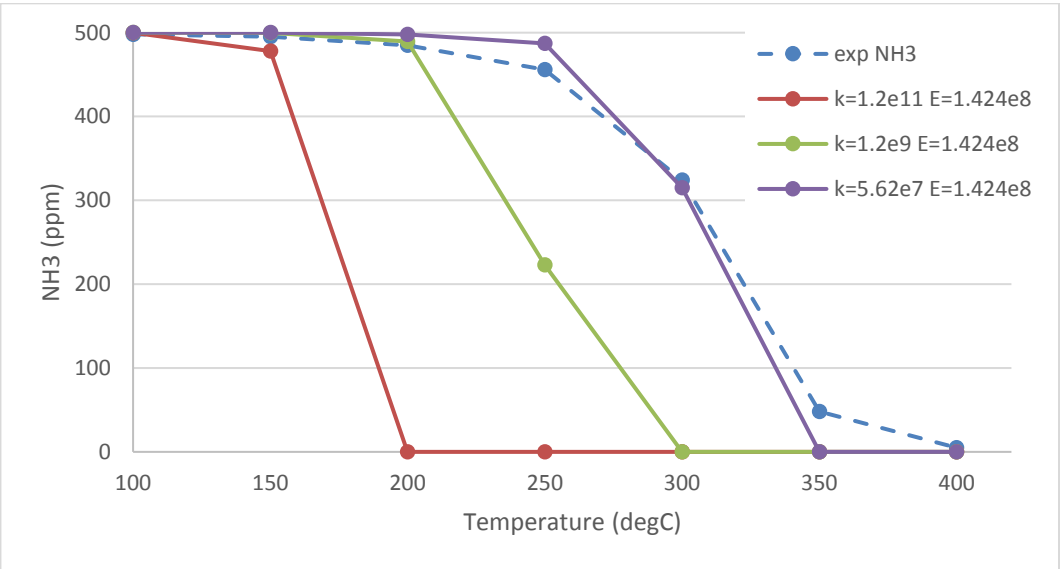

Figure 4-6: Demonstration of Outlet NH3 Level from Pre-Exponential Factor change

After reducing the overall ammonia oxidation reaction rate by a lowered pre-exponential factor, the result is plotted in Figure 4-6. As pre-exponential factor value is lowered, simulation result start moves toward to experimental result closer and closer, in the complete temperature range. When pre-exponential factor value is set to 5.62E+07 with activation energy 1.42E+08, the outlet ammonia level is increased to around 498ppm at the temperature below 200°C. 487ppm at 250°C and 315ppm at 300°C, in the contrast experimental results are 489ppm, 456ppm and 324ppm at 200°C, 250°C and 300°C respectively. This set of reaction rate is close to the experimental result, but the error at 250°C and 350°C are still significant. By repeating this procedure of finding reaction rate, a reasonable combination of activation energy and pre-exponential factor can be found. But it needs a pair of reaction rate to produce two sets of the result as guidance.

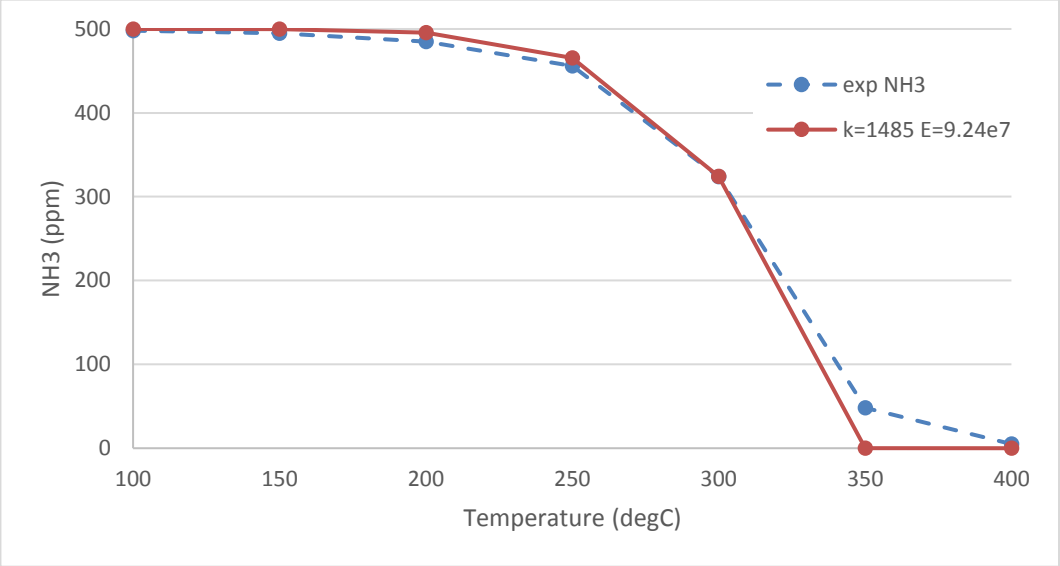

Figure 4-7: Final Values for NH_3 Oxidation Calibration

After several attempts, Figure 4-7 shows the final values for ammonia oxidation rate and its simulation compare to experimental data. It matches experimental data well from 100°C to 325°C, and the error is less than 3%. But the difference between 325°C and

400°C is still substantial. And at a higher temperature, both simulation and experimental result are tending towards 0.

In general, this combination of activation energy and pre-exponential factor produces a simulation result fits experiment data well in the temperature range 100°C to 400°C, so it can be used in later models for further study.

4.1.3 NO Oxidation

The NO oxidation process is relatively simpler as the oxidation happens in the gas phase; there is no ad/desorption in the process. Here is NO oxidation chemical equation,

$$NO+\frac{1}{2}O_2 \longleftrightarrow NO_2$$

In NO oxidation model calibration, the inlet temperature increases from 100°C to 500°C, the result is recorded at every 50°C change. The composition of the inlet mixture gas is 500ppm NO, 8% O2 and 5% H2O and Argon gas. In order to find a suitable combination of activation energy and pre-exponential factor, the same principle and procedure are applied to NO oxidation calibration.

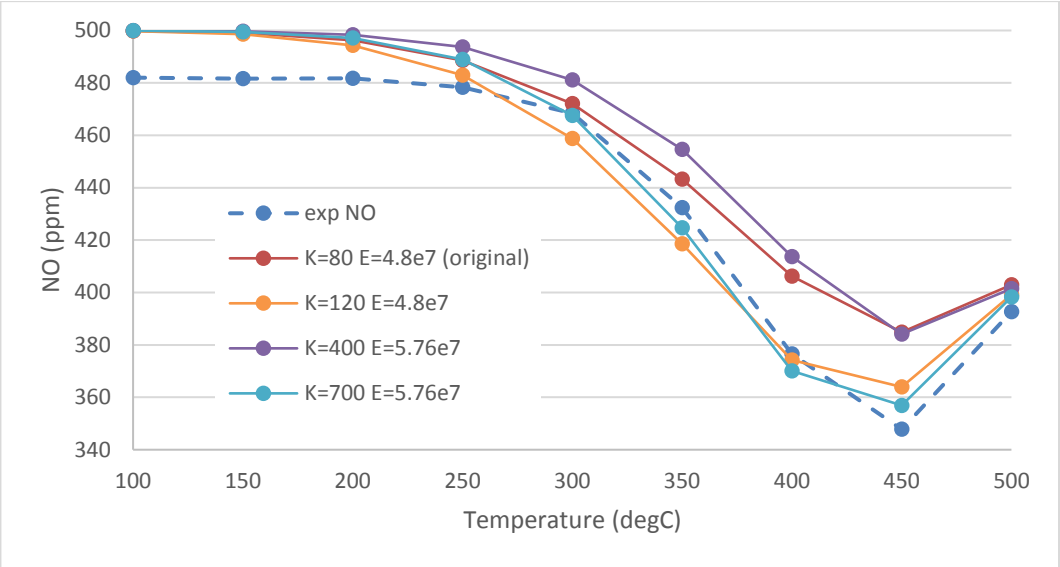

Figure 4-8: Outlet NO Level vs Temperature Variation for NO Oxidation

From Figure 4-8, NO level at the outlet, the original reaction rate is able to produce good result around 300°C. But the NO concentration is higher than experimental results at 350°C and above. In the low-temperature range, 100°C to 250°C, the average error between the two results is 3.4%; and in the temperature range 350°C to 500°C, the error is 2.5% for 350°C and 500°C; the most significant error is greater than 8% at 400°C and 450°C.

In order to achieve lower NO level at the outlet in a high-temperature range, the reaction rate needs to be increased a little. Increasing K values is a way to increase the reaction rate without change too much in the response sensitivity to temperature changes.

After increase pre-exponential factor to 120, the result at temperature250 and above is close to the experiment result. To be exact, the error from 100°C to 200°C is the same, but the error at 250°C drop to 0.97%. At 300°C and 350°C, the error is -2% to -3%. And the most significant error appears at 450°C, that is 4.65%. This set of reaction rates has a good result on all temperature range but 450°C.

Activation energy can be increased slightly to have higher NO concentration result at 450°C, which is closer to experimental value, it also lowers the result at the low-temperature range as the error in this range is around positive 3%. A set of reaction rate is found to be a much better fit than others, that pre-exponential factor is 700, and activation energy is 5.76E+7. The result of this set of reaction rate has an error less than 1.5% in the temperature range from 300°C to 500°C and the same error as other sets at 100°C to 250°C.

NO oxidation is a reversible reaction; both NO and NO_2 concentration need to be examined. NO_2 concentration at the outlet is plotted in Figure 4-9.

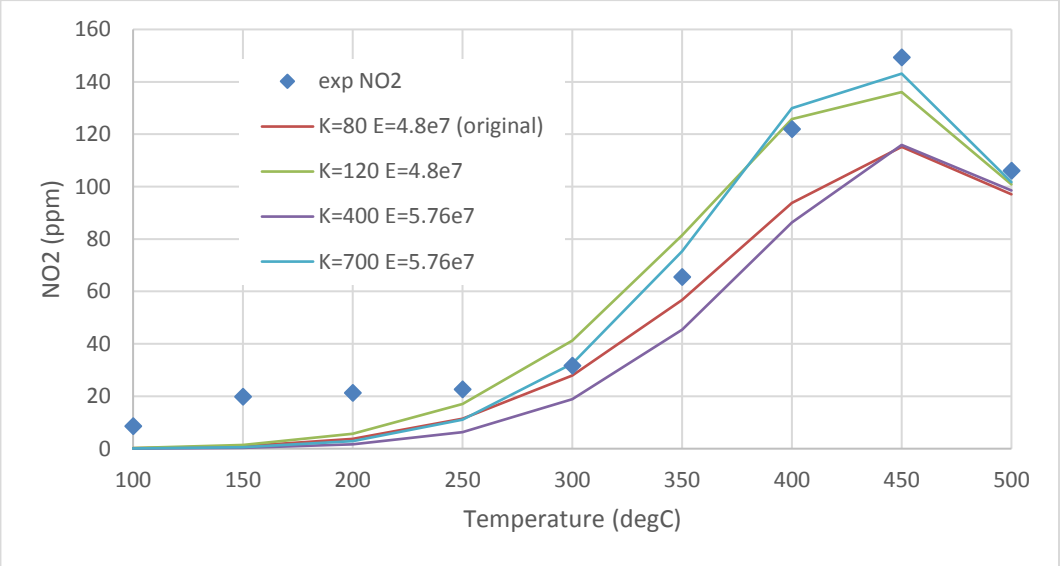

Figure 4-9: Outlet NO_2 Level vs Temperature Variation for NO Oxidation

The results' tendency is a similar situation to those on NO concentration. The best match is from the same set of reaction, and the error is within an acceptable level. This confirms that reaction rate with 700 for pre-exponential factor and 5.76e7 for activation energy, produces a satisfying result and can be used in later studies.

4.1.4 NO_x Conversion Reactions

Regard to NO_x conversion in SCR, there are 4 reactions, as listed below,

$$4NH_3(S)+4NO+O_2 \rightarrow 4N_2+6H_2O+S$$

$$2NH_3(S)+NO+NO_2 \rightarrow 2N_2+3H_2O+S$$

$$4NH_3(S)+3NO_2 \rightarrow 3.5N_2+6H_2O+S$$

$$NH_3(S)+ 2NO_2 \rightarrow N_2+ N_2O+ 3H_2O+S$$

These 4 reactions form a set of NO_x conversion reaction with 3 variables: NH_3, NO and NO_2. It cannot be calibrated and validated one by one like ammonia ad/desorption, oxidation or NO oxidation. Therefore, they are treated as one set; all reactions rates of the SCR reaction set were adjusted at the same time by the same percentage. Thus rate constants and activation energies are multiplied or divided by the same number to reach the best match. The downside of this method is the relation between those reactions is also change as multiplication and division. Thus, a smaller number is preferred to keep relations with SCR reactions as small as possible.

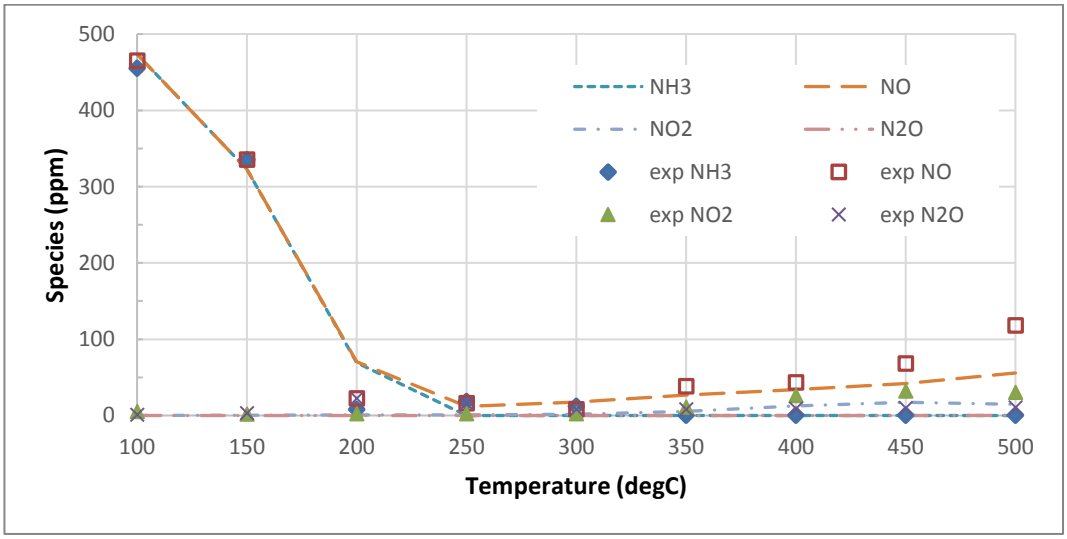

Figure 4-10: deNO_x Result and Comparison

Figure 4-10 only shows the best result of the set of SCR reaction rates. This figure shows all species concentration at the channel outlet from 100°C to 500°C, against the experimental result. This set of values provides a good match between simulation result and experiment data in spite of NO level at high temperature is slightly off. Since the purpose of this model is to study the general trend of SCR performance on new catalyst structure, the comparison is made between different structures using the same model. And this result reflects the correct tendency and level of all species from 100°C to 500°C, apart from NO level at 500°C. therefore, this only difference of NO level at 500°C can be compromised.

4.2 Geometric Downscale

The purpose of this geometric downscale is to increase the speed of the simulation process. But this downscale is only to cut the channel shorter for faster simulation. The only change in this reduced model is the length in the longitudinal direction, 30mm is reduced to 10mm while all other geometries remain the same. With this change, total mesh quantity is reduced to third. Thus computation expense is down to third. In order to exam this reduced model, the parameters of interested are monitored and compared.

The first one is the velocity profile in the channel.

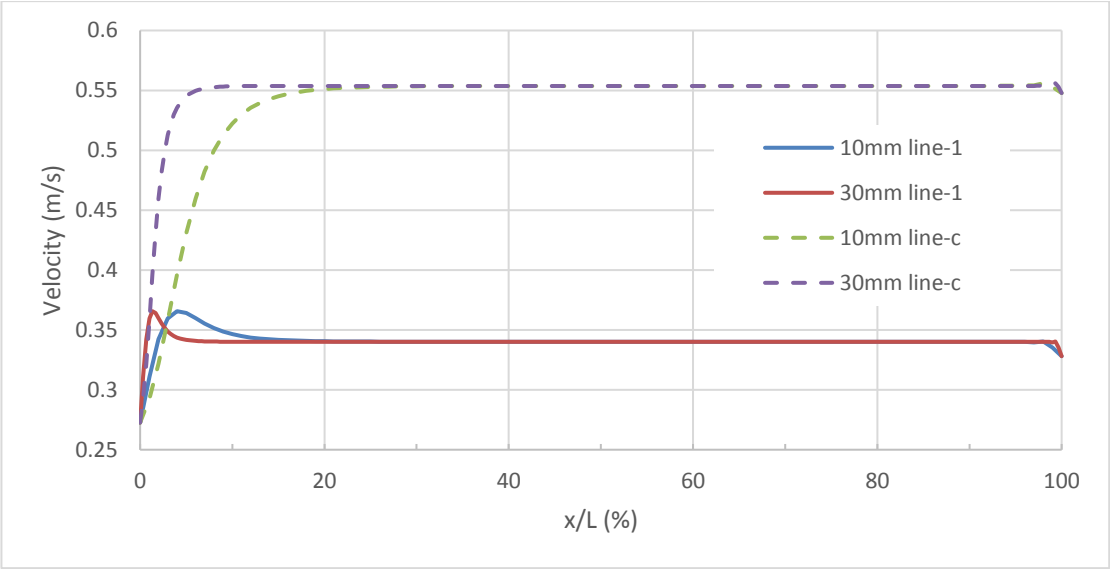

Figure 4-11: Longitudinal Velocity at line-1 and line-C, 10mm vs 30mm

Figure 4-11 compares the velocity value alone the channels, the monitor lines from the inlet to outlet in both cases, line-c is the centre line, and line-1 is at a random location. Since one case is 30mm and the other one is 10mm, X-axis is shown as x/L in percentage. The only difference between 10mm and 30mm case is the velocity in the inlet region, the first 20% of the total length. velocity value on the monitor lines from 20% to the end are identical.

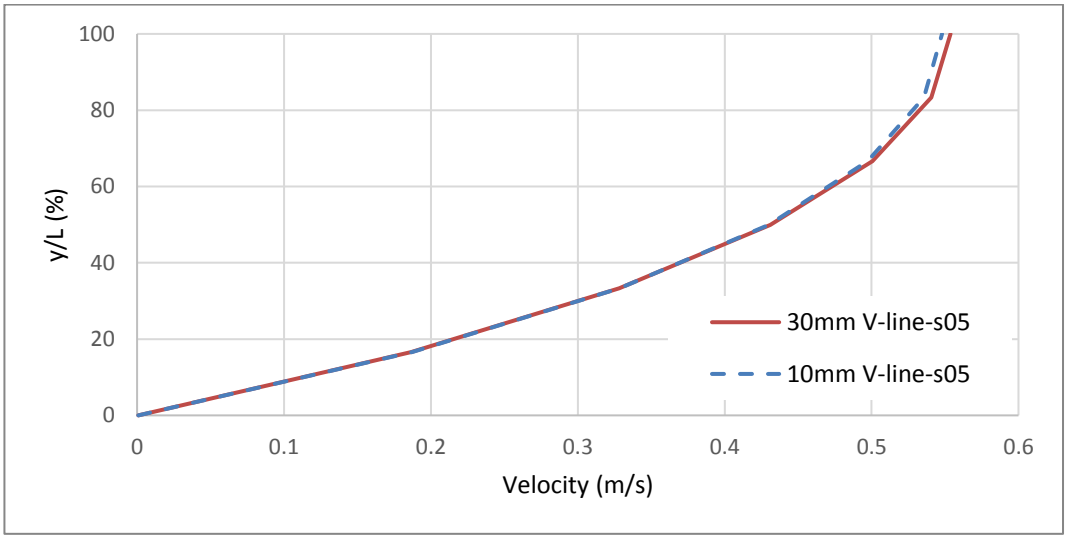

Figure 4-12: transverse velocity at V-Line-s05, 10mm vs 30mm

In the transverse direction, the velocity profile is plotted in Figure 4-12, V-line-s05 is a line perpendicular to the wall surface, located at 5mm from the inlet for 30mm case, and 1.667mm from the inlet for 10mm case. That is 16.67% of the total length from the inlet. Since there is no change in the channel's width or shape, velocity profiles on these two lines are the same as expected.

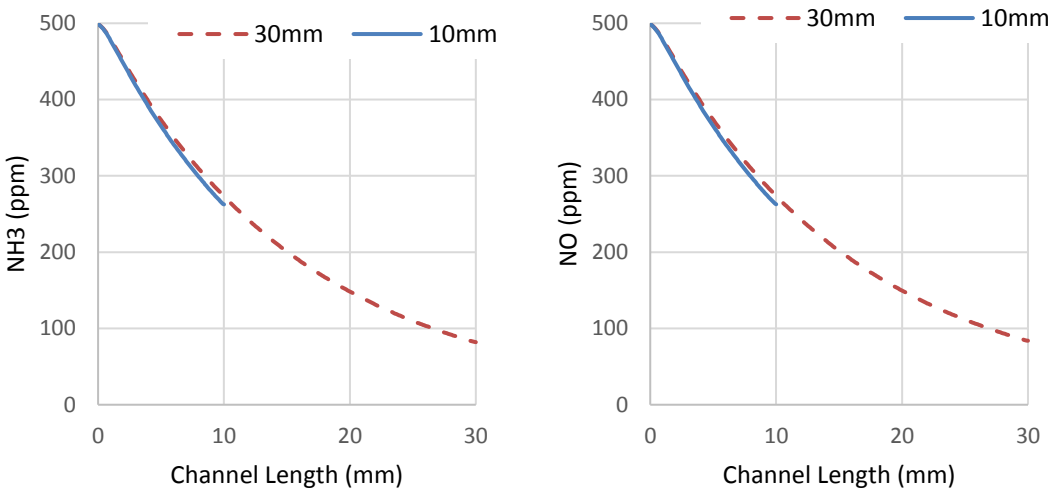

Figure 4-13: NH_3 and NO concentration at the centre line at 200°C

As 30mm channel is reduced to third, the catalytic site is also down to third. Thus, deNO and deNH3 performance are expected to be lower by 2/3 maximum, and the species concentration in the channel of 10mm case should have the same value as the first 10mm in the 30mm case. The comparison of NH_3 and NO concentration is shown in Figure 4-13. Both NH_3 and NO concentration in the 10mm case are similar to the first 10mm from 30mm case. These figures can be seen as proof that reduces the length of the catalyst model has only slightly affected the results, less than 3% in this case. But the computation time is less than half compared to the full-length case.

Figure 4-14 shows NH_3 and NO reduction rates between 10mm case and 30mm case. As mentioned earlier, the maximum performance drop is expected 2/3, and this happens at

100°C where 30mm catalyst has 5.29% deNH3 rate and 5.3% deNO rate and 10mm case is 1.821% and 1.825% respectively. This difference is getting smaller as temperature goes up to 300°C, after 300°C both cases perform the same. This is because at a low temperature all of the catalytic sites are taking part in the SCR process so that the total length of the channel makes the difference to outlet species concentration. However, the reactions are getting faster and faster as the temperature is further increased and almost all the NH_3 are consumed within 10mm from the inlet, the length of the catalyst makes no difference if there is not enough ammonia in the mixture.

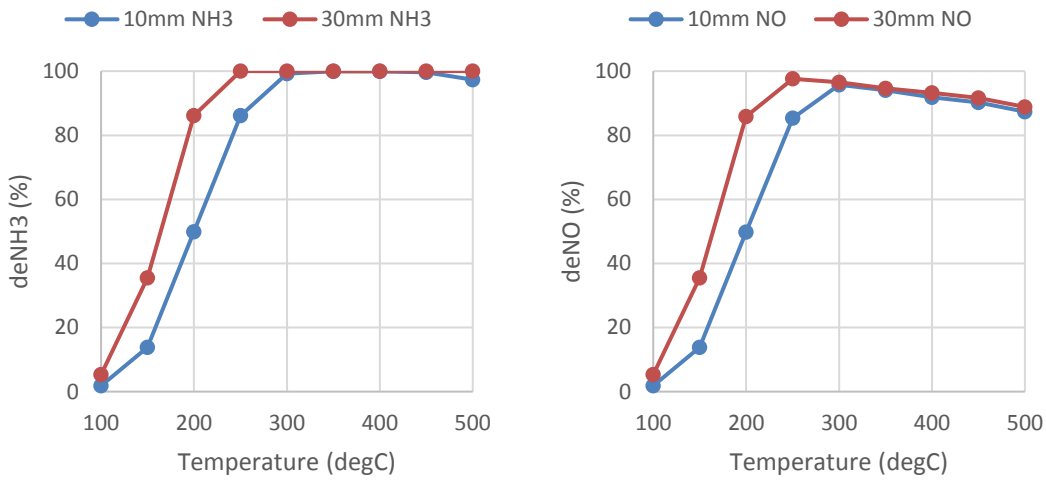

Figure 4-14: NH_3 and NO Conversion Rates Comparison

In order to prove the above view, ammonia concentration at the centre line of the channel under the temperature range from 100°C to 500°C is plotted in Figure 4-15. This figure clearly shows that almost all ammonia is consumed around 7mm from the inlet when the temperature above 300°C. Due to the lack of reductant, there are no more SCR reactions after 8mm.

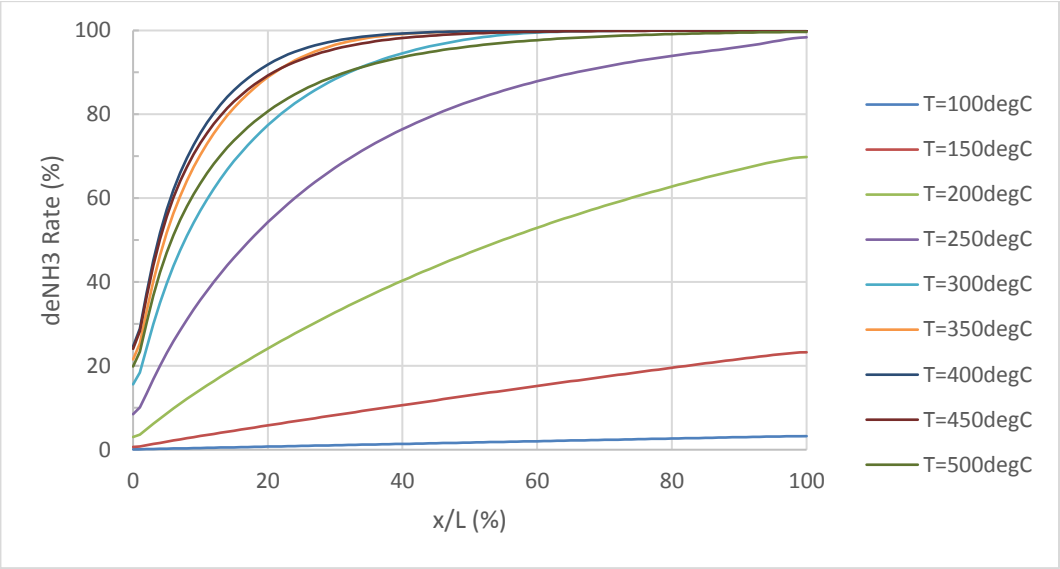

Figure 4-15: 10mm FT NH_3 Reduction Rate Against Channel Length

As seen in Figure 4-16, deNO rate for temperature above 300°C shows no change from 70%. For temperature 250°C, there are about 7% of ammonia left in mixture gas at location 8mm. Therefore there is further deNO reaction happens in the channel. Thus, in Figure 4-16, temperature 250°C shows better deNO rate at the end of the channel.

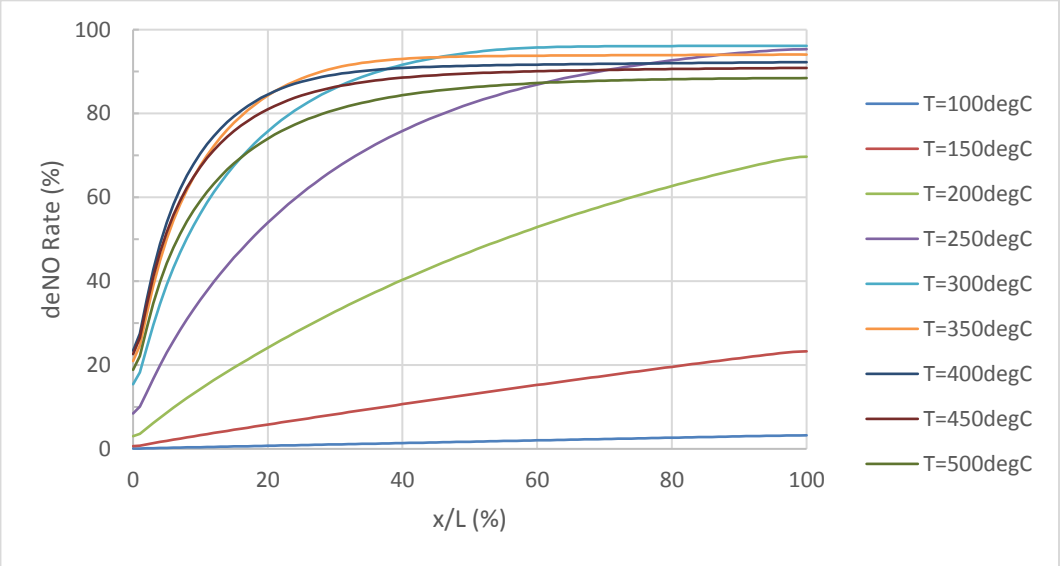

Figure 4-16: 10mm FT NO Reduction Rate Against Channel Length

As a result, reducing channel length from 30mm to 10mm has no major difference to deNO performance from 300°C to 500°C; the performance under 300°C is predictable and reasonable. Despite 3% error is exist, as in Figure 4-13, the computation time is significantly reduced. This is an excellent saving of time in the later stage when porous media is added into the model.

4.3 Summary

All reaction rates are calibrated and validated against Olsson's experimental results[70]. In overall, most of the results match experimental data very well. There are only 2 results are less satisfying: outlet NO level during the deNO_x process under temperature 450°C and 500°C unable to provide a satisfying result, but it shows a correct trend that NO level is increasing from 400°C and above. Thus, this can be tolerant due to the purpose of these reaction rates are used simulation models, and the comparison is between the simulation models.

	Pre-Exponential Factor	E_a (J/kgmol)
NH_3 Adsorption	0.93	0
NH_3 Desorption	1e8	1.72e8
NH_3 Oxidation	1485	9.24e7
standard SCR NO+O2	14375	5.943e7
Fast SCR NO+NO2+O2	1.1875e9	5.957e7
Slow SCR NO_2	687.5	5.061e7
NO Oxidation	700	5.76e7
N2O formation	2.25	3.031e7
Site Density	0.0545 (mol/m2)	

Table 7: Calibrated Reaction Rates

All validated rate constants and activation energies are listed in the above table, and these values are only valid for this CFD model based on all the assumptions made in earlier sections. However, to be noted that all these values are only valid in this model with all the assumptions made in the earlier sections.

Also, the comparison results of the downscale model and full-scale model show positive signs as there is no significant performance difference, or physical changes to the flow, as in Figure 4-13. And the performance drop at the outlet fits the expectation. Therefore, 10mm channel model can be used for further study.

5. Results: WF SCR and WF SCR with Fins

In this chapter, there are two sections of simulation results, one is for WF model, and the other one is for WF-Fin model, they are run under the same boundary conditions but discussed separately in this chapter. Each of them, the result of the overall conversion rate of the species along the length of the channel, velocity profile in channel longitude wise, the mass flow rate on each of the sections on channel's wall and reaction rates are showed and discussed.

5.1 WF SCR

For the following simulation results, boundary conditions are set to inlet velocity 0.3m/s to 1.0m/s; species composition is NH_3 500ppm, NO 500ppm, H_2O 8% and balanced by inert gas Argon, the temperature is varied between 100 and 500°C at 50°C increment. For the cases with velocity variation, the temperature is set to 300°C, and for the cases with temperature variation, inlet velocity is set to 0.3m/s.

5.1.1 NH_3, NO Conversion Rates

As the goal of such a catalyst is to add the functionality of NO_x conversion to diesel particulate filter, the first attention is the result of the species' reduction rate on the catalyst surface. The overall reduction rate only considers the species at inlet and outlet of the channel, it is calculated as

$$\frac{(C_{in} - C_{out})}{C_{in}} * 100$$

where is C_{in} is species level at the inlet and C_{out} is species level at the outlet.

The following figures, Figure 5-1 and Figure 5-2, are the overall NH_3 and NO reduction rate respectively between 100°C and 500°C with inlet velocity variation from 0.3m/s to 1m/s. In these results, generally inlet velocity change has a great effect on conversion rates between 100°C and 250°C. As the velocity increase, the conversion rates drop. This dropping rate is higher at low velocity and getting smaller at high velocity; It is merely because the increment of inlet velocity was set disproportionately.

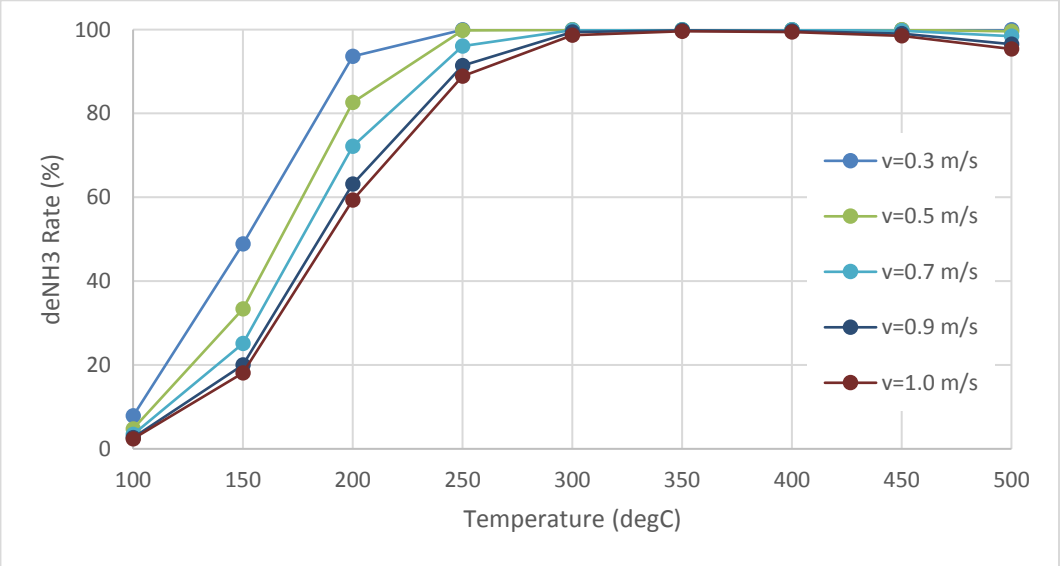

Figure 5-1: WF Overall NH_3 reduction Rate vs Temperature

Conversion rates of NH_3 and NO are slow in both cases at low temperature, and this is within the expectation as SCR reactions become more active from around 200°C at the least [77, 78].

Conversion rates falling while inlet velocity is increasing is due to reactant has shorter resident time on the catalyst surface. Since SCR reactions are generally low below 200°C and short resident time means the catalyst (locally) is unable to process that much species while they are passing through, so unreacted species escape from catalyst and flow to

downstream. Due to this reason, the velocity increase at the low-temperature range has undoubtedly impact conversion rates.

At a temperature above 300°C, inlet velocity increased from 0.3m/s to 1m/s have minimal effect on overall NH_3 and NO conversion. As SCR reaction rates and diffusion rate are higher in the high-temperature range, it is difficult to decide if it is a diffusion-controlled reaction or reaction controlled based on these results. But one thing can be sure, and there is not enough ammonia left in the gas for further NO conversion. A possibility is another reaction rate, ammonia oxidation for an instant, is higher than SCR reaction rates; a small part of ammonia is consumed by ammonia oxidation. Therefore, the NO conversion rate cannot maintain the same rate and falls between 300°C and 500°C.

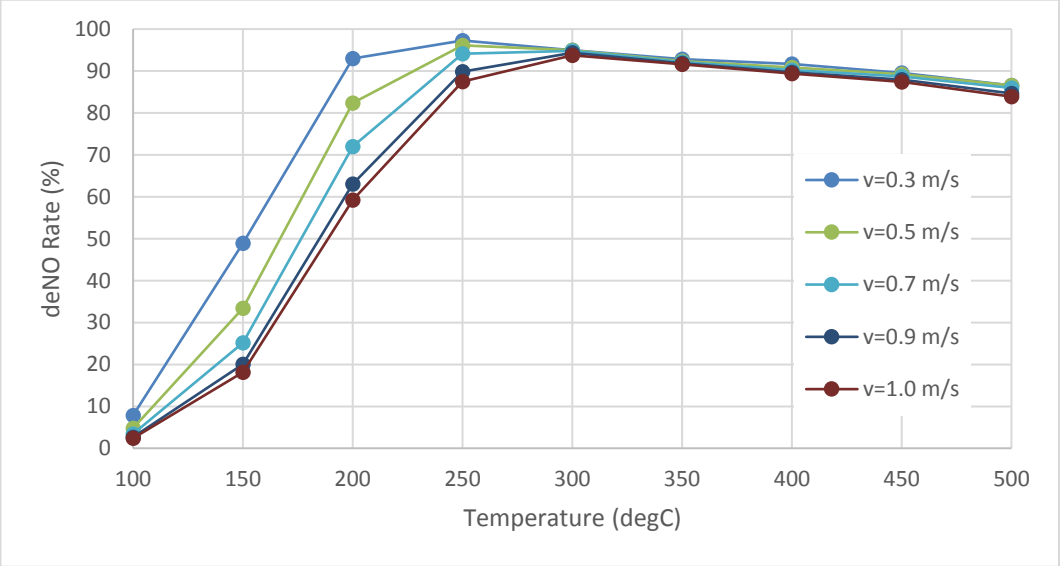

Figure 5-2: WF Overall NO Reduction Rate vs Temperature

In Figure 5-3, the ammonia conversion rate is plotted against the distance along the length of the catalyst channel. The data is collected from the central line in the outlet channel, overall reduction rate for the temperature at 200°C is acceptable, as it takes advantage of a complete section of catalyst, nearly 93% reduction is reached at the outlet of the channel. Whereas temperature 250°C and above, all of them reaches 98%, 99% by using about 40%

of the catalyst length. Temperature between 100°C and 150°C is a different story; the ammonia reduction rate starts at 1% and 7.4% at the inlet respectively. Because of their low reaction rate, the length of the catalyst provides very limit boost to overall conversion rate, at the end of the catalyst channel, deNH3 rate only reach 7.61% at 100°C and 47.7% at 150°C.

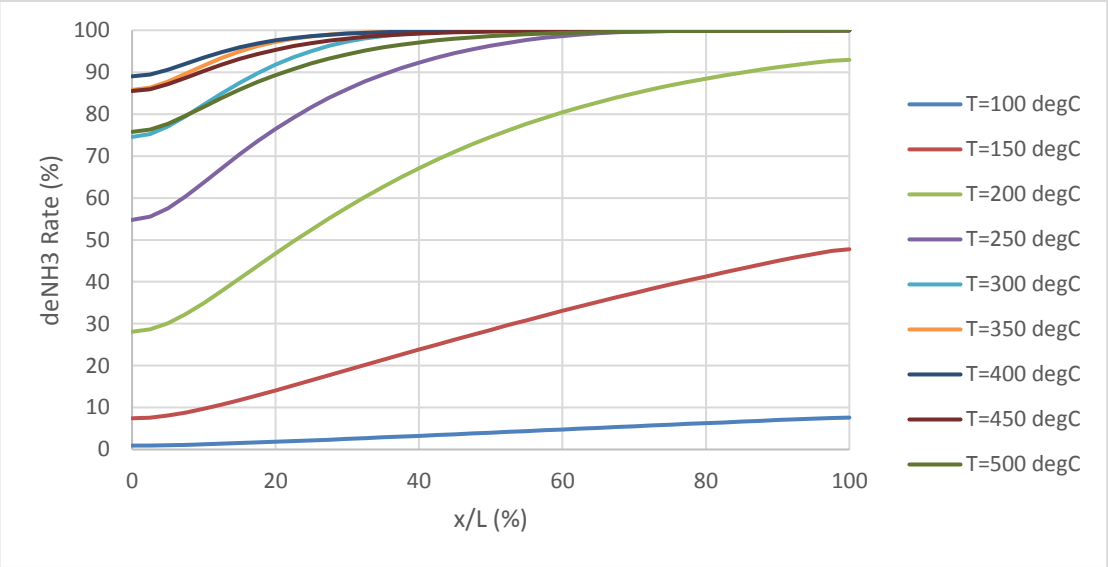

Figure 5-3: deNH3 Rate in The Outlet Channel (Longitudinal Direction)

The same figure is also plotted for the NO reduction rate as shown in Figure 5-4. The maximum NO reduction rate is about 48% at the outlet for the temperature lower than 150°C. When the temperature is above 200°C, NO reduction rate reaches 86% and 97% at the outlet, and it can be higher if there is more ammonia. In fact, NO reduction rate reaches around 90% only takes 4mm or 5mm of the catalyst, and there is no further reduction of NO beyond 6mm. That is because there is no ammonia left in the channel after 6mm from the inlet. The only case is at 200°C, and there is still ammonia gas left in the mixture as ammonia oxidation rate at this temperature still low and not consuming all the ammonia, so NO reduction rate reaches 92% at the end of outlet channel at 200°C.

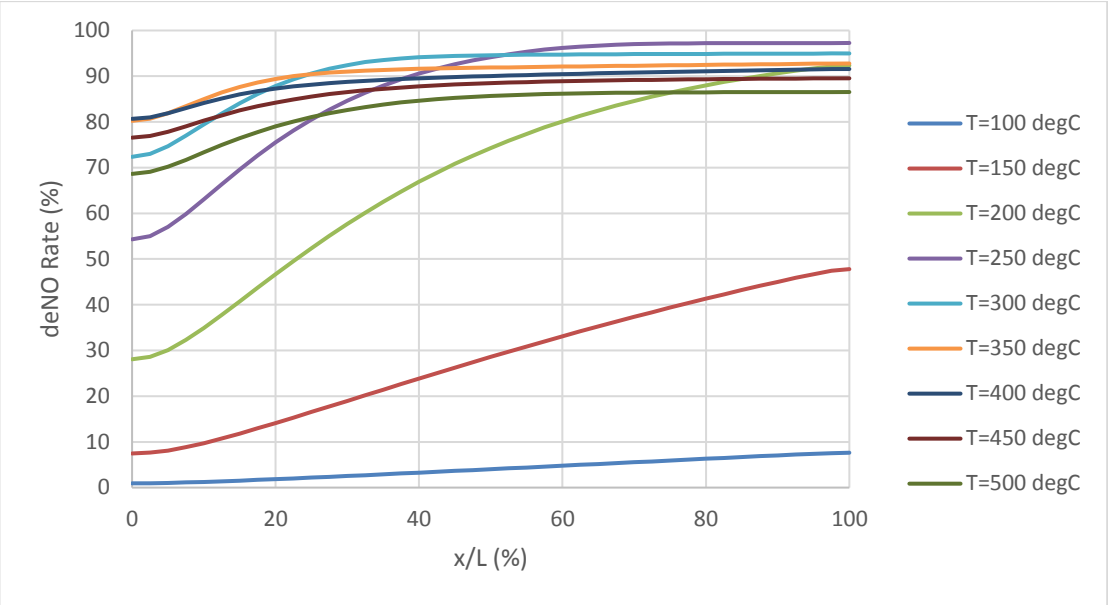

Figure 5-4: deNO Rate in The Outlet Channel (Longitudinal Direction)

Figure 5-5 and Figure 5-6 are plotted to show the conversion rate of NH_3 and NO along the channel length as in some cases reach the same conversion rate, but the maximum capacity is unable to compare by overall conversion rate alone. Two sets of data are collected from the centre line of the outlet channel and discussed.

Figure 5-5 shows the ammonia conversion rate against channel length in percentage. For all the cases, velocity 0.3m/s to 1.0m/s, they reach 96% and beyond at catalyst outlet, but 3 or 4 out of 8 velocities use the whole catalyst length to reach that conversion level. On the other hand, the case with velocity 0.3m/s reaches 99.2% by using half of the catalyst. As the velocity increase, the usage of the rear section of the catalyst is getting higher. The majority of ammonia conversion happened in the front part of the catalyst and based on this case the rear part only deals with the maximum of 15% of ammonia.

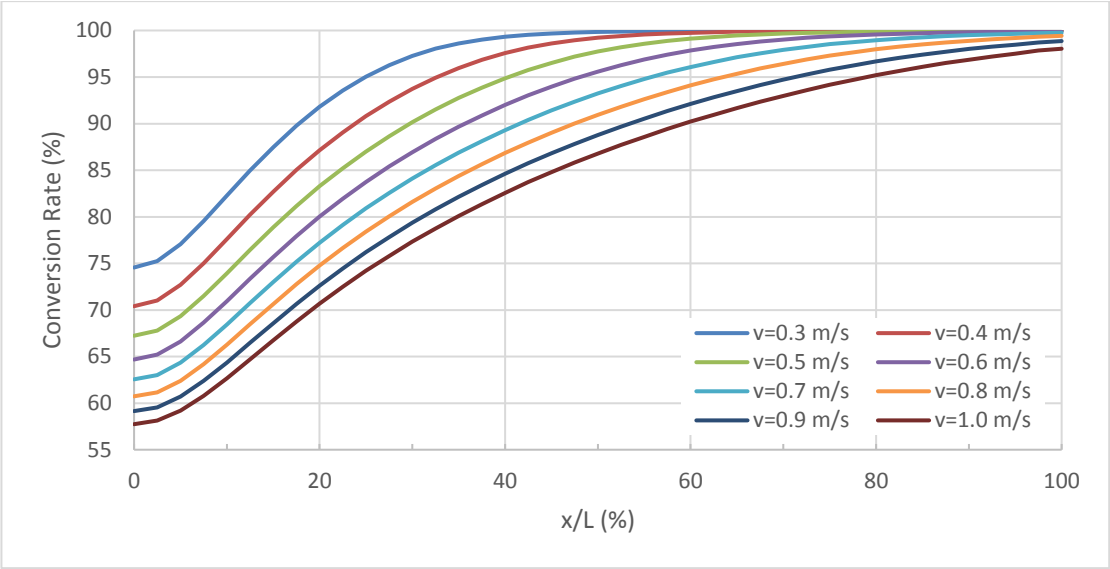

Figure 5-5: NH_3 Conversion Rate under Various Inlet Velocity (300°C)

And there is a similar situation in NO conversion rate, but the rate is limited to 95% due to the lack of ammonia. For all the cases in NO conversion, conversion rates stop to climb at ammonia species is wholly consumed.

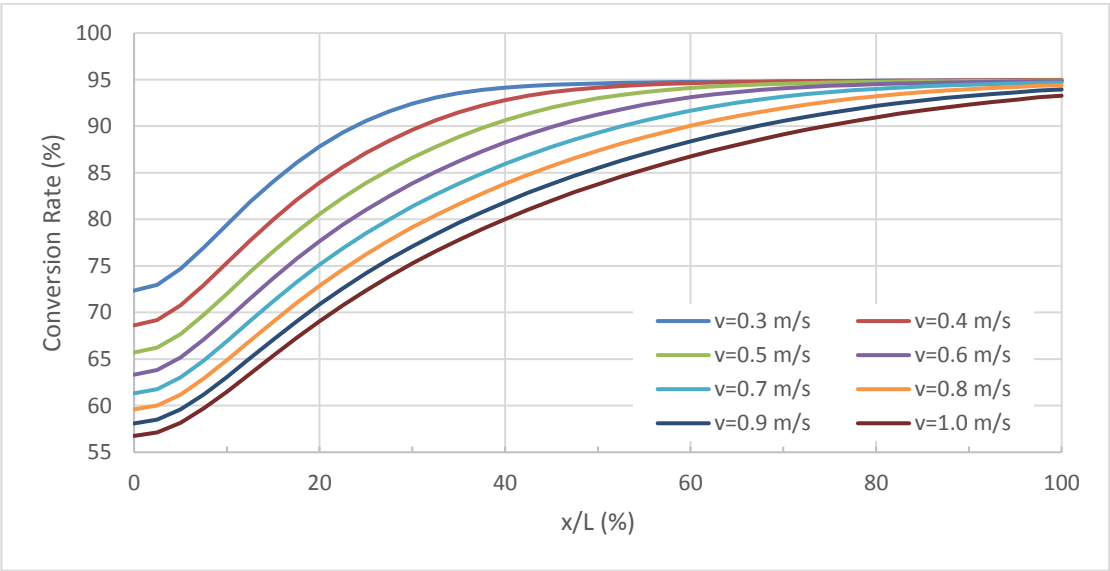

Figure 5-6: NO Conversion Rate under Various Inlet Velocity (300°C)

In general, higher velocity cause flow travels faster and reduces the conversion rate, and the rear part (80% to 100%) of the catalyst is used only when velocity is higher than

0.7m/s. if an extra section of the catalyst can be used at high-velocity range, it can maintain very high conversion.

5.1.2 NH_3(S) in Porous Wall

Ammonia storage in the catalyst material is an essential factor in SCR performance. For a wall flow type catalyst, the catalyst material is coated into the catalyst wall, which is porous media. The level of absorbed ammonia on-site surface in the porous wall is extracted to plot figures and discussed.

Figure 5-7 shows the level of NH_3(S) on the surface wall in the inlet channel. Lin-por-1-1 represent the midline on the wall surface in the inlet channel. While inlet velocity is fixed at 0.3m/s, the temperature is changing from 100°C to 500°C.

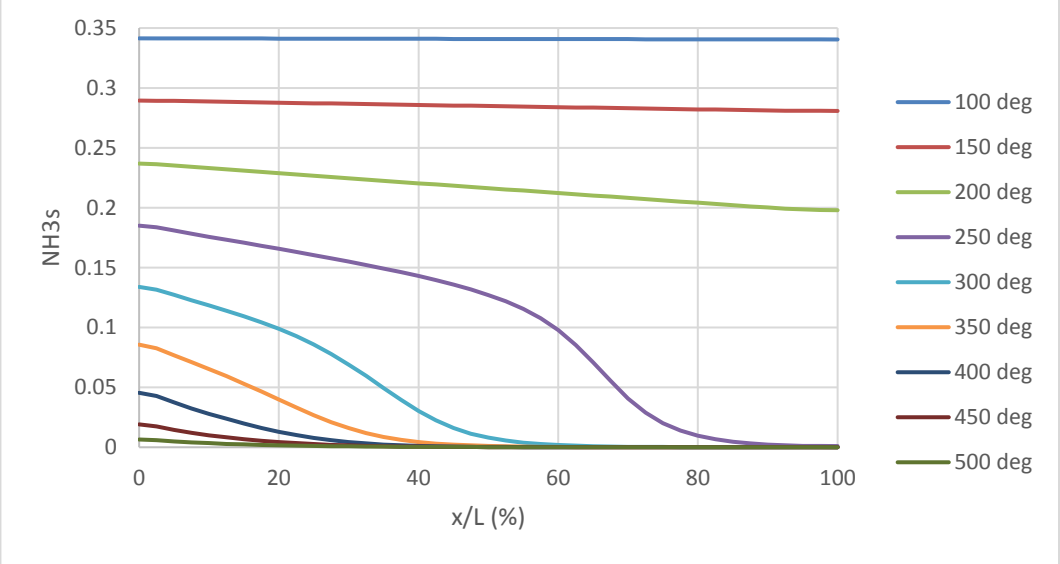

Figure 5-7: NH_3(S) Level at The Central Line of Porous Wall Surface (v=0.3m/s)

As well known that ammonia storage is decreasing as temperature goes up, this can be seen in Figure 5-7, from the inlet (0%) to about 5% of channel length NH_3(S) level decrease proportionally at every 50°C change. NH_3(S) level at the rear part of the catalyst

channel is a different story; it decreases dramatically at the end of the catalyst. During temperature rise process absorbed ammonia in the rear part of the porous wall is disappeared before the front part of it.

The data of NH_3(S), in Figure 5-8, is collected from the centre line of the porous wall at 300°C with various inlet velocity, X-axis is the length of catalyst channel in percentage. 18% is its maximum level at 300°C, despite there is a slight change with different velocity. The level of NH_3(S) decreases along the channel length because of the consumption of SCR reactions.

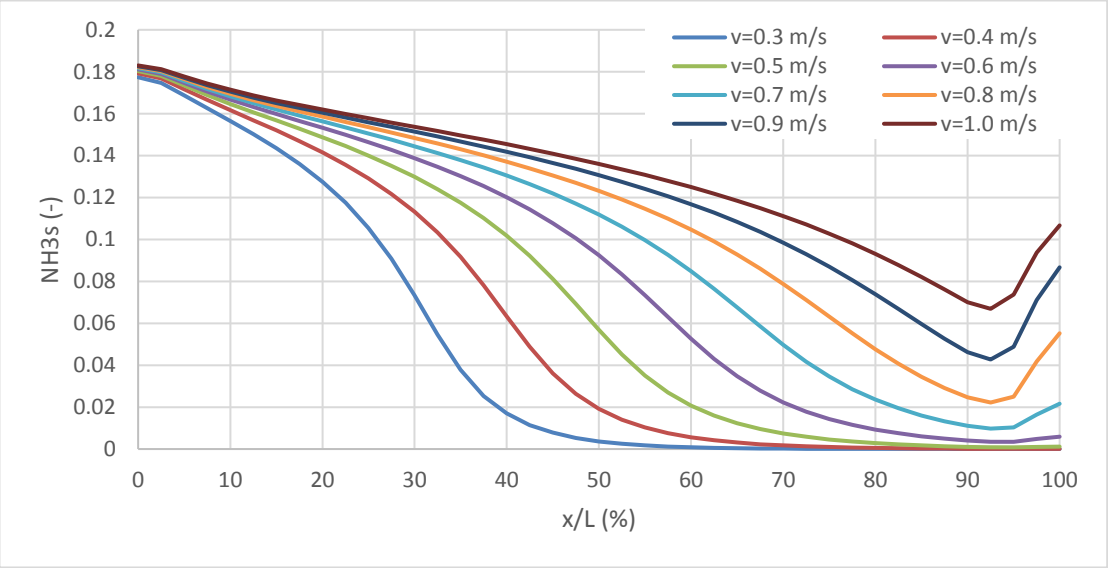

Figure 5-8: NH_3(S) Level in The Porous Wall vs Inlet Velocity (300°C)

In low velocity range, 0.3m/s to 0.5m/s, the species are consumed in the front section of catalyst by the reactions before they can travel to downstream, the fall of NH_3 level in this velocity range is between 20% - 40% for 0.3m/s, 25% - 50% for 0.4m/s and 35% - 55% for 0.5m/s. As the velocity increase, the gradient of this fall is less steep. There is the lowest point and followed by a sudden rise at around 93% in catalyst length in high-velocity range might be caused by extremely high local velocity. In overall, velocity change has a significant effect on NH_3(S) level, especially in the rear part of the catalyst.

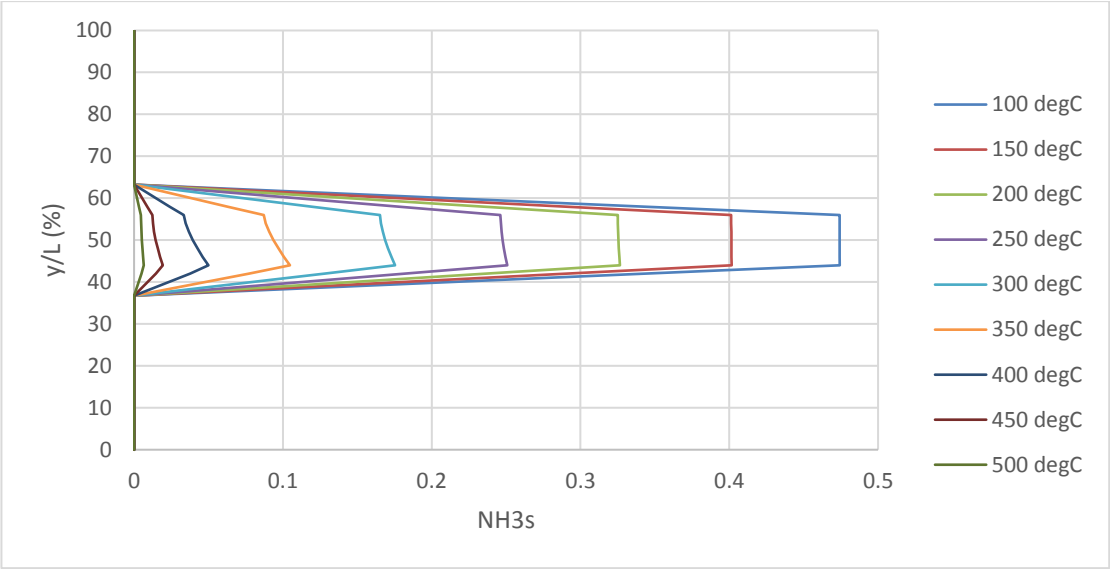

Figure 5-9: NH_3(S) Level Inside the Porous Wall (0.5mm from inlet)

Figure 5-9 is the result of NH_3(S) level inside the porous wall, and the data is extracted from a straight line perpendicular to the wall surface at location 0.5mm from the inlet. Y-axis is the distance in percentage from the centre of inlet channel to the centre of the outlet channel, so 0-40% and 60%-100% is inlet channel and outlet channel respectively, the porous wall is between 40% and 60%. The result indicates NH_3(S) level decreases with temperature increase. NH_3(S) level is similar on both sides of the wall at a temperature between 100 and 200°C. The difference begins to climb after 200°C, NH_3(S) level is higher on the side of the inlet channel. This is because when absorbed ammonia in the site storage is consumed during SCR reactions, the vacant site is quickly occupied by upstream ammonia from the inlet mixture and this process keeps repeating. Most of the ammonia in the mixture gas is absorbed and consumed before they can reach to the other side of the wall.

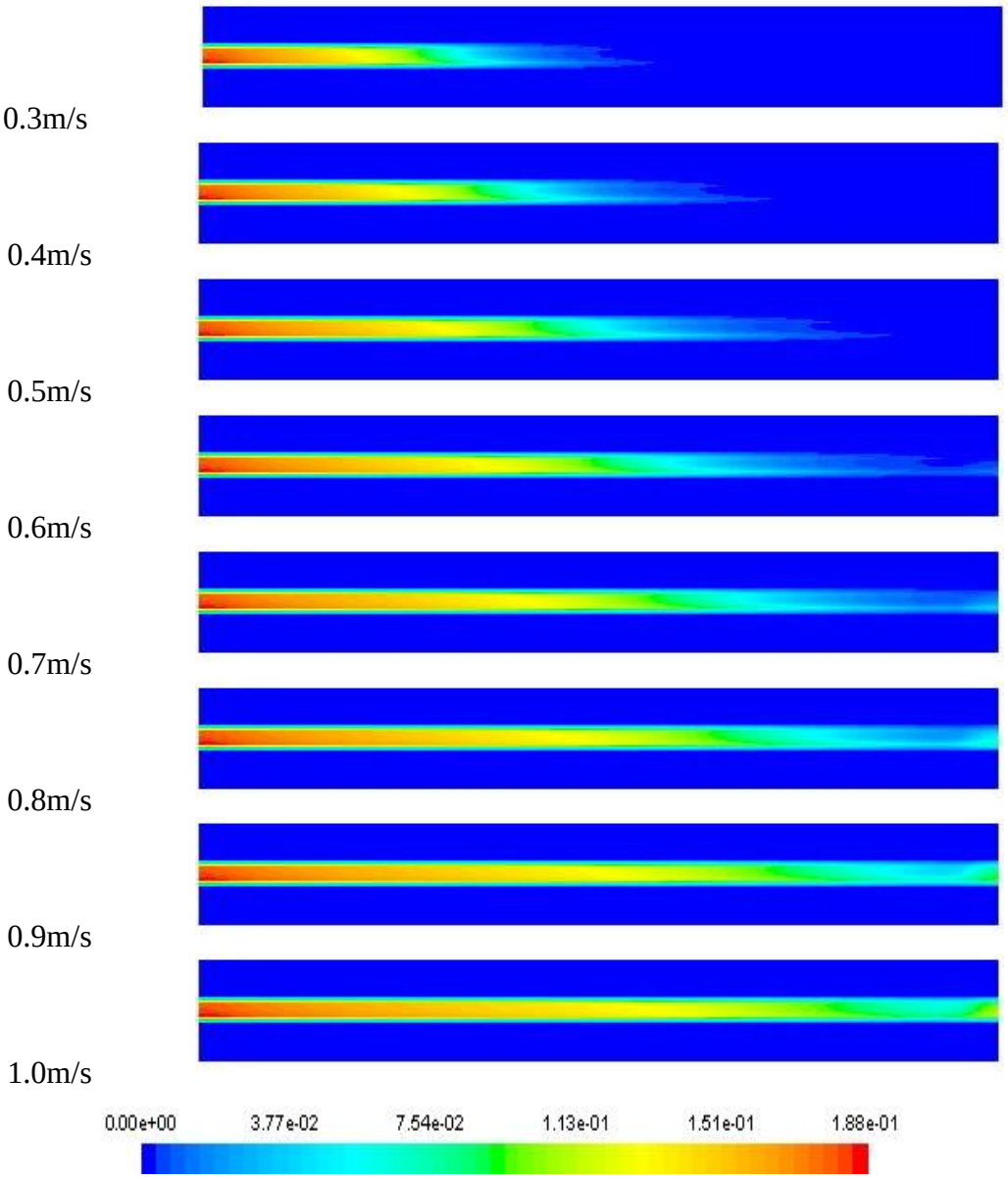

Figure 5-10: NH_3(S) inside the porous wall under various velocity (T=300°C)

Above contours, Figure 5-10, is showing the NH_3 level in the porous wall at 300°C under various inlet velocity effect. These contours are on the symmetric side panel, the top blue part is the outlet channel, and bot blue part is the inlet channel. The middle part is a porous wall. Mixture gas enters the channel from the left-hand side of the inlet channel at 0.3m/s and exit from the right-hand side of the top channel. The highest NH_3(S) at the beginning part of the wall and ammonia level decrease along the length of the catalyst. The maximum NH_3(S) level is 18.8% for all the cases as the temperature is the same; site storage is only affected by temperature and catalyst material.

In low-velocity range, the rear part of NH_3(S) in the porous wall is fading region and the level of NH_3(S) on the surfaces of is higher than that in the porous wall. In high-velocity range, there a region has the lowest NH_3(S) level. Since the temperature is the same and this region has the highest velocity, it can be guessed this region has higher NH_3 or NO consumption rate per unit times.

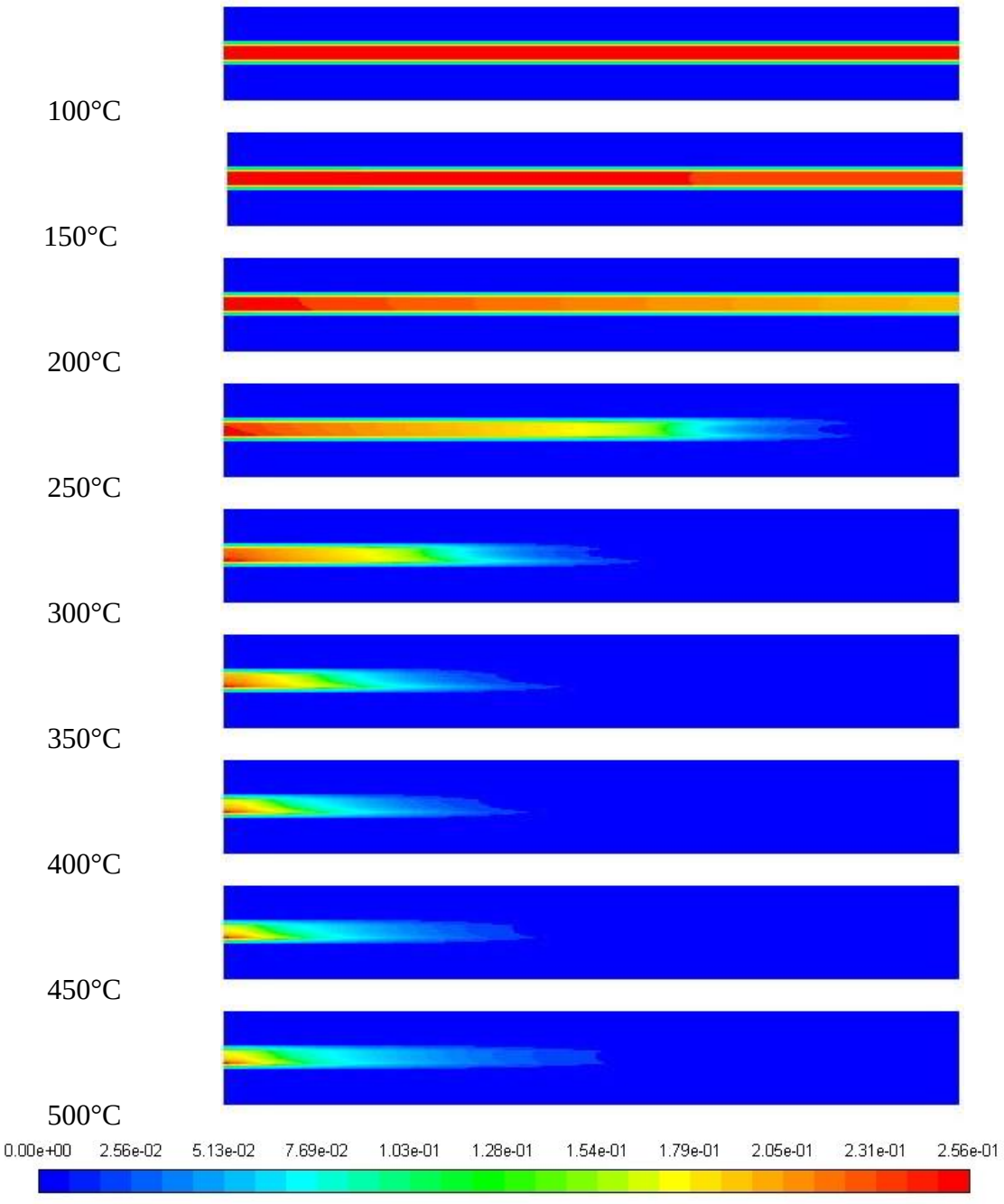

Figure 5-11: NH_3(S) inside the porous wall at 100°C to 500°C (v=0.3m/s)

While keeping inlet velocity as 0.3m/s, the temperature is increased from 100°C to 500°C, the contours of NH_3(S) level are extracted from the symmetry panel for the change under temperature effect.

In Figure 5-11, 250°C is clearly a threshold, the profile of NH_3(S) level in X direction changes greatly beyond this temperature. NH_3(S) level drops to below 5% in the rear part of the porous wall at around 70% of total catalyst length. At the end of the catalyst (between 90% and 100%) where has no absorbed ammonia left in that area. This is in a longitudinal direction. While in the high-temperature range, transverse direction, higher NH_3(S) level is shown on the surface of inlet channel side at the front part of the catalyst, and this difference becomes smaller in the middle of the catalyst, this is different from that in Figure 5-10 at 300°C. That phenomenon only appears in the range of 250°C and 300°C based on these results.

These contours of NH_3 level in the porous wall also explain the reason for majority NH_3, and SCR conversions happen in the front part of the channel. High velocity causes a lower reaction rate, but it can be compensated by the longer catalyst and low velocity tend to have a better conversion in the shorter catalyst, there is a compromise to be made.

5.1.3 Velocity and Mass Flow Rate

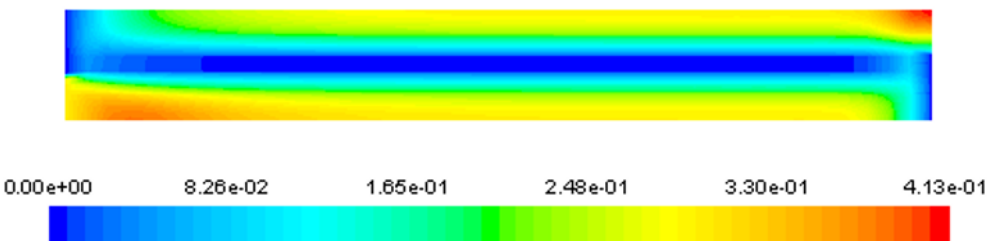

Figure 5-12: Velocity contours of the symmetric side panel at 0.3m/s

Figure 5-12 is the velocity contours of wall-flow catalyst on the symmetric side panel; higher velocity region appears in the porous wall at both ends of the channel: inlet and outlet regions. Together with the following figure, Figure 5-13, this high-velocity region covers 20% of the total length from the inlet and the last 10% at the outlet.

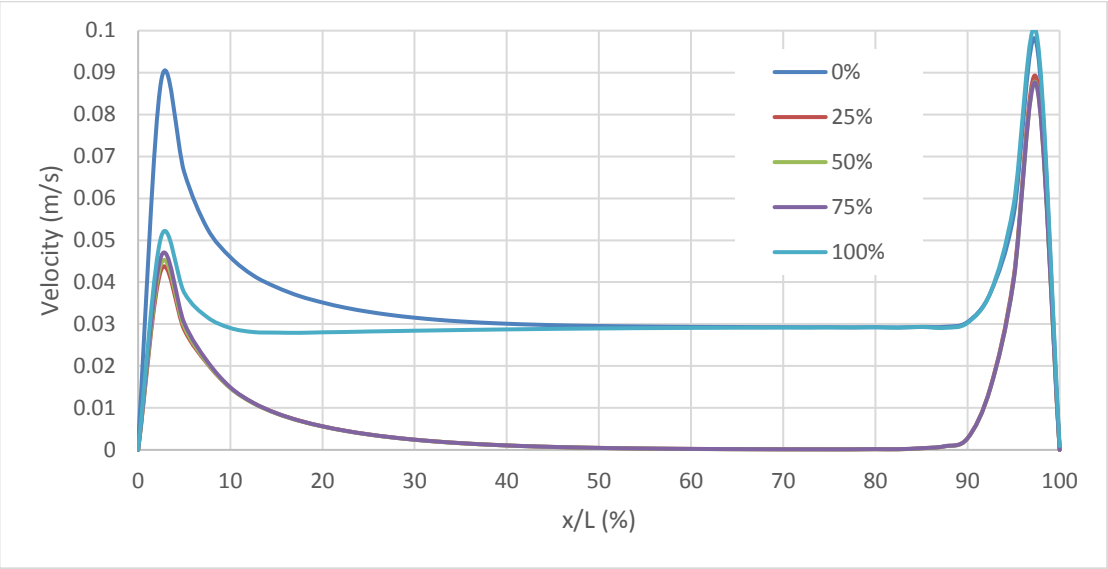

Figure 5-13: Velocity in the longitudinal direction inside the porous wall (inlet 0.3m/s)

The name of each series represents the distance (in percentage) from surface wall to the location of that data line, 0% means the data is collected from the surface of porous wall in inlet channel side, and 100% is in the outlet channel side, 25%, 50% and 75% are inside the porous wall, 25% 50% and 75% of total wall thickness respectively. In comparison, this case has inlet velocity 0.3m/s and the velocity adjacent to the wall surface is 0.03m/s when fully developed (can be seen in Figure 5-13), the velocity inside the front part of the porous wall is almost half of that speed at the same location on the surface.

In the middle part of the catalyst, between 2mm and 9mm, should have better SCR performance due to low velocity in the region. Lower velocity allows reactants to have more resistance time on the catalyst surface. Therefore, more species can be reacted

completely. Resistance time is critical to the diffusion rate, while temperature stays unchanged, conversion rate certainly benefitted from longer resistance time.

In the reaction-controlled situation, the diffusion rate is higher than the reaction rate, so there are always available species waiting to be reacted. Diffusion rate has no effect on the overall conversion rate of species under such condition. Higher velocity brings more reactants the catalyst surface for SCR reactions, but shorter resistance time. This has not a problem if it is the reaction-controlled situation. Therefore, velocity change only affects conversion rates when the reaction is diffusion-controlled.

As in Figure 5-13, comparing the high-velocity region to the low-velocity region, the ratio is roughly about 3 to 7, 30% of the channel has high velocity, and the rest of them has uniform low velocity. In other words, fewer species pass through the porous wall in the low-velocity region (middle part of the catalyst) and more species pass through the wall from the high-velocity region (both inlet and outlet end). Providing NH_3(S) level is the same across the porous wall, more species are consumed in the high-velocity region if it is in reaction-controlled case, but it is an opposite situation in the diffusion-controlled case due to short resistance time.

In high-temperature range, the low-velocity region is a drawback, because the capability of conversion rate is high (in both diffusion and reaction rate), but there are not enough species for the reaction. This is one of the reasons that WF type catalysts perform better NO_x conversion rate than FT catalyst, even at the entrance of the catalyst.

Below figures measure mass flow rate on wall surfaces in inlet channel, Figure 5-14 shows the value of mass flow rate pass through each of the sections on the surfaces, and Figure 5-15 is plotted by comparing local mass flow rate to total mass flow at the inlet. The wall surface is divided equally into 10 sections, and each section is 1mm in length

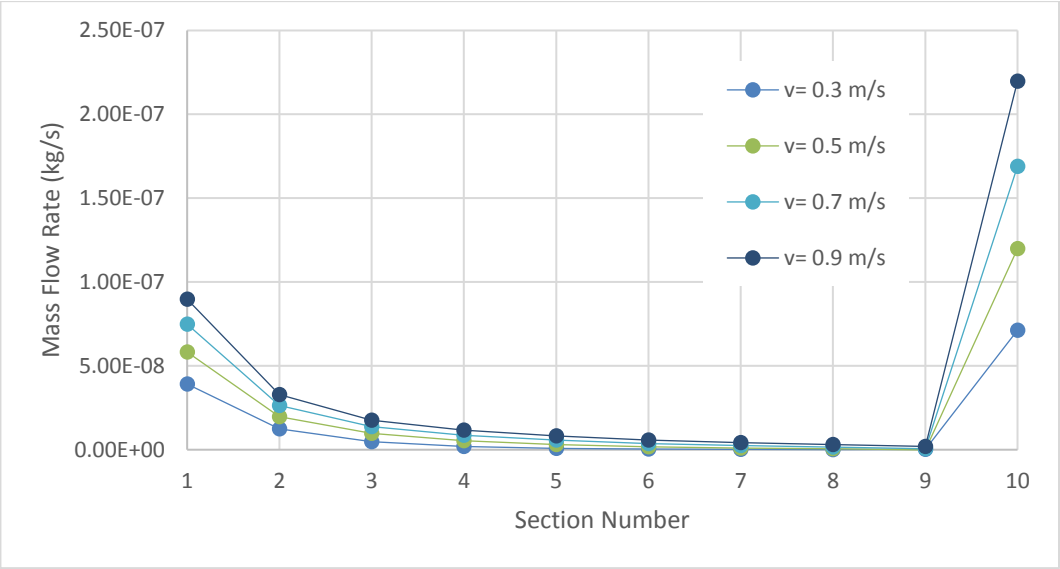

Figure 5-14: Mass Flow Rate on The Wall Surface (The Inlet Channel)

In Figure 5-14, section 1 to 3 is adjacent to flow entrance region in inlet channel, mass flow rate starts at 5E-8 kg/s for 0.3m/s in the first section and gradually decrease along the length of the channel and reach a more stable region in downstream where the flow is fully developed. The highest mass flow rate is in the last section, it 2.5 times the first section at the inlet.

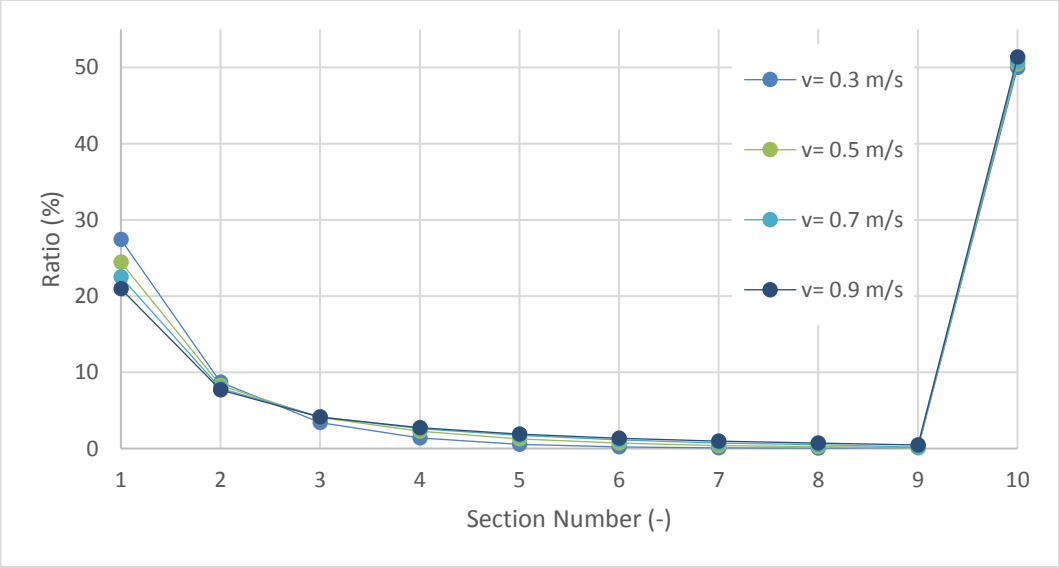

Figure 5-15: Mass Flow Rate Through Wall Surface (The Inlet Channel)

Figure 5-15 shows the ratio of how much of the mixture gas flows through the porous wall at each section. This ratio is in percentage as

$$Percentage\ (\%) = \frac{sectional\ mass\ flow\ rate}{total\ mass\ flow\ rate}$$

Comparing to total inlet mass flow rate, the first section account for 20% to 28% of the total mass flow rate and it drops to 7.6% in section 2 and half of the flow pass through porous in the last section. The over profile is similar at all velocity condition as the only difference is high velocity has a lower percentage of mass flow rate in the first section and higher percentage in section 4, 5, 6 and 7 when compared to low inlet velocity case. There is not much difference in section 2, 3 and the last section.

5.1.4 Species Distribution

Base on the reaction rate model, the amount of species in the local area is one of the factors that affect the reaction rate. In this section, 4 species compositions along the length of the channel are plotted, the result is from the centre line of inlet and outlet channel at inlet velocity 0.3m/s.

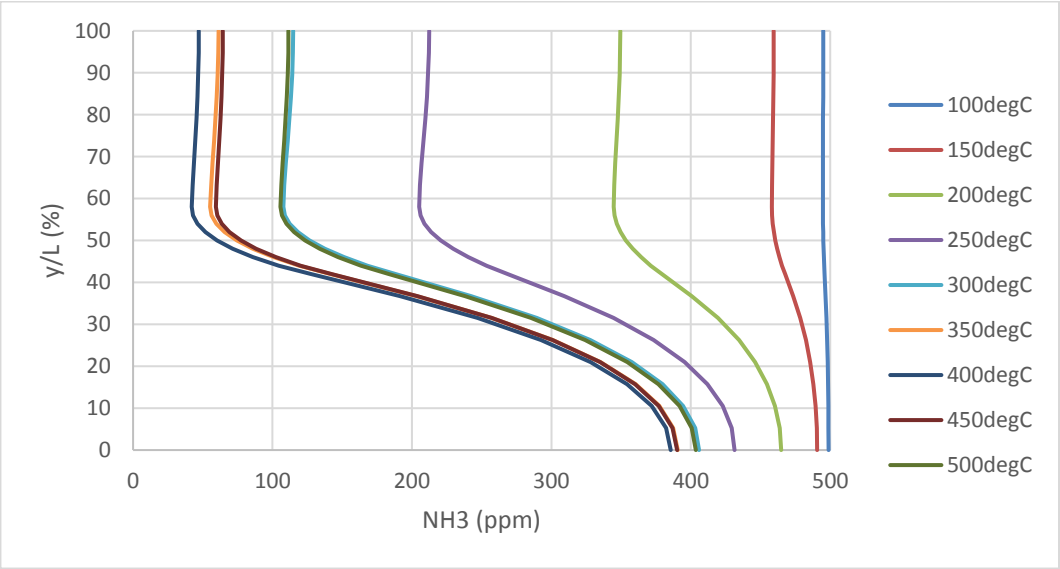

Figure 5-16: NH_3 Mole Fraction at 0.5mm from The Inlet (line C05)

Figure 5-16 shows the ammonia level at 0.5mm from channel entrance in the Y direction. Y-axis 0 to 40% is from the centre of inlet channel to surface wall, 40% to 60% is a porous wall and 60% to 100% is from upper surface wall to the centre of the outlet channel. 0.5mm from the inlet is in a location where most of SCR reaction happens. The gradient of ammonia reduction is small at 100°C to 200°C due to the slow reaction rate. In higher temperature range, the gradient is steep from y/L=10% all the way to 55%, where is beyond the central line of the porous wall, and then the value stops to change at that point. The significant reduction happens in the 2/3 of the porous wall on the side of the inlet channel. The other side of the porous seems like not contributing any effect to the reduction process.

The result in the following figures, Figure 5-17 to Figure 5-20, is shown in the X direction. The ammonia composition in the inlet and outlet channel from 100°C, 300°C and 500°C is shown in Figure 5-17. ammonia composition is nearly the same in the inlet, and outlet channel apart from the slightly falls along the length. While at a higher temperature, the inlet channel has a similar level of NH_3 composition at 300°C and 500°C, this is understandable due to the assumption of no homogenous reactions. The composition of NH_3 is pretty similar because nearly 100% conversion rate is reached by both temperatures. But 300°C shows less ammonia level at 2mm to 4mm in both inlet and outlet channel than the case with 500°C.

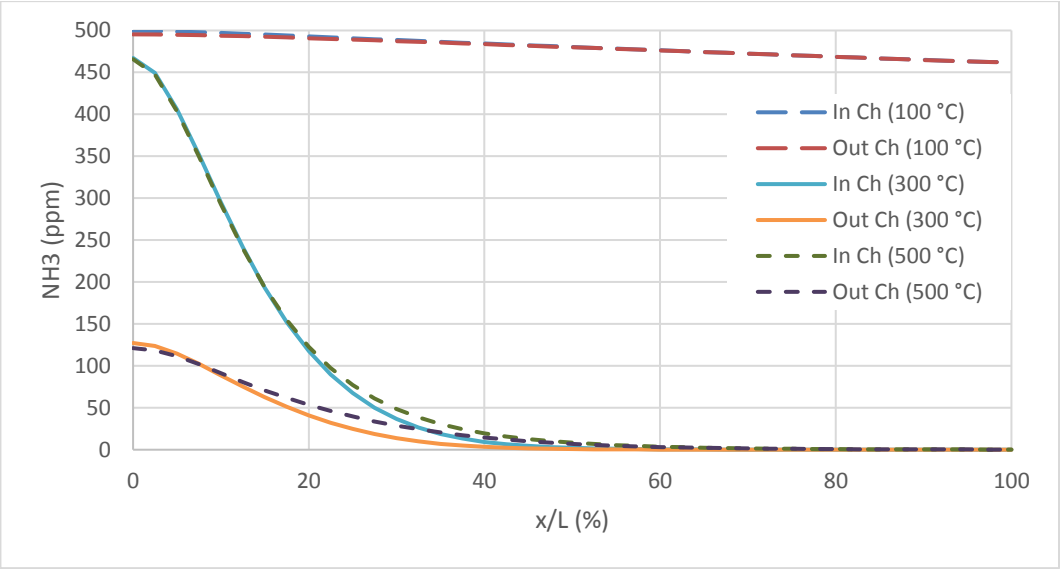

Figure 5-17: NH_3 Composition in The Channels (0.3m/s)

In the case of NO composition, Figure 5-18, the situation at 100°C is the same as the case of NH_3 composition at 100°C. At high temperature, most of NO is in the front part of channels (inlet and outlet). There are no further SCR reactions beyond 45% due to lack of ammonia, so the same NO composition level in both inlet and an outlet channel.

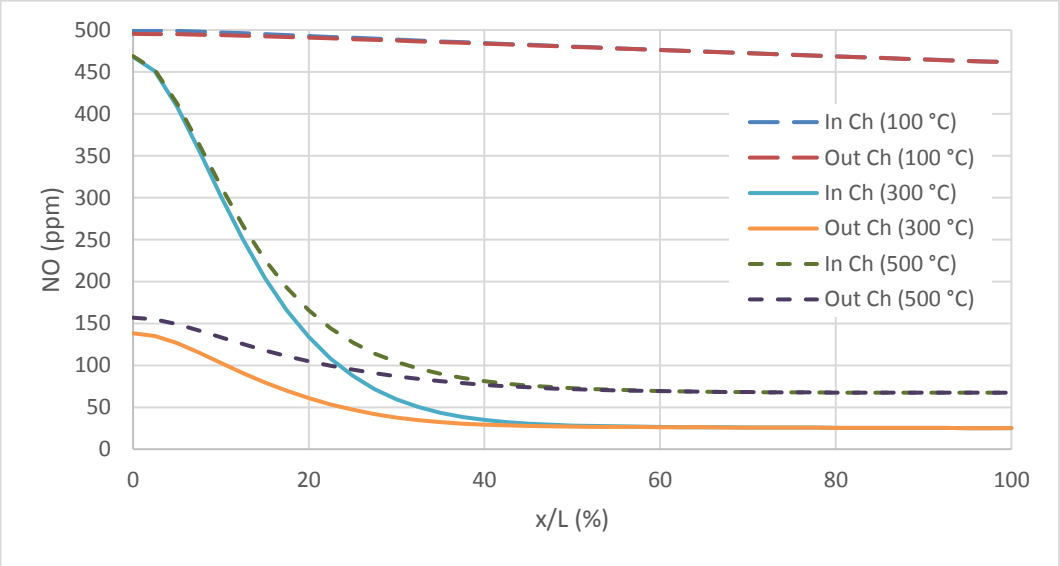

Figure 5-18: NO Composition in The Channels (0.3m/s)

The existence of NO_2, in this case, is due to NO oxidation. the result of NO_2 at 300°C, 400°C and 500°C are shown in Figure 5-19. For temperature below 300°C, NO oxidation rate is low, NO_2 composition is low and slowly increases along the length of the channel, it is less than 4ppm even by the end of the channel. NO_2 composition is 4ppm and 15ppm at the beginning of outlet channel at 400°C and 500°C, the level of NO_2 in the inlet channel is low in the front part due to it is surface reaction, it is reasonable that more product (NO_2) is available after the gas pass through porous wall.

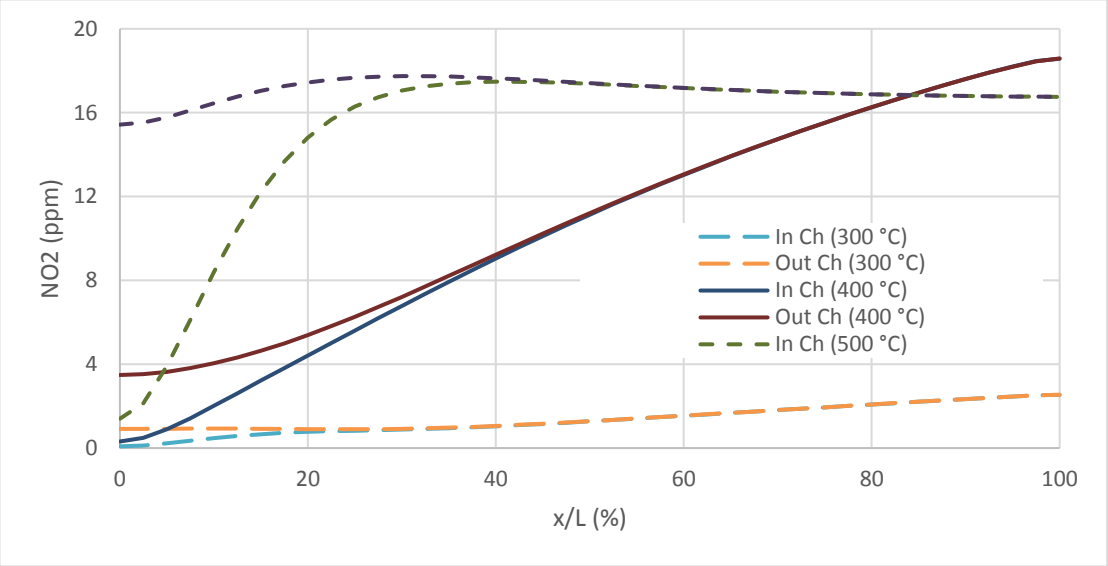

Figure 5-19: NO_2 Composition in The Channels (0.3m/s)

N_2O is a side product during SCR reaction; the composition of N_2O is deficient even at 500°C. In Figure 5-20, N_2O level starts at 0.01ppm at the entrance section of the inlet channel and rises to 0.16ppm at the outlet, and the starting value is less than 0.1ppm in the outlet channel. In the case here, all the N_2O is formed in the front 40% of the channel, and this is because the formation of N_2O requires the presence of NH_3. Due to the extremely low level of N_2O composition, it is neglected here.

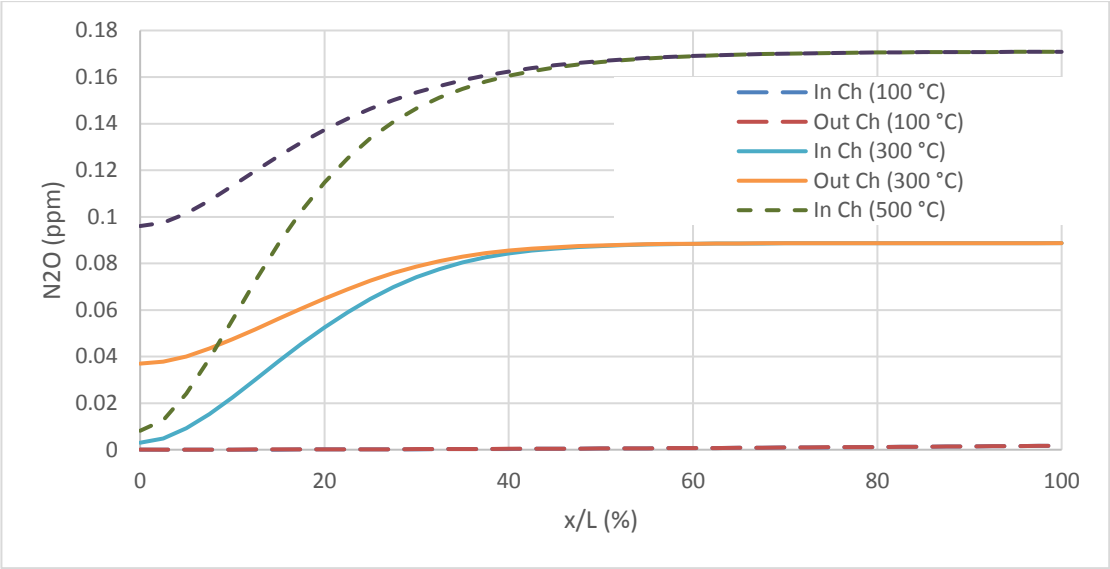

Figure 5-20: N_2O Composition in The Channels (0.3m/s)

5.1.5 Excessive Inlet NH_3 Concentration

This inlet mixture gas of 500ppm NH_3 and 500ppm NO is unable to reflect the whole situation in the rear half channel at a temperature above 300°C, a case with inlet mixture of 1000ppm NH_3, 500ppm NO and 8% O2 is simulated, the result is represented as follow. Figure 5-21and Figure 5-22 show NH_3 and NO reduction rate under the condition of double ammonia concentration from inlet respectively, velocity range from 0.3m/s to 0.9m/s.

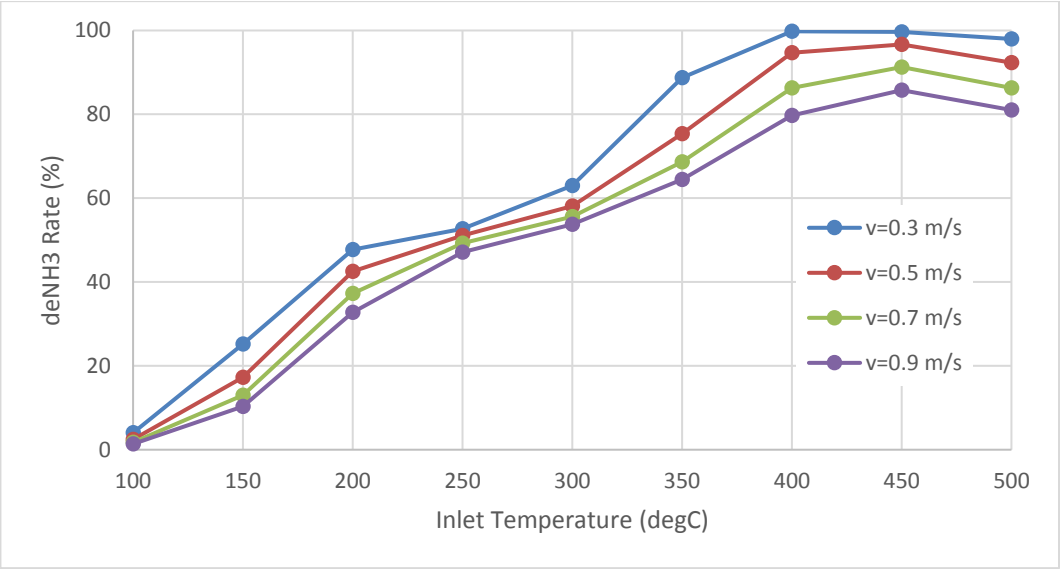

Figure 5-21: NH_3 Reduction Rate at Double Inlet NH_3 Concentration

When there is enough ammonia is available in the channel, NO conversion process continues to the end of the channel, and NO conversion rate reaches almost 100% at 300°C and maintains at this level at higher temperatures. At 300°C, around 50% - 60% of NH_3 is reacted with almost 100% of NO. Beyond 300°C up to 500°C, there are 10% to 40% of ammonia reduction is due to ammonia oxidation and excess is absorbed into the porous wall. Providing reaction rates and site density are correctly measured and set, this result can be used in conjunction with ammonia dosing strategy to achieve better control of ammonia slip at catalyst outlet.

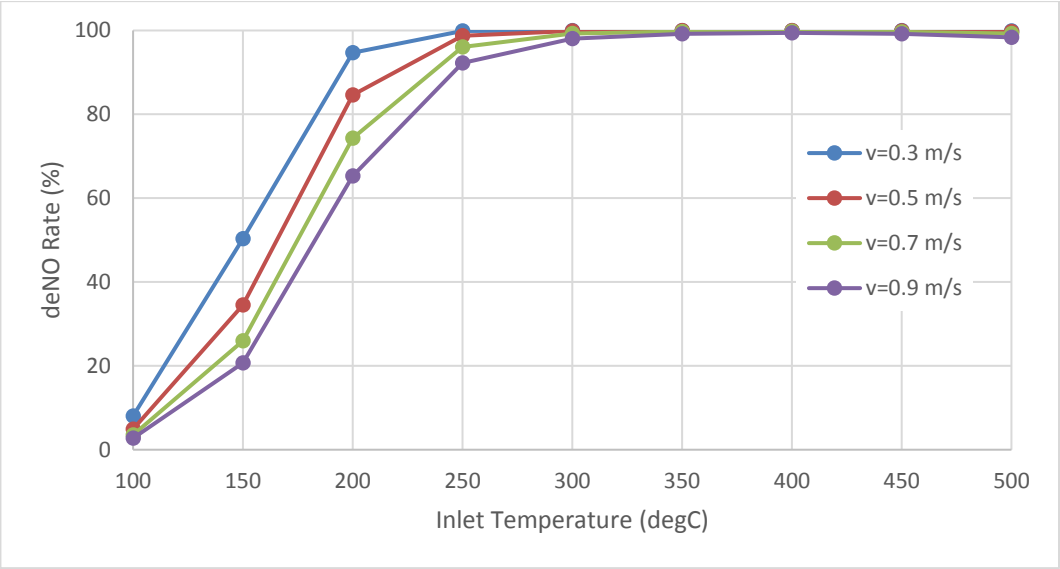

Figure 5-22: NO Reduction Rate at Double Inlet NH_3 Concentration

Conversion rate against the channel length is also plotted in Figure 5-23, in the case of excessive ammonia is supplied at the inlet, the conversion rate is expected to be low. Therefore, the focus point is at the change of velocity. Overall NH_3 conversion rate falls with every velocity increase. The maximum capability or the required quantity for the maximum NO conversion rate at 300°C with various velocity can be obtained. For instance, it requires 625.77ppm of NH_3 for 99.99% NO conversion at 0.3m/s and it requires 531.63ppm of NH_3 for 97.6% NO conversion rate at 0.9m/s. This quantity has taken account of the consumption of ammonia oxidation.

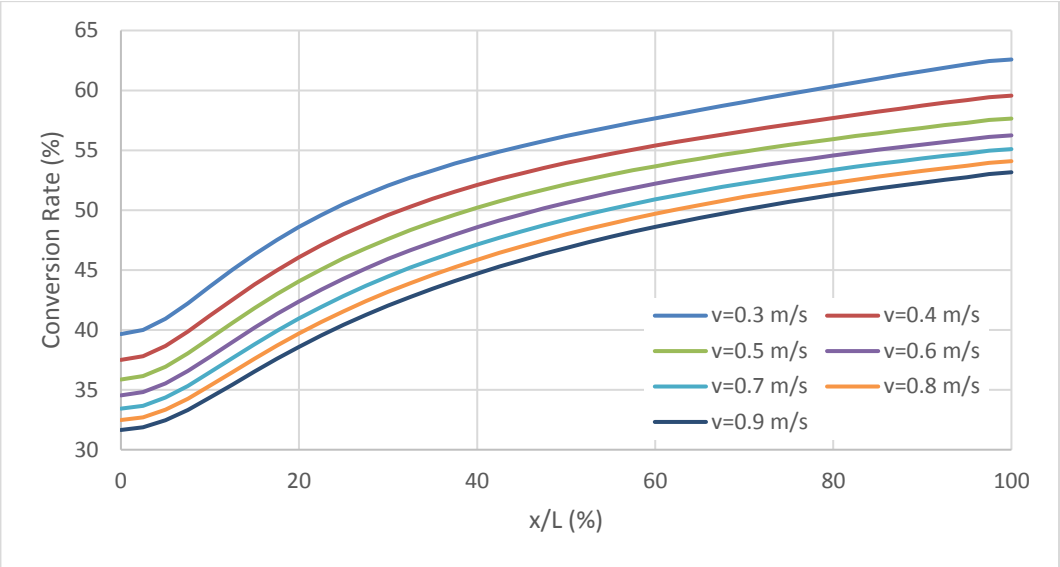

Figure 5-23: NH_3 Conversion Rate Against Channel Length at 300°C

Since excessive ammonia is available, NO conversion rate is expected to be higher, especially in the rear part of the channel. In Figure 5-24, the lowest overall NO conversion rate is 97.6% at the channel's outlet with inlet flow 0.9m/s. When low inlet velocity is used, 0.3m/s, 99% of NO is reduced at 47.5% of the catalyst length, and it means 4.75mm of catalyst reduces 99% of NO in this case. The conversion rate at high-velocity 0.7m/s and above benefits from the length of the catalyst, thus the overall conversion rate of NO is pretty good.

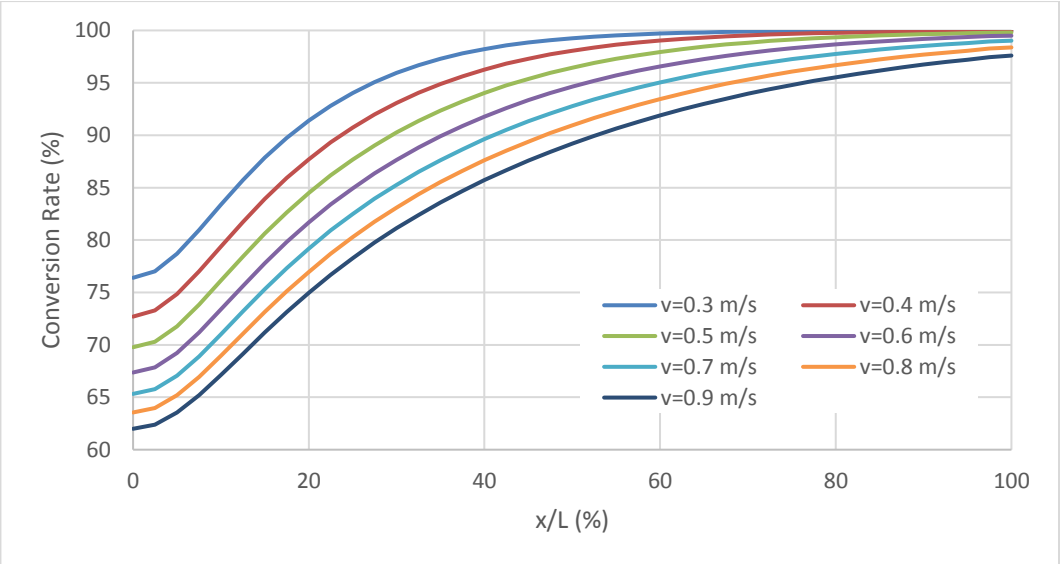

Figure 5-24: NO Conversion Rate Against Channel Length at 300°C

In a different view, Figure 5-25 and Figure 5-26 are plotted based on the result of inlet velocity at 0.3m/s; the temperature is increased from 100°C to 500°C.

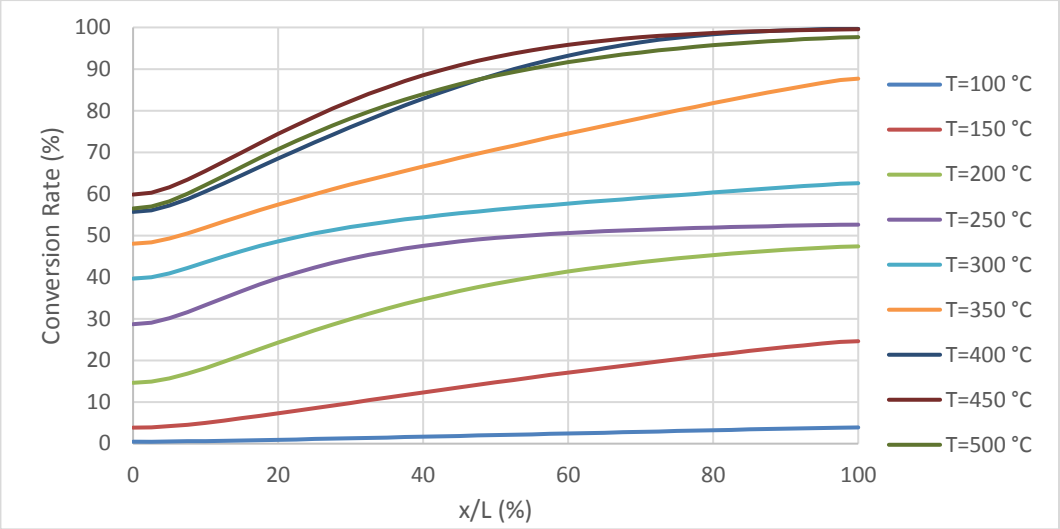

Figure 5-25: NH_3 Conversion Rate at 100°C to 500°C (0.3m/s 1000ppm NH_3 inlet)

In NH_3 conversion with various temperature, 100% reduction of 1000ppm NH_3 is achievable above 450°C. Based on the result of NO conversion rate in the last figure, roughly 55% is used for SCR reactions at 300°C, 5% of NH_3 is consumed by further NH_3 oxidation or absorbed in the porous wall.

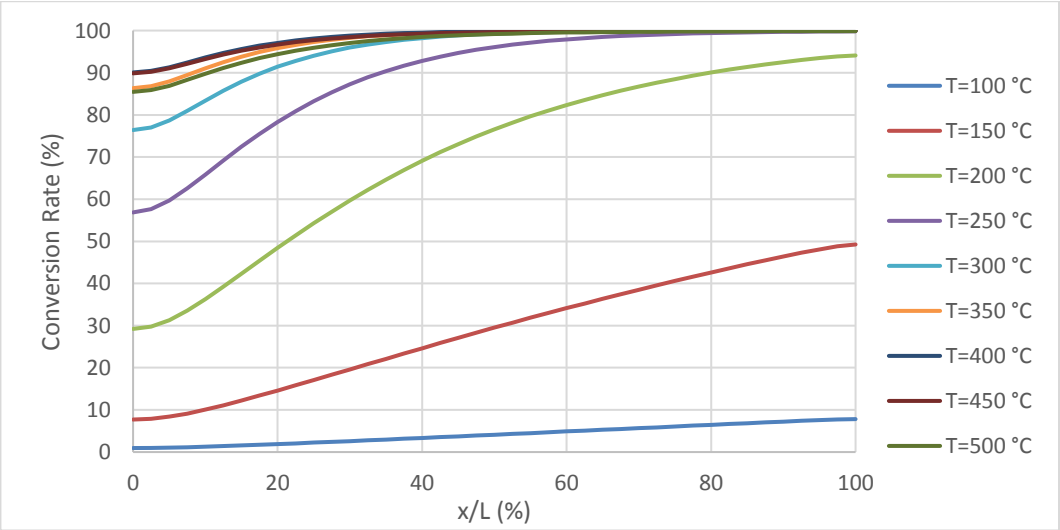

Figure 5-26: NO Conversion Rate at 100°C to 500°C (0.3m/s 1000ppm NH_3 inlet)

In the result of NO conversion in Figure 5-26, at high-temperature range 300°C and above, the conversion rate reaches 90% by using 47.5% of total catalyst length. Despite the fact that NO conversion rate can reach 94% reduction at the outlet of the catalyst at the temperature of 200°C. This is an indicator that NO conversion rate is much faster when the temperature is between 300°C and 500°C.

5.1.6 Reaction rates

The surface reaction rate is a critical factor to overall conversions. Reaction rate improvement is usually achieved by employing better catalyst material as a surface coating or using different washcoat preparation method and so on. By the study of reaction rates, different kind of improvement can be made. For example, using a specific surface coating or catalyst material or structure at specific locations to maximise the overall performance or specific performance in low temperature. In this section, the reaction rate contours in the porous wall of the selected reaction are shown and discussed the possible cause.

The first reaction is overall ammonia adsorption. The contours are displayed on the surface of cross-section panels, at 1mm interval. This reaction rate is calculated using the adsorption rate minus the desorption rate. The boundary condition for this example case is inlet velocity 0.3m/s, temperature 300°C and 500ppm NH_3, 500ppm NO and 8% O2.

The contours in Figure 5-27 shows the overall reaction rate of NH_3 adsorption in the front part of the catalyst, where x=0mm, x=1mm, x=2mm and x=3mm. in each of the contours, bottom left, and top right channels are inlet channels, and top left and bottom right are outlet channels. The strongest reaction rate is within the first millimetre, that is x=0mm. the reaction rate is the same on the surface wall, no matter of inlet channel or outlet

channel. but inside the porous wall, the higher reaction rate is beneath the surface wall of the inlet channel. this high reaction rate area takes up half of the porous wall around the symmetry panel and decreases as getting close to the corner. The moderate reaction rate is in the cross centre of the porous wall. But this rate falls rapidly and nearly disappear at 3mm from the inlet. Despite the low adsorption rate beyond 3mm, it is still a rate much higher than the SCR reaction rates.

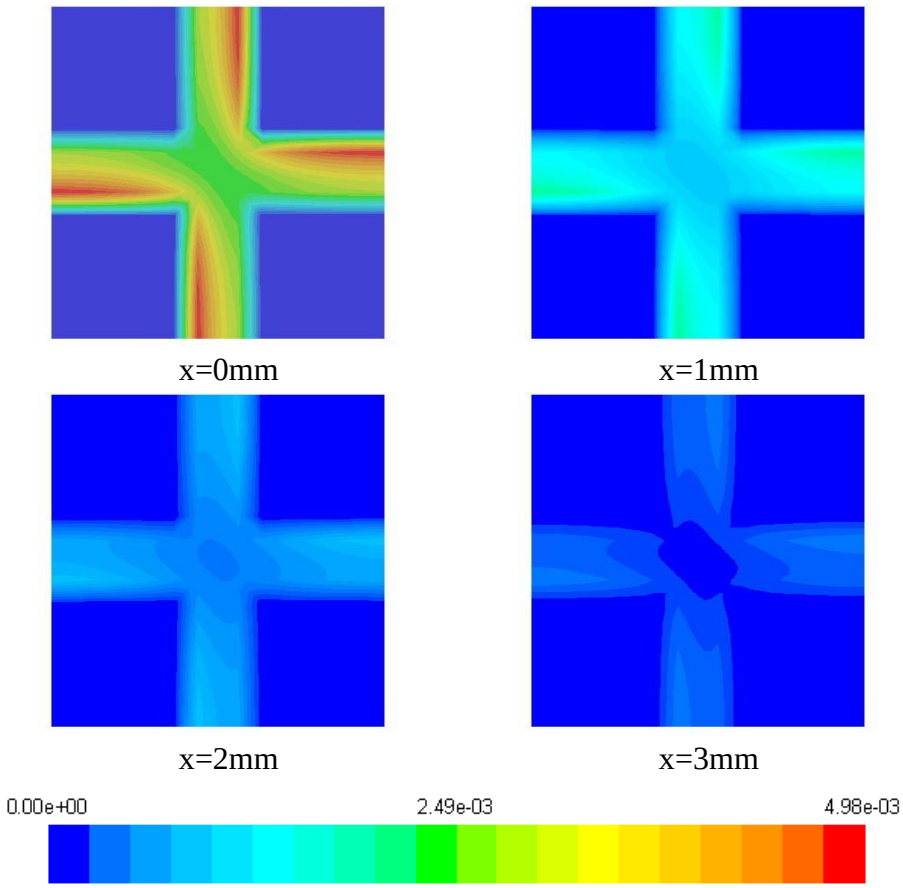

Figure 5-27: Overall NH_3 Adsorption Rate (Inlet: 0.3m/s, 300°C, 500ppm NH_3)

Since the highest reaction rate and the majority of ammonia is adsorbed in this section, it is an indication that all of the SCR reaction takes place in this region as NH_3(S) is unavailable in later sections. Also, as mentioned earlier in Figure 5-7, NH_3 level in porous starts 0.13 at 0mm and falls to 0.03 at 4mm and then slowly falls to 0 around 5mm. There is the reaction in the first 5mm of the channel, but the highest value of the colour map is

too high, 0.00498 kgmol/m3-s, the small values in the middle section is not showing in the contours.

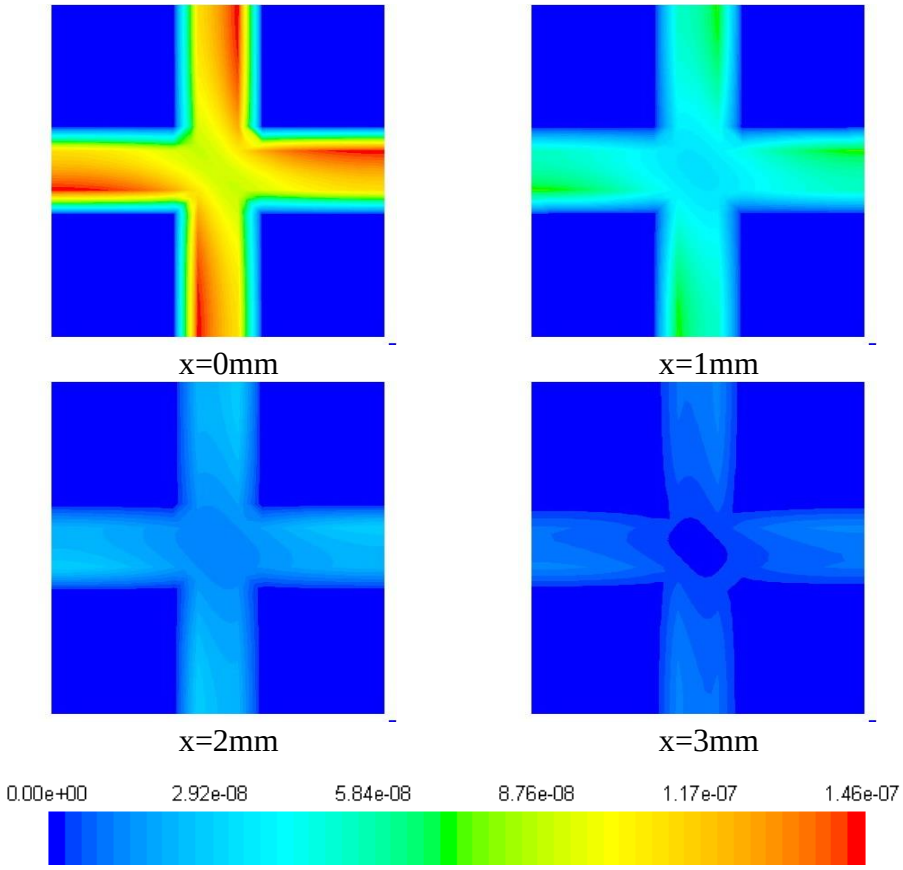

Figure 5-28: SCR Standard Reaction Rate (Inlet: 0.3m/s, 300°C, 500ppm NH_3)

The second reaction rate to show is standard SCR reaction, and the overall situation is very similar to the case in ammonia adsorption reaction. The difference is the high reaction rate region beneath the inlet channel surface extend almost to the wall surface of the outlet channel. Despite the same reaction rate profile, the maximum rate of standard reaction is 1.46E+7 kgmol/m3-s.

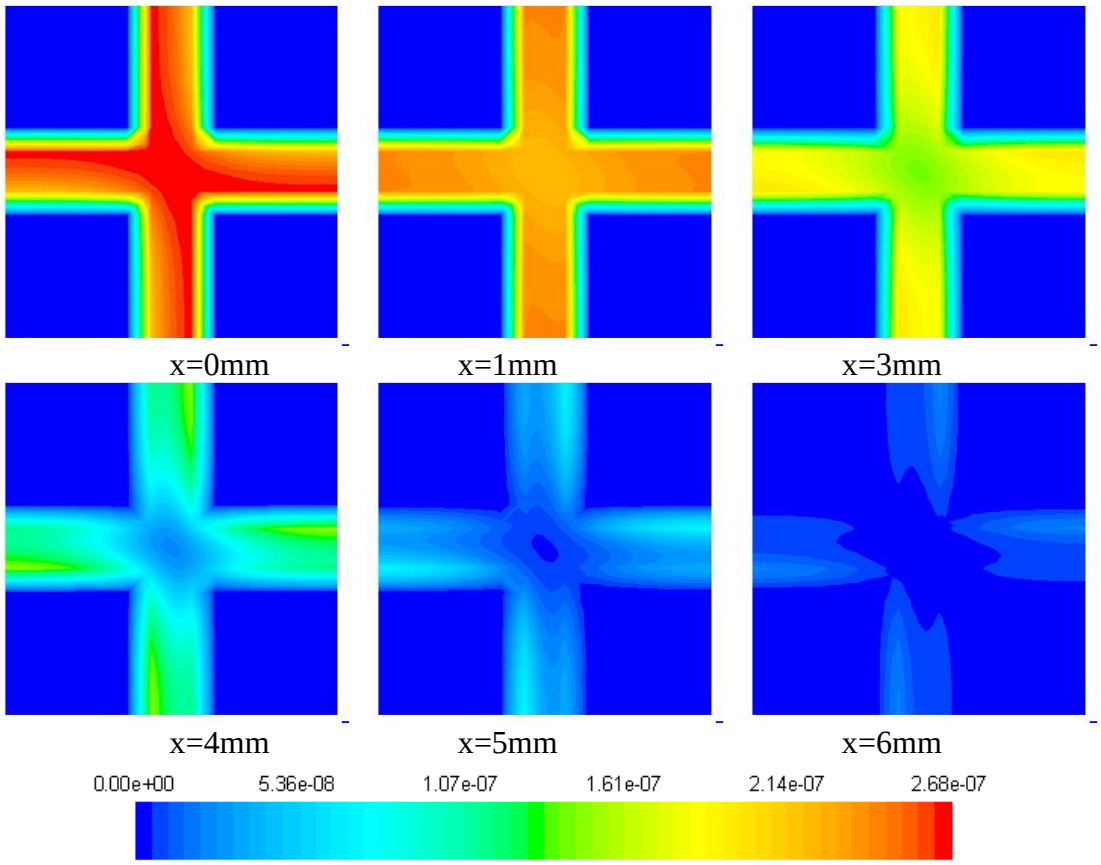

Figure 5-29: Ammonia Oxidation Rate (Inlet: 0.3m/s, 300°C, 500ppm NH_3)

In ammonia oxidation, the maximum reaction rate is almost twice the standard deNO rate. At the location x=0mm, high reaction rate region occupies the entire porous wall and evenly falls when it gets to the next section at x=2mm. This reaction rate profile provides evidence of ammonia oxidation rate are higher than SCR reaction rates, and the reaction rate is uniformly distributed in the porous wall.

While reaction rates are falling along the length of the channel, the region in the cross centre is first to disappear and the second region is near the surface in the corn of outlet channel, and then is the porous wall beneath the outlet channel. the last region is on the surface of the inlet channel. this order of reaction rate fading is showing the last contours of all three reaction rates.

5.2 WF SCR with Fin

While adding fins into the outlet channel, the fins were set to behave like solid material in the simulation, there is no fluid flow inside or pass through the fins. Thus the flow domain it modified to cut off the fins. Since the fins surface is covered by the same catalyst material as in a porous wall, surface reactions were set to the surfaces and the same reaction rates are used. After mixture gas pass through the porous wall, the fin provides more active site surface for SCR reaction for any remaining NH_3 and NO_x in the mixture gas.

In this section, similar results and contours are displayed. Due to both cases are wall-flow type catalyst, flow characteristic is more or less the same and extra fins actually bring some obstacle for the flow while exiting from the porous wall, so only the difference is mentioned and discussed.

5.2.1 NH_3, NO Conversion Rates

As mentioned in early sections, for the inlet condition with 500ppm NH_3 and 500ppm NO, there is a lack of ammonia at a high-temperature range between 300 and 500°C. This causes the peak NO conversion rate stops at 90%. In order the study NO conversion tendency and behaviour in the temperature range at 300°C to 500°C, inlet ammonia concentration needs to be increased slightly to allow all NO are reacted. But for the consistency between model cases, WF with Fin model is firstly run in the condition of inlet mixture with 500ppm ammonia. Once it is finished, the inlet ammonia supply is doubled, to 1000ppm for further study.

In the first inlet condition, the overall conversion rate of NH_3 and NO are shown in the below figures, Figure 5-30 and Figure 5-31. Both figures show a similar tendency as in the WF model. At 100°C to 250°C, reaction rates are low, only up to 50% of the NH_3 and NO are removed under the lowest velocity 0.3m/s and 250°C. As the temperature climbs to 300°C, the reaction rates are fast enough to consume almost all of that 500ppm NH_3. At 1m/s inlet velocity, there are 20ppm NH_3 left in the mixture at the outlet and the only 2ppm that is 1% left when inlet velocity drops to 0.7m/s.

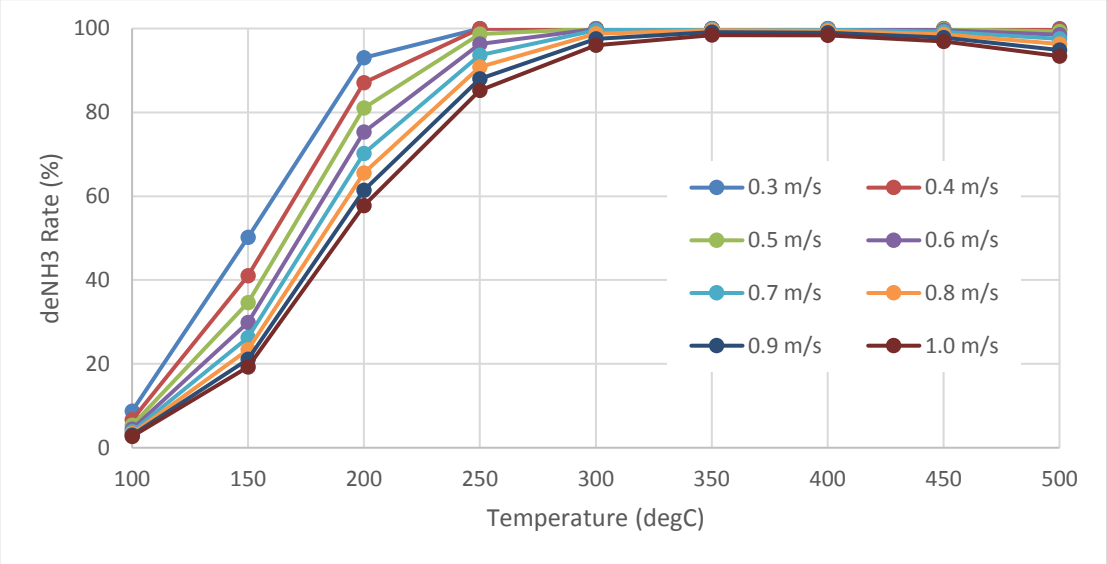

Figure 5-30: deNH$_3$ Rate (inlet NH_3 500ppm) for WF-Fin

There is still NH_3 left in the mixture at the outlet, around 20ppm, at 300°C. when the temperature is further increased, a large proportion of this ammonia is easily consumed by ammonia oxidation before they can react with NO. Therefore, there is an increase in the ammonia conversion rate at 350°C, but a further improvement on NO conversion is limited due to the lack of NH_3.

As shown in Figure 5-31, NO conversion rate stays between 80% and 90%. Even more, the NO conversion rate steadily drops off from 91% to 80% as the temperature increase from 300°C to 500°C. The reason is that ammonia oxidation rate is getting faster and

faster as temperature rises, the ammonia oxidation rate is nearly 200% faster than standard SCR reaction rate at 300°C. As a result, part of NH_3 is oxidized before it reacts with NO_x. Less reducing agent leads to less NO is consumed, thus lower NO conversion rate.

There is a difference in the NO conversion rate between this model and WF model, as NO conversion rate falls with velocity increase, for example, it falls 1% to 2% in WF model at 350°C to 500°C whereas 4% in WF-Fin model.

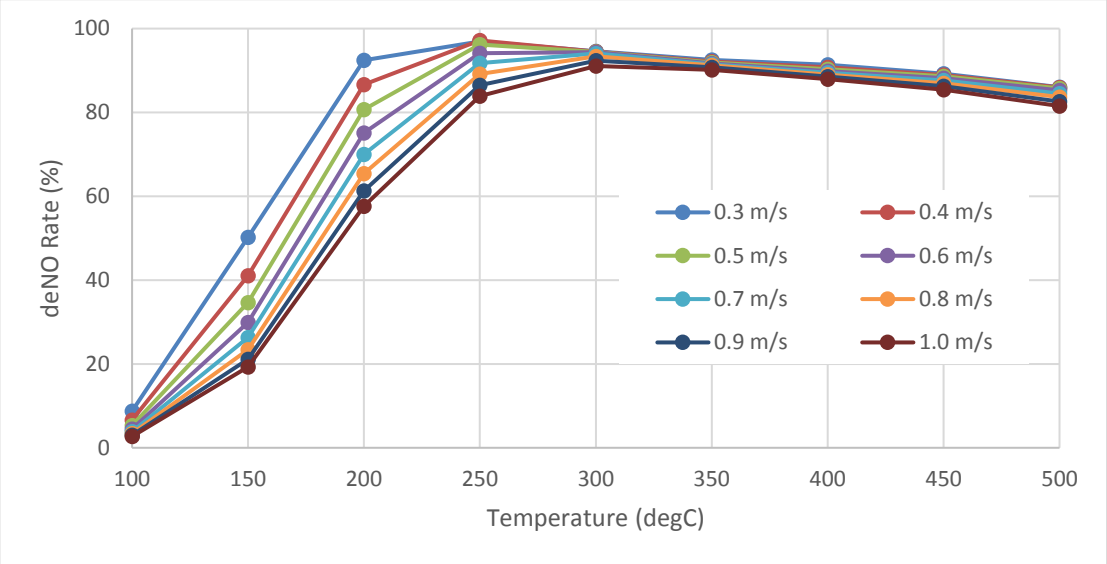

Figure 5-31: deNO Rate (inlet NH_3 500ppm) for WF-Fin

In general speaking, WF with Fin model has a similar tendency of NH_3 and NO conversion rate to the WF model under the condition of lack of NH_3 in high-temperature range due to low NH_3 concentration. Therefore, the model is rerun with 1000ppm NH_3 in the inlet mixture.

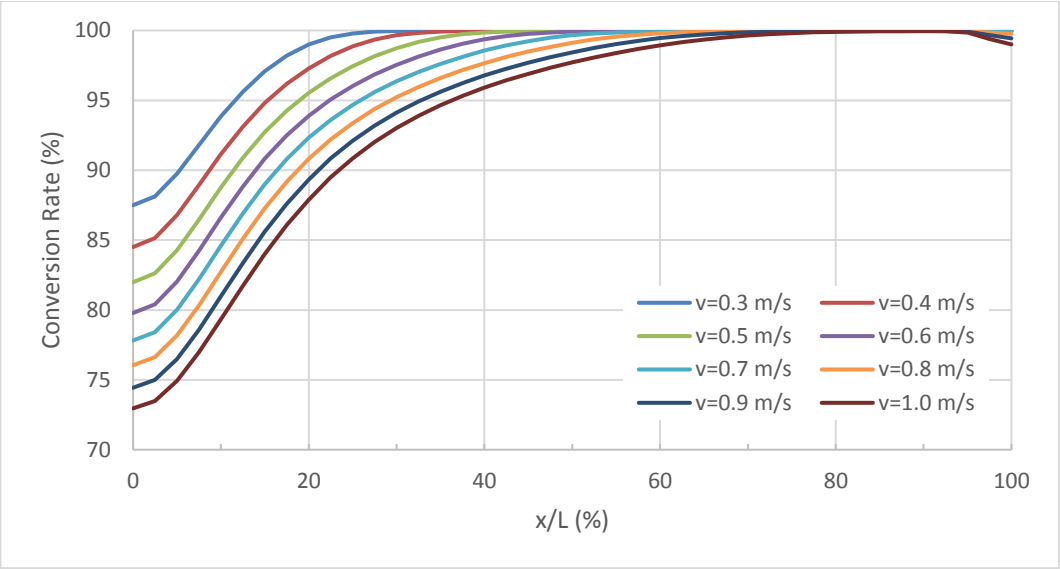

Figure 5-32: NH_3 Conversion Rate at Various Inlet velocities at 300°C for WF-Fin

For ammonia conversion rate at 300°C, WF-Fin model starts at 73.9% reduction with 1m/s velocity compare to 57.7% in the WF model. At the lowest velocity, 0.3m/s, NH_3 reduction is 87.5% in WF-Fin model compared to 75% in the WF model. In WF-Fin model, with 1.0m/s inlet velocity 99.99% reduction is reached by 70% of total channel length.

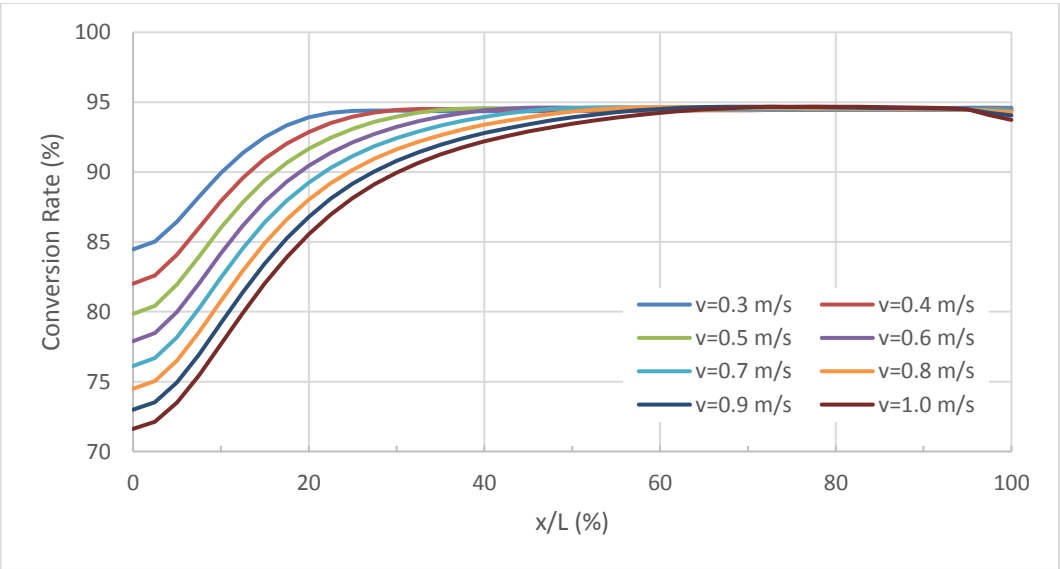

Figure 5-33: deNO Rate at Various Inlet Velocities at 300°C for WF-Fin

In NO conversion rate, the lowest reduction rate of NO is at the beginning of the channel at 1.0m/s inlet velocity, the rate is 71.6% and the same location with 0.3m/s, the rate is 84.5% whereas 56.7% and 72.3% in WF model. Due to the limitation of NH_3 unavailability, NO conversion rate in WF-Fin model is also limited to 94.6%

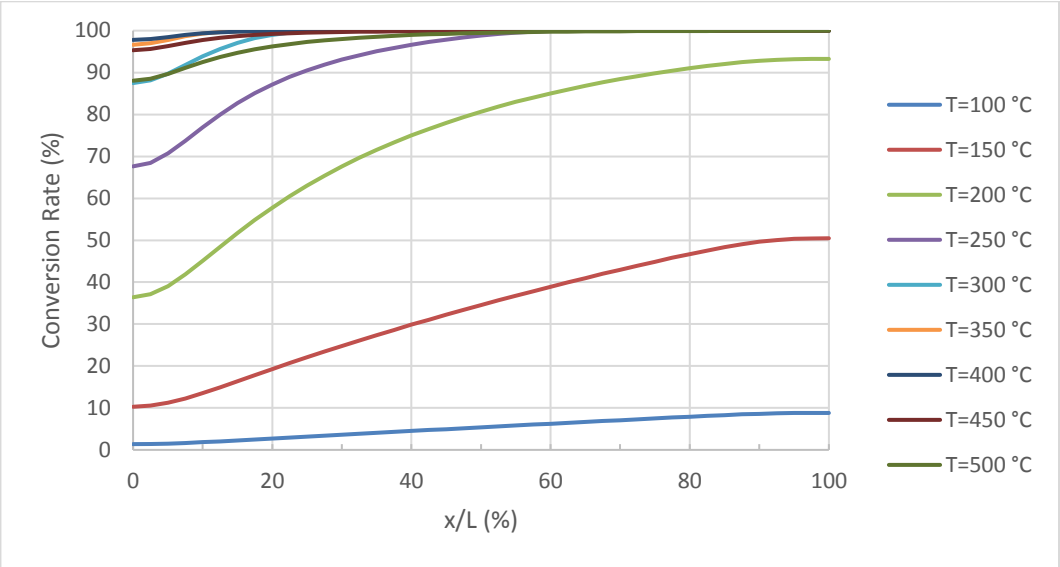

Figure 5-34: deNH3 Rate in The Outlet Channel for WF-Fin

The conversion rate of NH_3 (Figure 5-34) and NO (Figure 5-35) in the outlet channel under various temperature is plotted. The conversion rate of NH_3 is the same for the temperature below 200°C. As for temperature from 250°C and above, the maximum reduction rate of 99.99% is reached in the first half of catalyst in all the temperature cases. Moreover, with a temperature of 350°C to 500°C, the reduction rate starts from 95% at the beginning of the outlet channel.

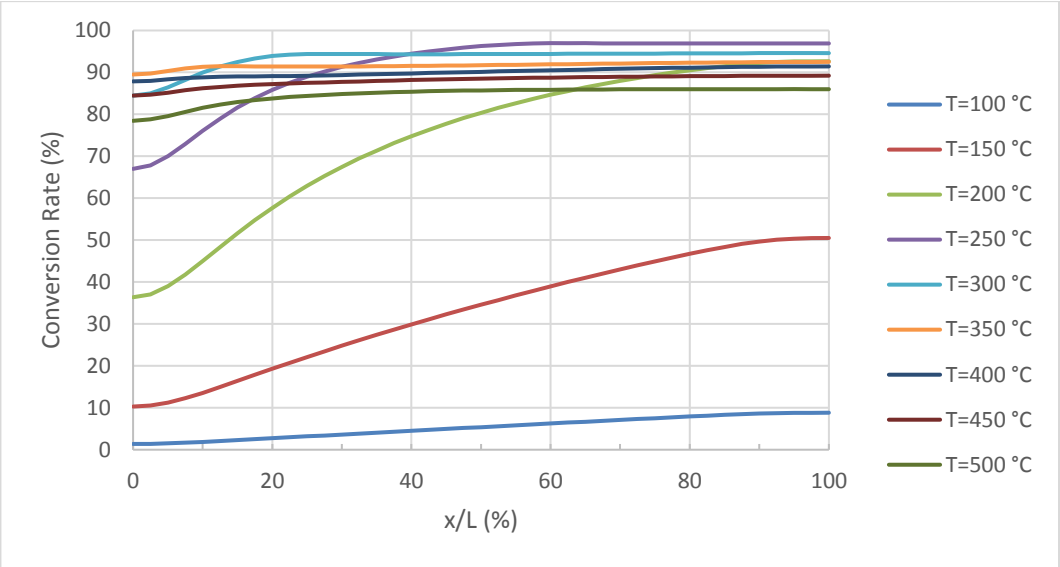

Figure 5-35: deNO Rate in The Outlet Channel for WF-Fin

A similar situation is in NO reduction rate, Figure 5-35, despite both cases reach a similar conversion rate at the outlet, WF-Fin case can get to the same conversion rate with the shorter catalyst. By a rough estimate is WF-Fin can get to similar overall conversion rate by only use 85% of total channel length at velocity is 0.3m/s. And it seems WF-Fin is affected by velocity change more significant than the WF model, as Figure 5-31 shows. A possibility is due to new fins provide more surface site, and ammonia oxidation takes advantage of this extra surface site.

5.2.2 Excessive Inlet NH_3 Concentration

With double NH_3 concentration in the inlet mixture, NO conversion rate at a high-temperature range (350 to 500°C) hovers around 96% and 97%, as in Figure 5-36. NO conversion rate does not change much below 150°C, but there is 2% increase in NO conversion rate at 200°C in the velocity range from 0.3m/s to 1m/s; and 3% increase when the temperature is 250°C.

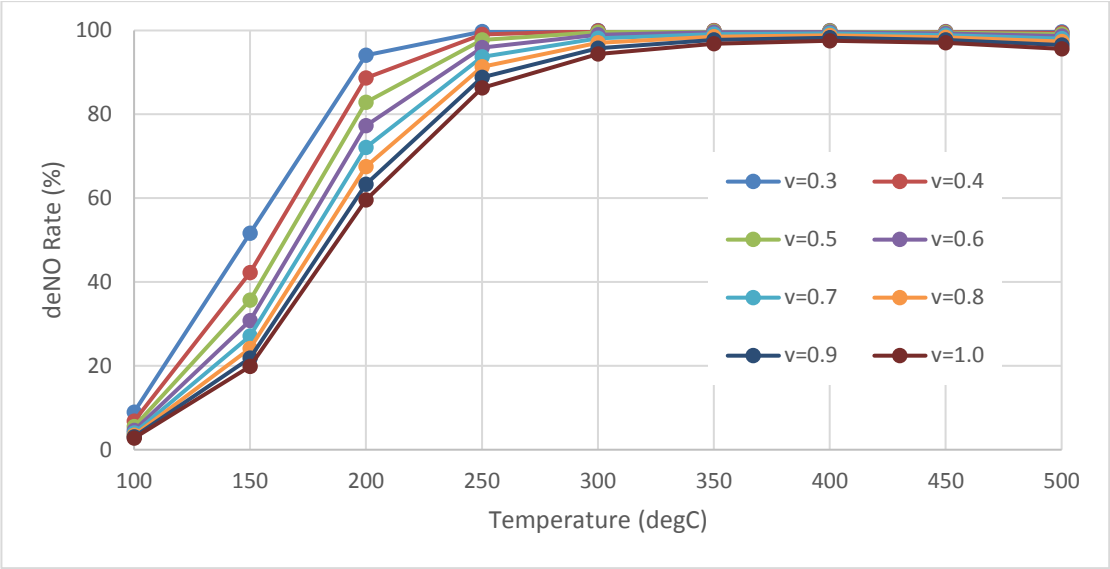

Figure 5-36: WF-Fin NO Reaction Rate (inlet NH_3 1000ppm)

There is a slight performance drop at 500°C when the temperature increases from 450°C. In general, low inlet velocity has better performance than high inlet velocity. The performance falls largely when the inlet velocity rate is increased. Performance drop reaches 1.53% at 1m/s inlet velocity when the temperature increases from 450°C to 500°C. This drop is insignificant during catalyst normal operation model, but it can be a problem during DPF regeneration model as the temperature is much higher.

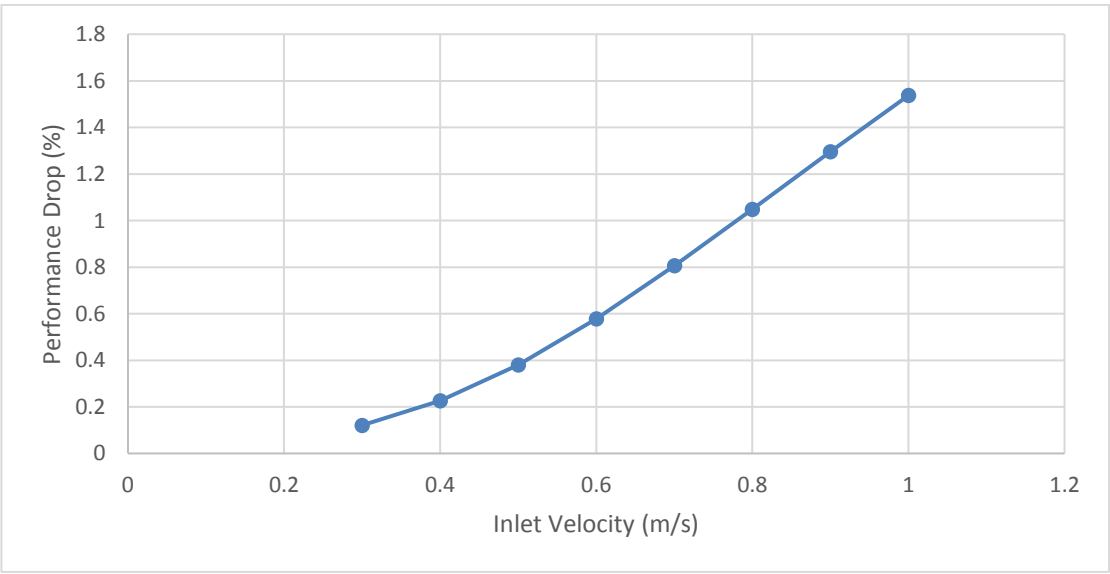

Figure 5-37: Performance Drop as Velocity Increase in WF-Fin Model (T=500°C)

One thing is certain that this performance drop is not caused by insufficient of NH_3 concentration, as Figure 5-38 shows around 20% NH_3 is left unreacted at the outlet for 1m/s inlet velocity from 400°C to 500°C.

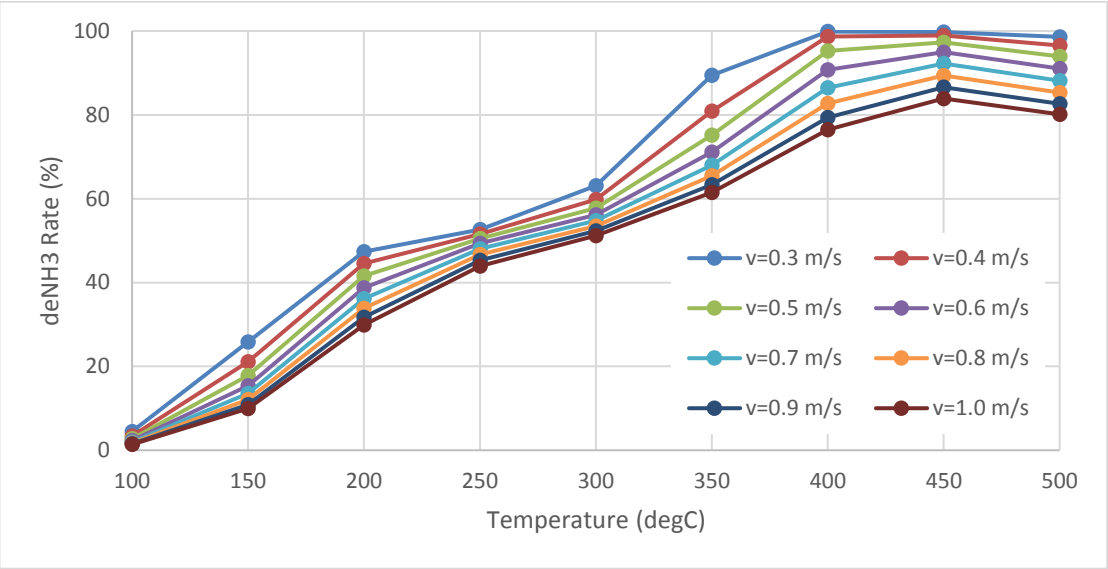

Figure 5-38: WF-Fin NH_3 Reaction Rate (inlet NH_3 1000ppm)

At 0.3m/s and 0.4m/s inlet velocity, 96% to 98% of the NH_3 is consumed from 400°C to 500°C. As velocity increase, the NH_3 conversion rate drops clearly, by average 2.5% from 150°C to 500°C. Whereas NO conversion rate is average 4% and 0.5% for temperature 100°C to 250°C and 300°C to 500°C respectively. A possibility is the diffusion rate is lower than NH_3 oxidation rate, even at high-temperature NH_3 conversion is decided by the diffusion rate.

Since the above figures are showing the overall conversion rate of NH_3 and NO, the difference between WF and WF-Fin model is difficult to tell. Below are the figures of conversion rate against the length of the catalyst; this should show some difference between the two models.

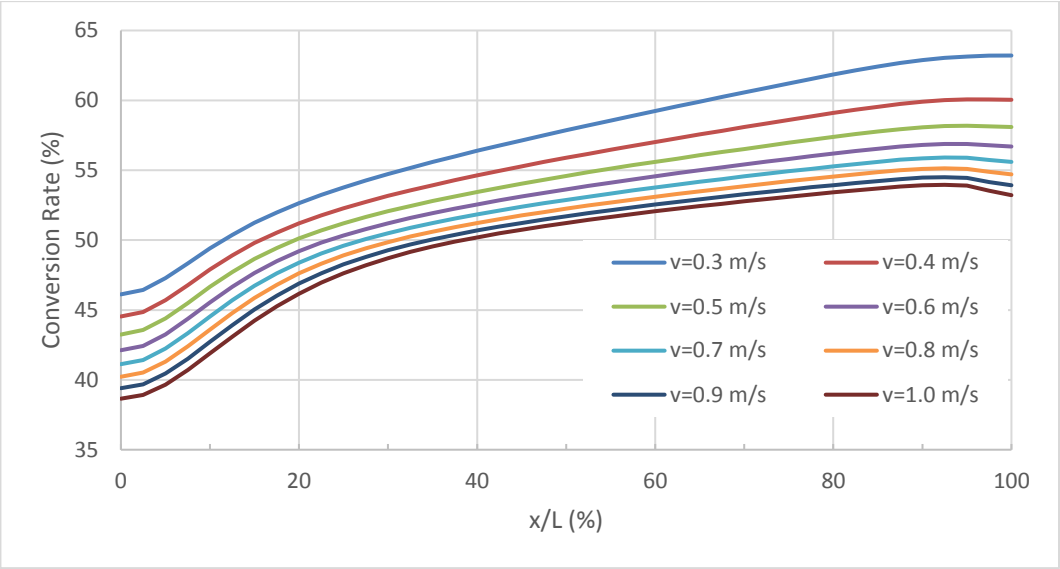

Figure 5-39: NH_3 Conversion Rate Against Channel Length at 300°C for WF-Fin

The first case is NH_3 conversion rate, the starting point at the beginning section of the channel at all inlet velocities are clearly better than WF model, 46.15% at 0.3m/s compare to 40% in WF model, and 39.4% at 0.9m/s compared to 31.64% in WF model. That is around a 7% difference. In the rear part of the channel, conversion at low velocity climbs faster the high velocity. But they all reach a similar conversion rate in the end. It is because there is a sudden turning point at location 90% to 100%, conversion rate stops to climb or even drop in this region.

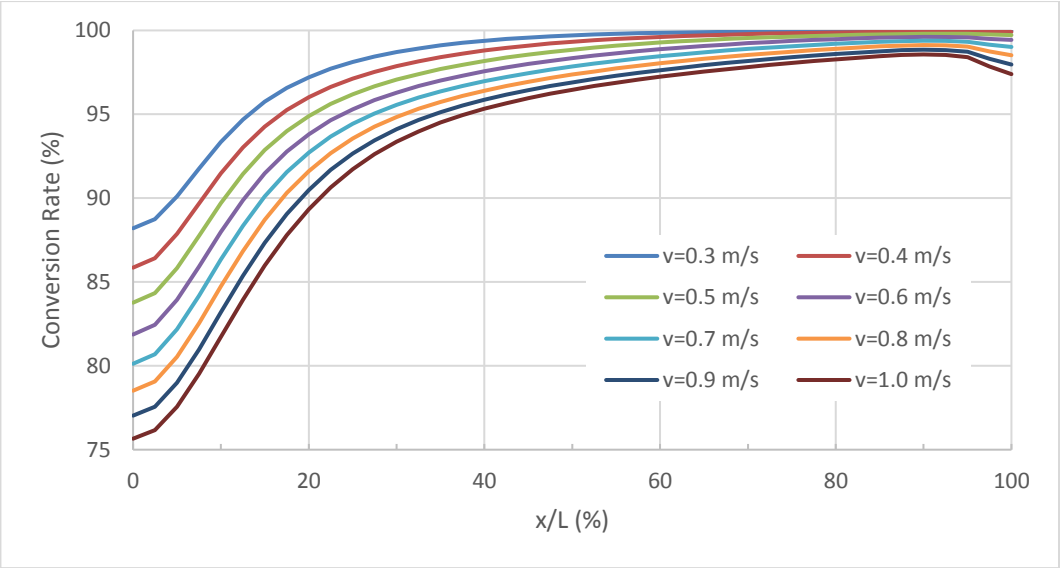

Figure 5-40: NO Conversion Rate Against Channel Length at 300°C for WF-Fin

The same situation happens to NO conversion rate as well. The starting point is excellent in WF-Fin model with an average 10% higher than that rate in the WF model. But the overall conversion rates are very similar at the outlet, and it is all because of the sudden drop.

Figure 5-41 and Figure 5-42 is the conversion rate of NH_3 and NO along the channel length under a wide temperature range.

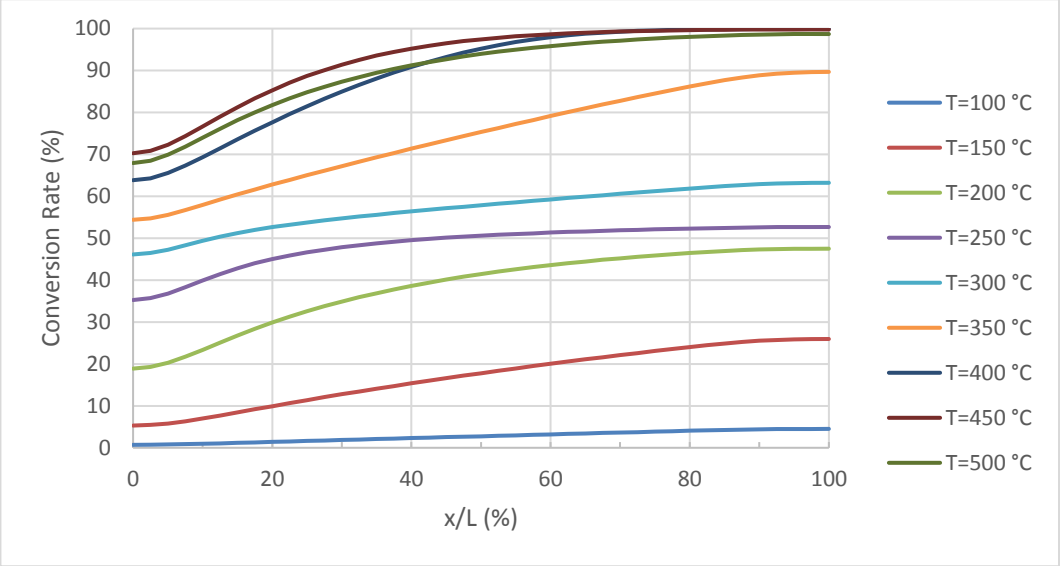

Figure 5-41: NH_3 Conversion Rate at 100°C to 500°C (0.3m/s) for WF-Fin

Despite the fact that excessive NH_3 is fed into the catalyst, WF-Fin model manages to achieve a good result. The starting point in the inlet section, the difference between the reduction rate is small at a low temperature, like 100°C and 150°C. At 200°C, WF-Fin conversion rate is 5% higher, 19% compared to 15% in the WF model. This difference is getting larger and larger as temperature increase. At 500°C, WF-Fin has 70.25% reduction rate whereas WF model only has a 60% reduction rate. Again, the outlet conversion rate is similar, only 1% or 2% difference, but WF-Fin reaches the same at location 85%, 8.5mm.

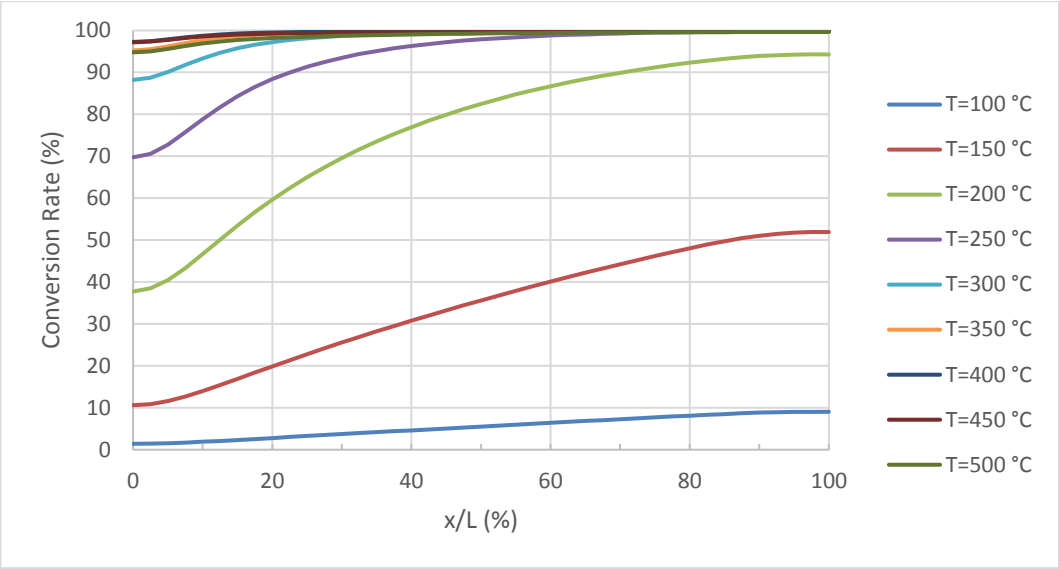

Figure 5-42: NO Conversion Rate at 100°C to 500°C (0.3m/s) for WF-Fin

In NO conversion rate with 1000ppm NH_3 inlet, conversion rate of 100°C, 150°C and 200°C start at a very low point from the inlet region, the rates continue to rise until 80% of the channel, it is still increasing but in a meagre rate. For 250°C, the maximum reduction of 99.6% is reached with half of the catalyst. As for high-temperature range, complete reduction happens in the first 10% of the channel.

Generally speaking, based on above results adding extra fins in the outlet channel helps the conversion reach its maximum level in shorter catalyst length. Although the overall conversion rate is similar at the outlet, WF-Fin model is capable of handling a much higher level of species concentration.

5.2.3 Velocity and Mass Flow Rate

Velocity vector in Y and Z direction inside the porous wall is shown in the longitudinal view in Figure 5-43, and the same setting is used in Figure 5-45 and Figure 5-46. There are three parts to be noticed in this figure, the first one is the difference of velocity

magnitude between the inlet part and outlet is easily noticed, the second one is the distance of those high-velocity region travels, and the third one is that the lowest velocity magnitude is in the middle of the channel and it gradually rises as it reaches to inlet and outlet.

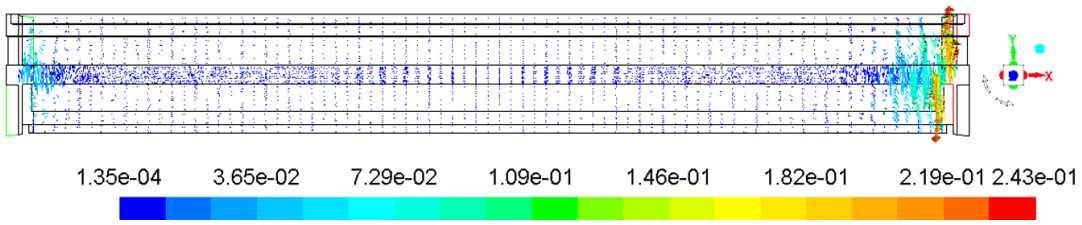

Figure 5-43: Velocity Vector of Porous Wall Interior (Left: Inlet, Right: Outlet)

This figure indicates most of the fluid pass through the porous wall from the rear part, and the front part of the channel and the middle part has the lowest velocity thus the least fluid goes through from there. A monitor line is added into the porous wall and an XY figure, Figure 5-44, is plotted base on above contour, results of two inlet velocities are shown. When inlet velocity is low at 0.3m/s, velocity magnitude at the front part of the channel (0-20%) starts from 0.043m/s and drops to 0.000173m/s; the value between 20% and 80% stays around 0.00015m/s and its average values is 0.000155m/s; the rear 20% of the channel has the highest value as it starts from 0.000249m/s and ends at 0.21m/s. In the case of 1.0m/s inlet velocity, velocity magnitude at the first 20% of the channel starts at 0.11m/s and drops to 0.001m/s. the average values in the middle 60% are 0.00163m/s, and the value of velocity magnitude rises from 0.0016m/s in the last 20% of the channel.

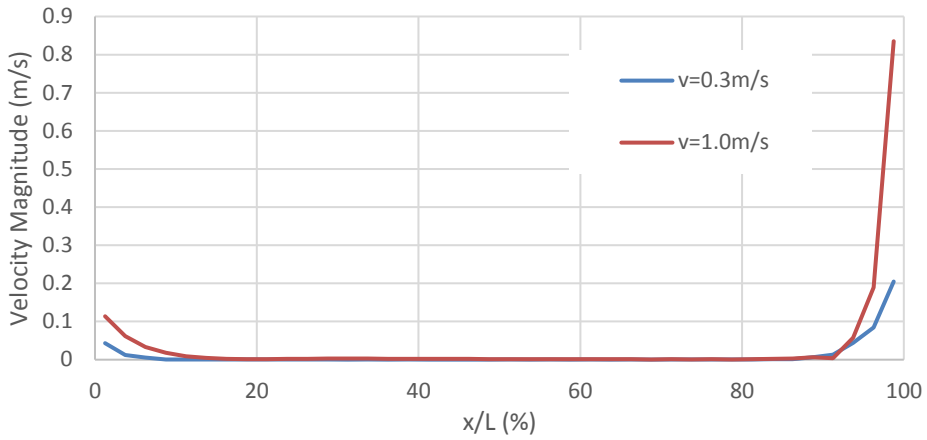

Figure 5-44: Velocity Magnitude in Porous Wall

When compare velocity magnitude value from front 20% and rear 20% to the average value of the middle part, the major drop in velocity is within the first 10% of the total length, and the significant rise in the rear part of the channel start after 90% of the total length.

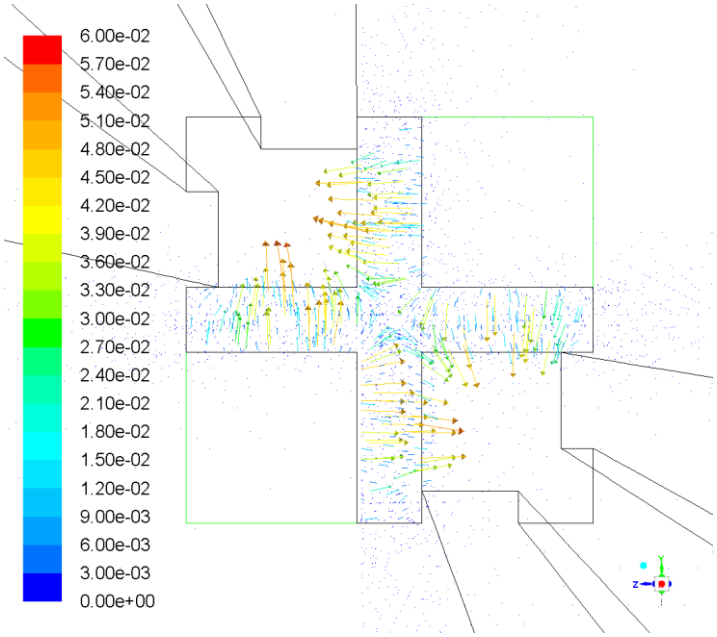

Figure 5-45: Velocity Vector in Porous Wall at The Inlet (v=0.3m/s T=200°C)

The velocity vector of porous wall interior at the inlet region is shown in Figure 5-45. Since this only shows the velocity inside the porous wall, the value is minimal, the velocity range in this figure is set between 0 and 0.06m/s which is indicated by the

colourmap on the left. The green squares on top-right and bottom-left are inlet channels, and the cross in the middle is porous wall and top-left, and bottom-right are outlet channels with two fins in each of them. As view angle, this figure is looking at the inlet region from the middle part of the channel. The area of interest in the porous wall is the location around the fins. As the fin is set to a solid material, it is cut out from the fluid domain and cannot be penetrated by any fluids. This creates an obstacle to the flow in the porous wall and changes local flow behaviour. As can be seen from the picture, the velocity in these areas is much smaller than another part of the porous wall. This low-velocity region might have a positive effect on NO_x conversion performance when diffusion is faster than reactions, as resistance time is longer than the high-velocity region. On the other hand, it brings a negative effect to when reactions are fast and no enough reactants for reactions.

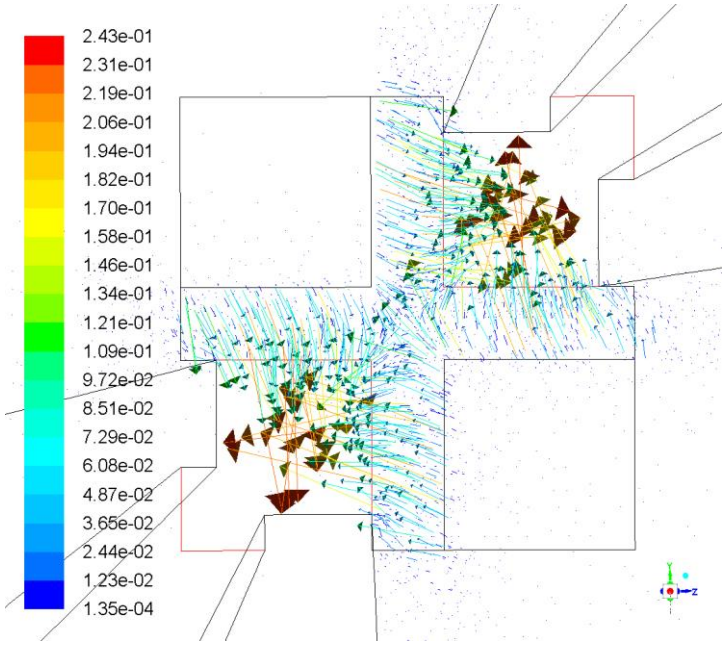

Figure 5-46: Velocity Vector in Porous Wall at The Outlet (v=0.3m/s T=200°C)

Figure 5-46 shows the velocity vector on the outlet end, and there are two important points to be noticed, one is clearly larger velocity magnitude on this end of the channel compared

to the inlet, the other one is that the largest velocity magnitude occurs at the location close to the fin. Velocity magnitude in Figure 5-47 is taken from a monitor line on the surface of the porous wall in outlet channel, 0% is at the bottom of the fin, and 100% is in the corner where two porous walls perpendicular to each other and this monitor line is 0.4334mm. When inlet velocity is 1m/s, the maximum velocity magnitude is between 23% and 33% of the monitor line. The peak velocity magnitude is 2.8 times the value in the corner, and it covers the distance (in Z-direction) about 0.45mm.

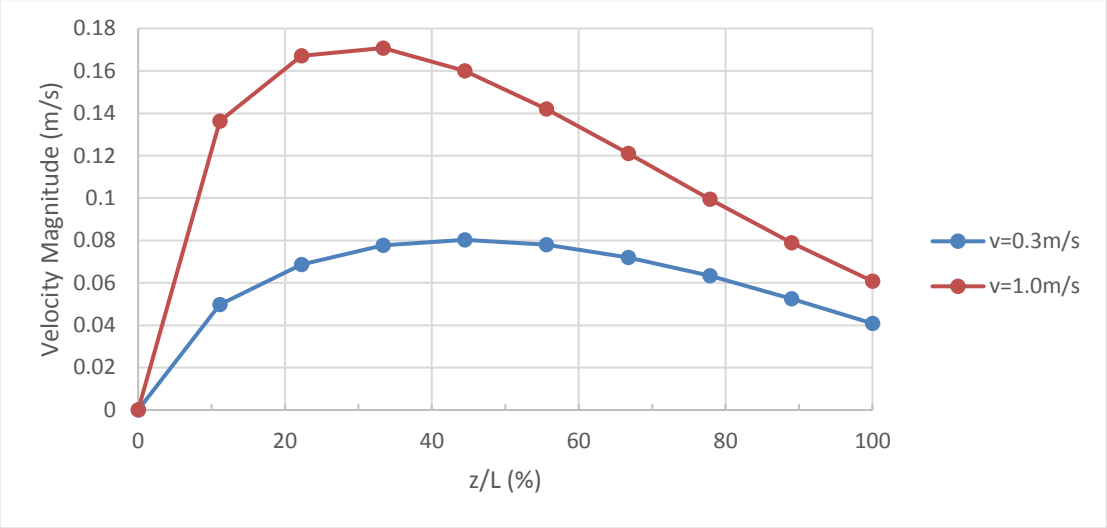

Figure 5-47: Velocity Magnitude on The Porous Wall Surface (Outlet Channel)

When inlet velocity drops to 0.3m/s the maximum velocity from 33% to 55%, the peak value is only twice of the velocity in the corner. When consider the highest 25% velocity magnitude, the case v=0.3m/s is from 0.06 to 0.08 m/s and 0.1275 m/s to the peak velocity for the case v=1.0m/s, that high velocity region covers nearly 60% of the monitor line in the case of v=0.3m/s compares to 50% for the case of v=1.0m/s. When inlet velocity rises, the major change in velocity magnitude on Z direction is between 5% and 45%, the change on both ends, in the fin's bottom and in the corner shows no change or roughly between 50% and 100% of change. But the change is 2 times or 3 times in the region between 0.021mm and 0.195mm from the fin.

Monitor lines ‘Por’ lies in the middle of the porous wall, from the cross centre toward the fin. ‘Por-0.5’ means the line is 0.5mm away from the inlet and ‘Por-9.5’ is located at 0.5mm from the outlet, that the distance in the x-direction is 9.5mm from the inlet. Below figure is velocity magnitude inside the porous wall in Z-direction, one is 0.5mm from the inlet, and the other one is 0.5mm from the outlet. In this figure, inlet velocity is 0.3m/s, z/L=0% is at the centre point of the porous wall cross, and z/L=100% is right below the fin.

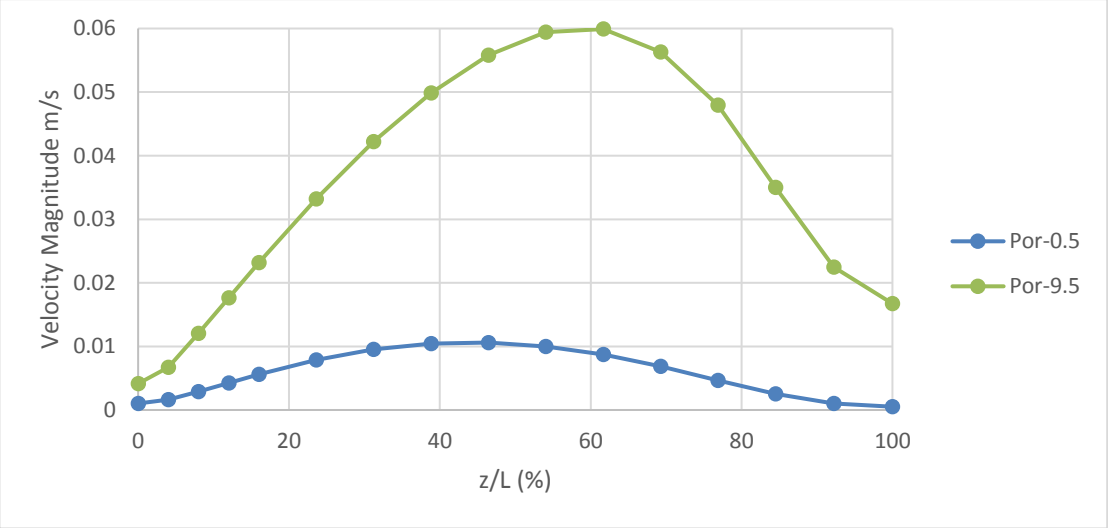

Figure 5-48: Velocity Profile on The Porous Wall at Both Ends of The Channel (v=0.3m/s)

At the inlet region, the peak velocity appears almost in the centre of the monitor line, and it is about 46%. The reason is that the flow still in the entrance region, it is not yet fully developed. Therefore there is little difference between the velocity value in the corner and the value on the wall. After a short distance through the porous wall, it becomes developed flow profile. The peak velocity location,46%, is the middle point in the outlet channel when the fin is considered as a solid material. In the outlet region, the velocity profile is in a similar situation but with much larger values.

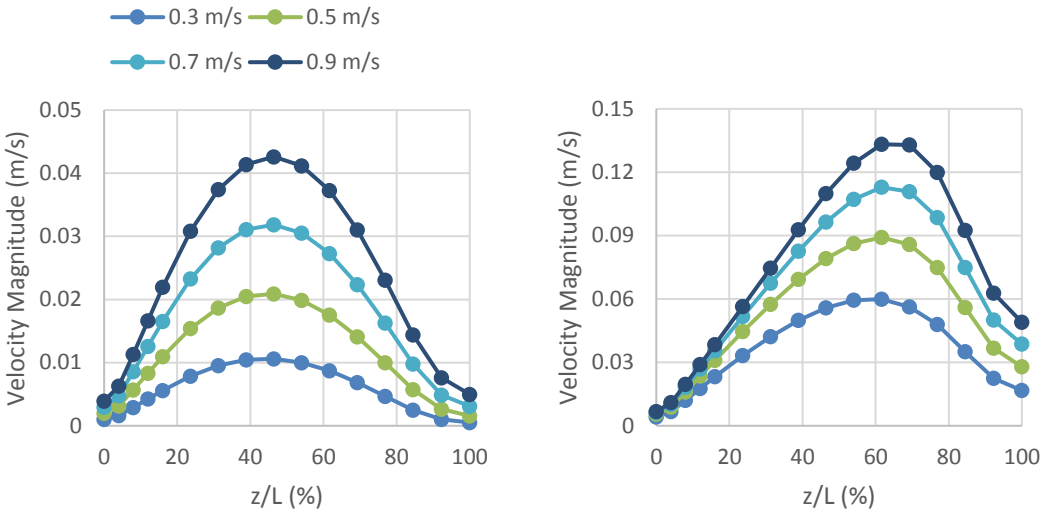

Figure 5-49: Velocity Magnitude in Porous Wall (left: x=0.5mm, right: x=9.5mm)

As plotted in Figure 5-49, velocity inside the porous wall at the outlet end is faster than that at inlet end in whole inlet velocity range from 0.3m/s to 1m/s. when inlet velocity increase, velocity profiles in both cases stay the same, and the value increases accordingly. However, the difference of velocity value between these two location changes as inlet velocity change.

The relation is plotted in Figure 5-50, using the peak value from the outlet region (Por-9.5) divided by the peak value from the inlet region (Por-0.5). As the figure shows, outlet result is more than 5 times of the inlet result when inlet velocity is 0.3m/s, and it decreases as inlet velocity goes up. The changes in these multiple values in the low-velocity range (0.3-0.6m/s) is higher than the value in the high-velocity range (0.7-1.0m/s). In a reaction rate dominated situation, about 4 times more NH_3 and NO_x are reacted in rear-end porous wall compares to front end porous wall.

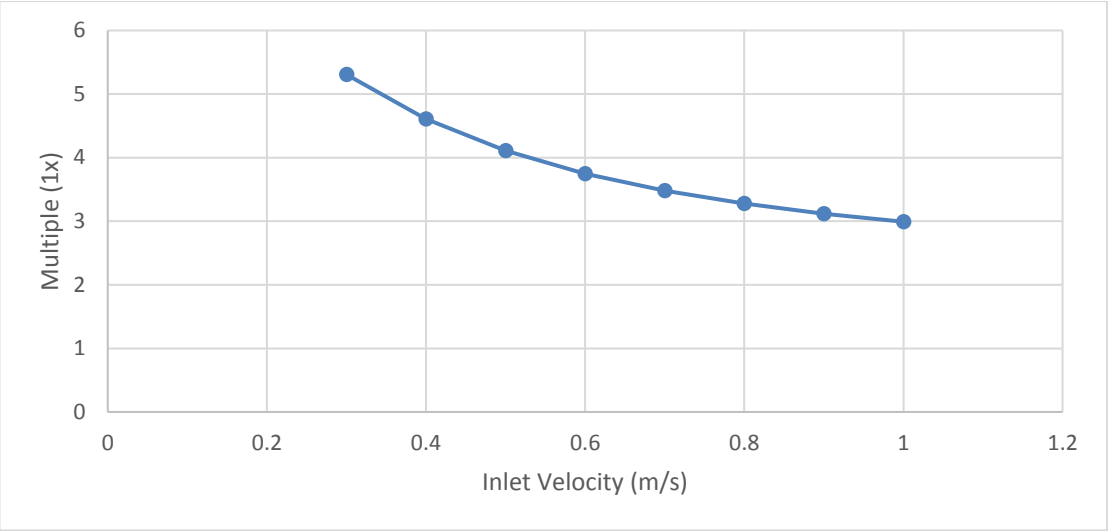

Figure 5-50: Velocity Difference Between Por-9.5 and Por-0.5

At the low-velocity range, the relative velocity at the outlet is much higher, that means the majority of mixture gas goes through from rear end porous wall. Local reaction rate improvement can be a solution to increase the overall performance of the complete catalyst.

The data from below figures (Figure 5-51, Figure 5-52 and Figure 5-53) are collected from one of the wall surfaces in inlet channel, and the wall surface is equally divided into 10 sections, the length of each section is 1mm. Section 1 is the first 1mm of the surface from the inlet, and section 2 is the second 1mm area which is from x=1mm to x=2mm and section 3 is from 2mm to 3mm area and so on.

Mass flow rate data is extracted from each of the sections. By definition, the mass flow rate through an interior surface is computed by summing the dot product of the density times the velocity vector and the area projections over the faces of the zone. When the same fluid is on both side of the wall surface, the data is less accurate than those wall boundary zones due to the inconsistency of area vectors as the flux for a cell face is

calculated with respect to its area vector. This inconsistency causes computation error when summing up the dot products.

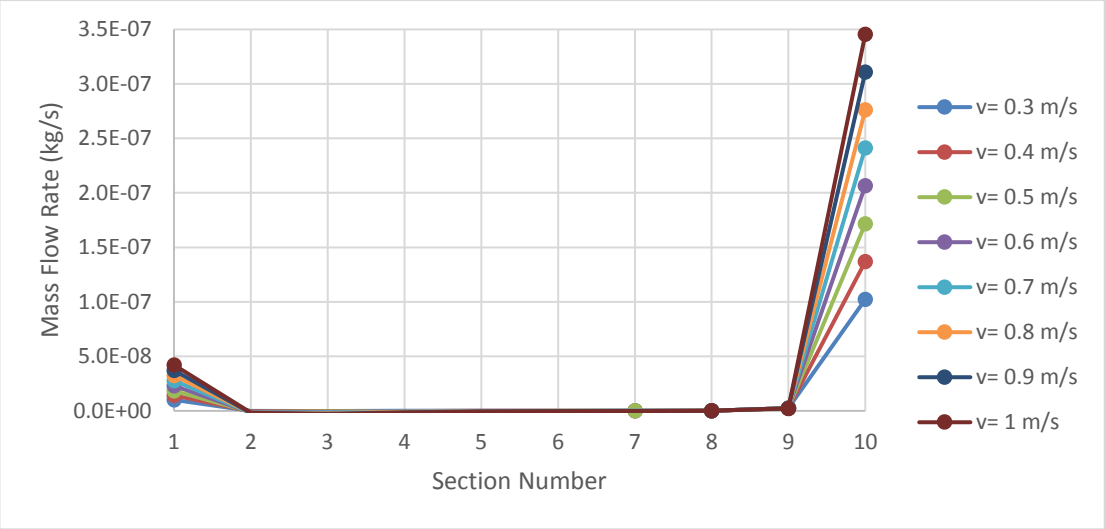

Figure 5-51: Mass Flow Rate on The Surfaces of The Inlet Channel (positive values)

Figure 5-51 shows the mass flow rates in each of the sections under inlet velocity from 0.3m/s to 1m/s. The highest mass flow rate is in the last section which is the outlet region. Although the inlet region has the second highest rates, it is 7 times lower than the values in the outlet region.

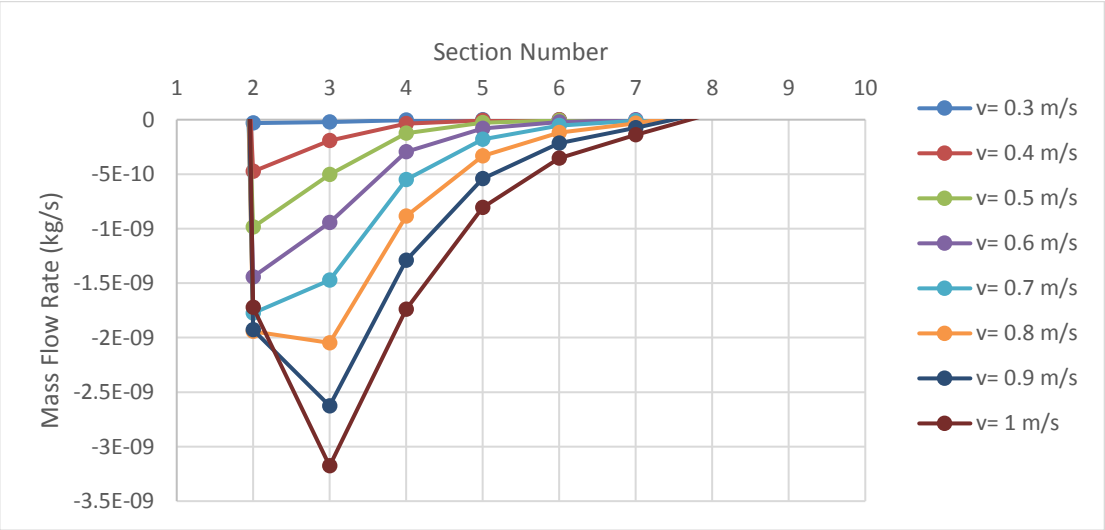

Figure 5-52: Mass Flow Rate on The Surfaces of The Inlet Channel (negative values)

Figure 5-52 shows the negative values of mass flow rate on the surface, that indicates the fluid goes in other directions, more likely is downstream in the X direction, rather than pass through the porous walls to the outlet channel. Moreover, the values on the negative side are minimal and can be neglected here.

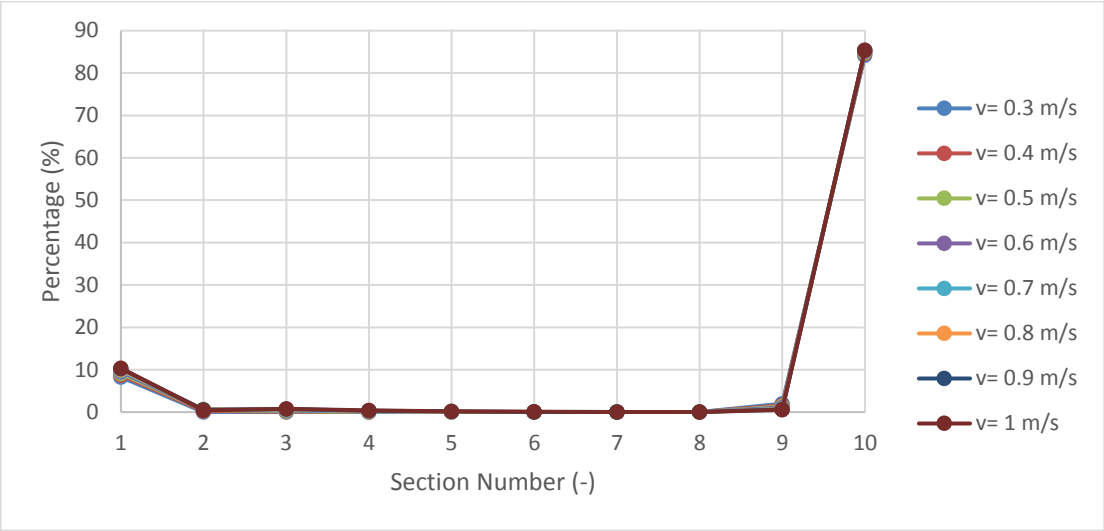

Figure 5-53: Mass Flow Rate Distribution on The Surface of Inlet Channel

In order to quantify the mass flow on the surface of the inlet channel, Figure 5-53 is plotted. The flow rate on each of the section is compared to the inlet mass flow rate, and the result is shown in percentage. As the figure, all inlet velocities have very similar distribution on the surface of the inlet channel, change of inlet has no effect on flow distribution on the surfaces in the inlet channel.

5.2.4 Species Distribution

For the species concentration along the channels of WF-Fin. Results of NH_3 level at 100°C, 200°C and 300°C with 0.3m/s inlet velocity is shown in Figure 5-54. Because in this case, the profile of the ammonia level is almost the same for 300°C, 400°C and 500°C. The results in this figure can be divided into 3 groups, and one is the result at low

temperature, 100°C, the second one is the mid-temperature at 200°C and high temperatures for 300°C and above.

Low-temperature performance is low and difficult to tell the difference. NH_3 level in the first 10% of inlet channel is the same as the WF model, but WF-Fin has higher NH_3 concentration in the rest of the inlet channel, although inlet conditions are the same. It is an opposite situation in the outlet channel, WF-Fin has lower NH_3 level for 95% of the length, and the last 5% is similar to the WF model. The result at 300°C is in the same situation as 200°C case, and the difference is NH_3 level in outlet channel drop to 1ppm at 25%, compared to 50% for WF model.

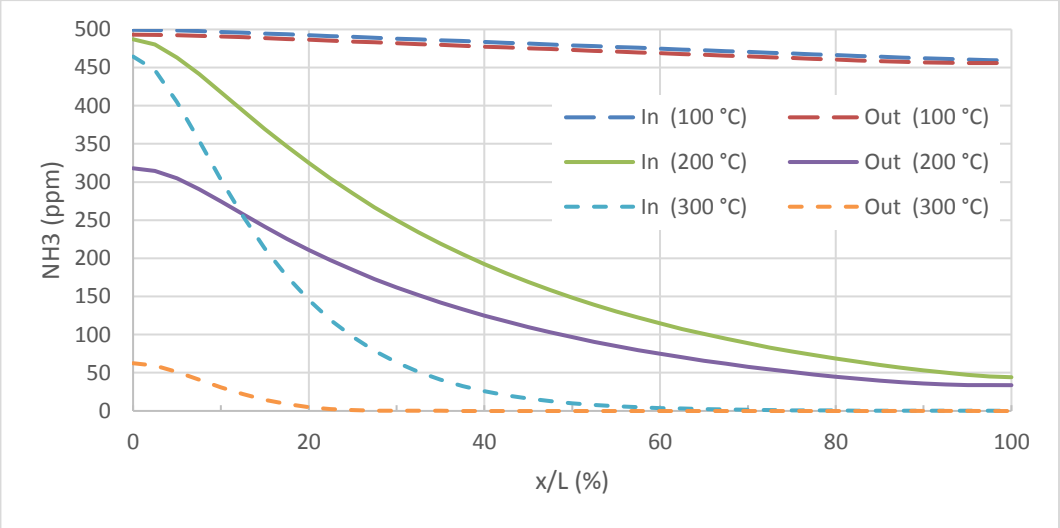

Figure 5-54: NH_3 Level (v=0.3m/s) for WF-Fin

In NO level result in Figure 5-55, only the results of 200°C and 300°C are focused as they are typical cases. At 200°C, NO conversion is not yet limited due to lack of NH_3, NO level at x=0 in outlet channel is about 318ppm and gradually falls to 36.7ppm at the end, whereas 360ppm and 38.2ppm in WF model, the difference is 42ppm in the front part, and 1.5ppm in the rear end.

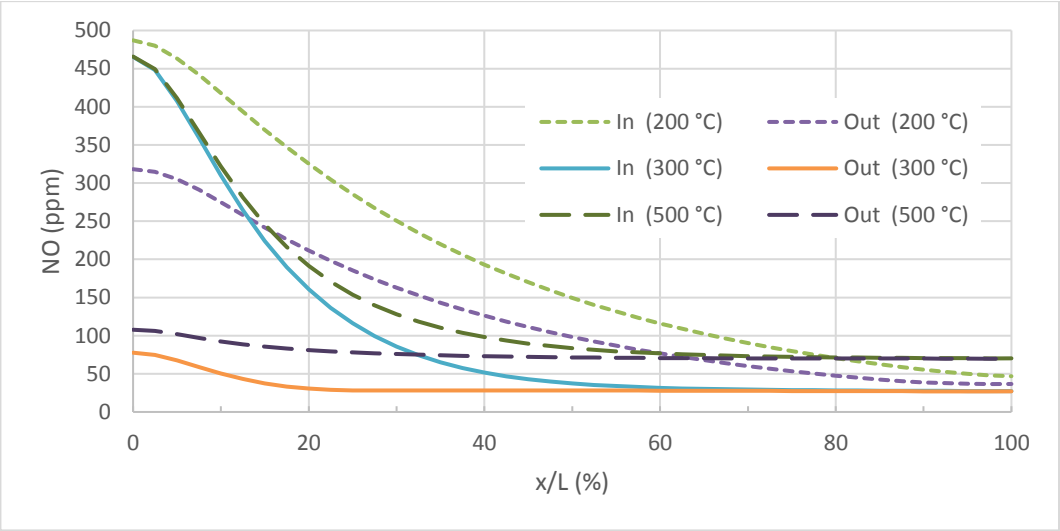

Figure 5-55: NO Level (v=0.3m/s) for WF-Fin

At 300°C and above, NO level in inlet channel is similar to each other with only less than 10ppm difference, but the NO level in outlet channels of WF-Fin catalyst is affected by ammonia oxidation, higher temperature, more NO is left in the outlet.

When compared to the WF model, WF-Fin in low temperature performs the same, at the mid-temperature, it consumes more NO species in the front section, but poor performance in the rear section.

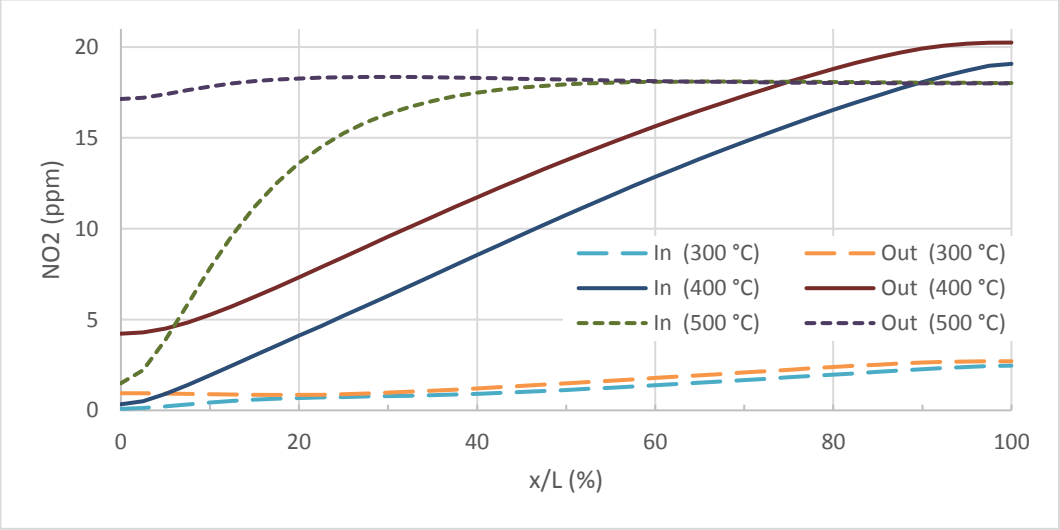

Figure 5-56: NO_2 Level (v=0.3m/s) for WF-Fin

Figure 5-56 shows NO_2 level in the channels. NO_2 level at a temperature below 300°C can be neglected due to low reaction rate and little to none impacts to overall performance. It kicks in at 400°C and has a clear impact on NO conversion performance with only 20mm in the last 10% of the outlet channel. At 500°C, the production of NO_2 rapidly increase in the front section of the inlet channel and stops at the middle. This is because no more NO is available from this point and no more NH_3 neither for any further reaction. Thus, that amount of NO_2 flows directly to the outlet.

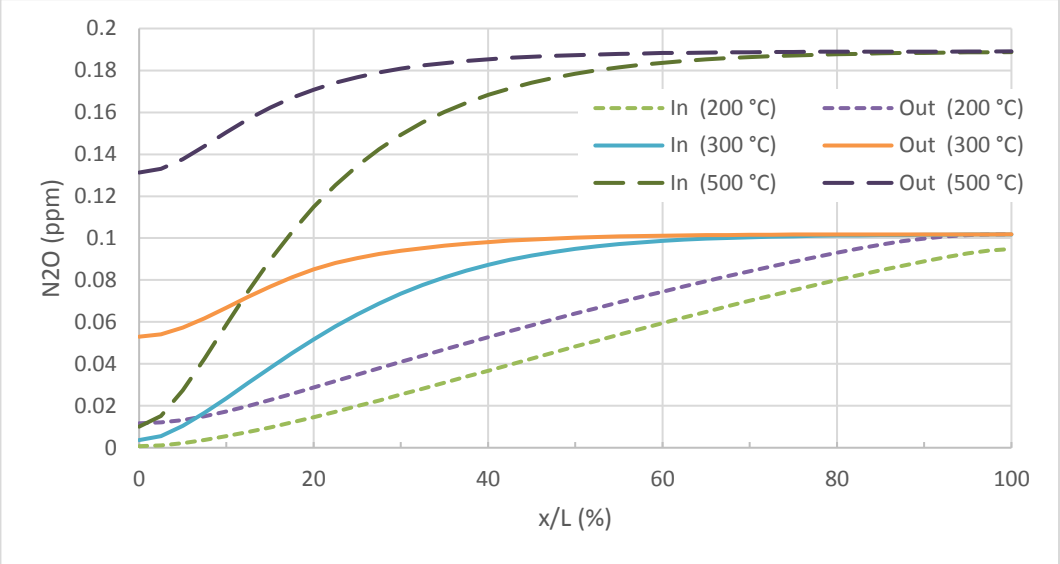

Figure 5-57: N_2O Level (0.3m/s) for WF-Fin

The results of the unwanted side product, N_2O, is plotted in Figure 5-57. With maximum composition less than 0.2ppm at 500°C, N_2O formation rate is very small, and the amount of quantity has an insignificant effect on system performance. It therefore neglected.

In overall, a more significant difference between the inlet and outlet channel of WF-Fin model means a larger amount of species are reacted in the front part of the catalyst, but the performance in rear section is rather poor even under mid-temperature range. So, the poor performance of WF-Fin in rear section gives the WF model a chance to catch up and ends up with a very similar overall conversion rate in the outlet.

5.2.5 NH_3(S) in Porous Wall

In terms of NH_3(S) in the porous wall, two sets of results are produced under the same boundary conditions and plotted for the same monitor line. The monitor line is located in the centre of the porous wall, it can be representative monitor line in WF model, but might not be that much representative in WF-Fin model as a solid fin is added to outlet channel and it crates obstacle and affects the direction of the flow and species. Moreover, this is only the NH_3(S) in the porous wall, and there is an extra surface area on the fin for NH_3(S) adsorption. This is discussed in a later section of fins effects.

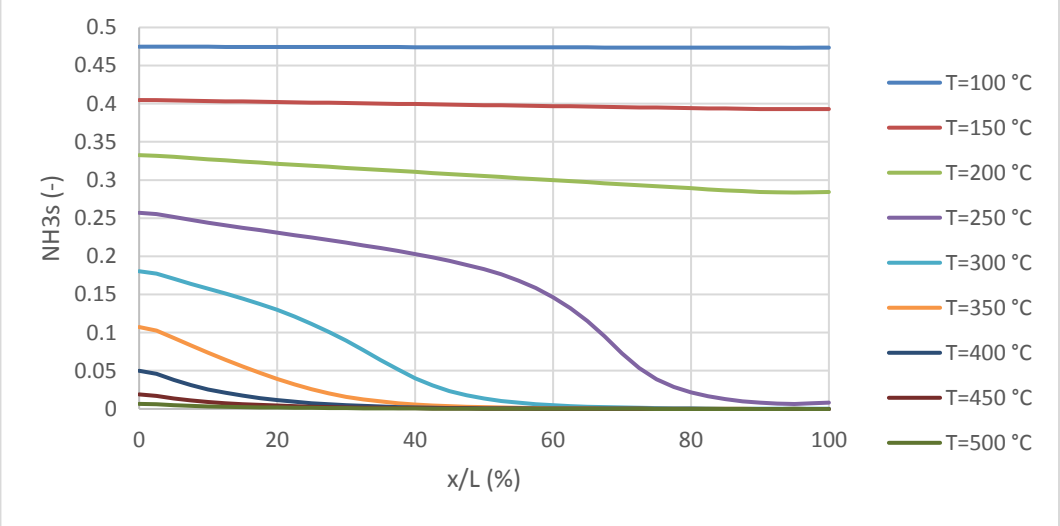

Figure 5-58: NH_3(S) Level in The Porous Wall (0.3m/s) for WF-Fin

Figure 5-58 shows the effect of temperature change on the NH_3(S) level in the porous wall. General speaking, overall profile and tendency along with channel length of WF-Fin NH_3(S) in the porous wall is the same as in WF model, the difference is NH_3(S) level in WF-Fin model is around 1% higher than WF model ina middle-temperature range of 200°C to 300°C. But it performs the same at both low and high-temperature range. For the middle section porous wall at 250°C, 300°C and 400°C, the falling of NH_3(S) level

are slower and smoother than that in the WF model. These little differences are most likely caused by an extra fin in the outlet channel.

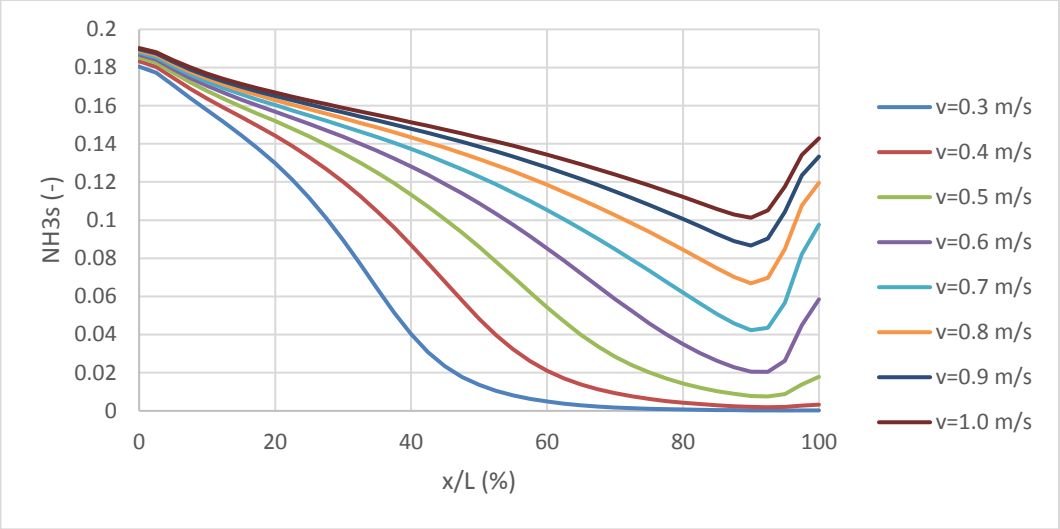

Figure 5-59: NH_3 Level in Porous Wall at 0.3m/s to 1.0m/s (300°C) for WF-Fin

In regarding velocity effect, the results are plotted in Figure 5-59. WF-Fin model performs pretty well compares to the WF model. The maximum level of NH_3(S) is the same, and they also fall along the channel length. The different is, the falls are less steep as in the WF model. It withstands the change of velocity. However, based on the result above, it cannot say that the NH_3(S) level in the whole catalyst withstands velocity change as the monitor line in WF-Fin is less representative.

5.2.6 Reaction Rates

Reaction rates in this section mainly refer to the reaction rates in the porous wall. As in the reaction rate section of the WF model. The same reactions are selected to demonstrate

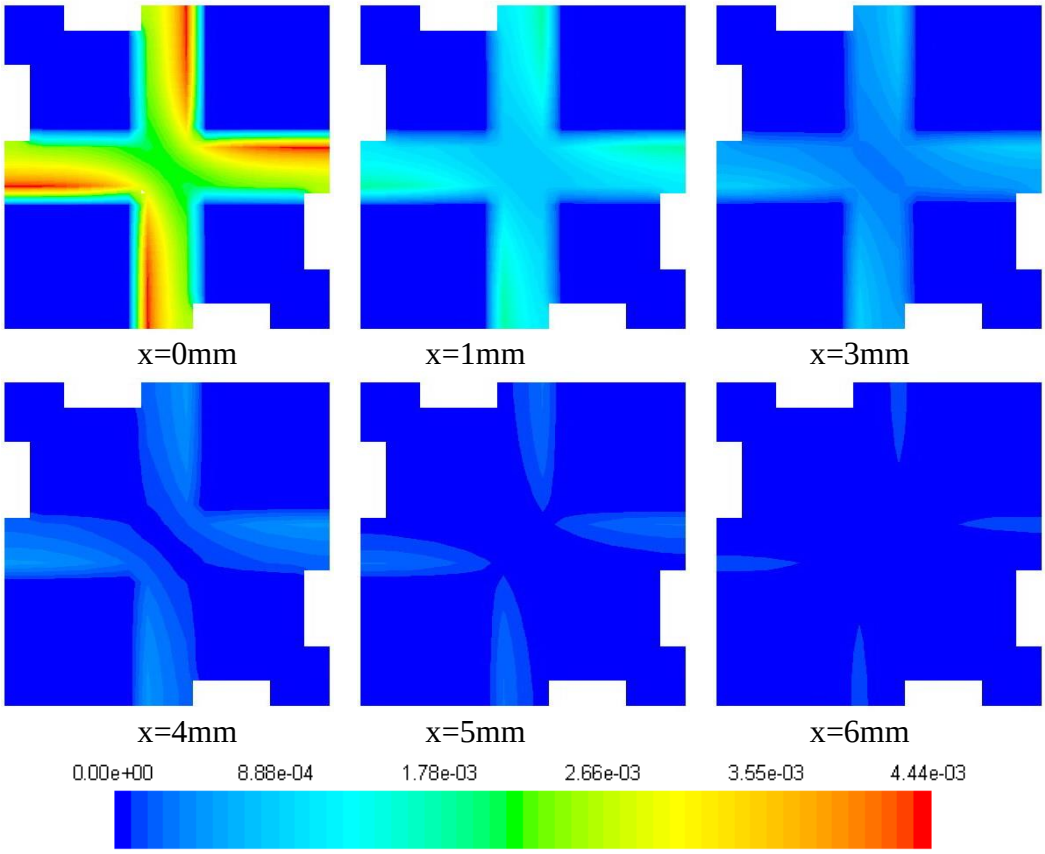

Figure 5-60: Overall NH_3 Adsorption Rate in Porous Wall for WF-Fin

Start with overall NH_3 adsorption, in Figure 5-60, the profile of the reaction rate is the same as is in the WF model. Only the maximum rate is 0.00444 kgmol/m3-s, in this case, compare to 0.00498 kgmol/m3-s in WF model. Besides the 10% reduction at peak reaction rate, there is not much difference.

The same thing happens to standard SCR reaction, and ammonia oxidation, Figure 5-61 and Figure 5-62, reaction rate profile is unaffected, and peak reaction rate drops 10% compared to the rate in the WF model. Since boundary conditions are the same, only variable in reaction rate the concentration of species. So, a possible reason is adding extra fins leads to a change of flow profile and species concentration.

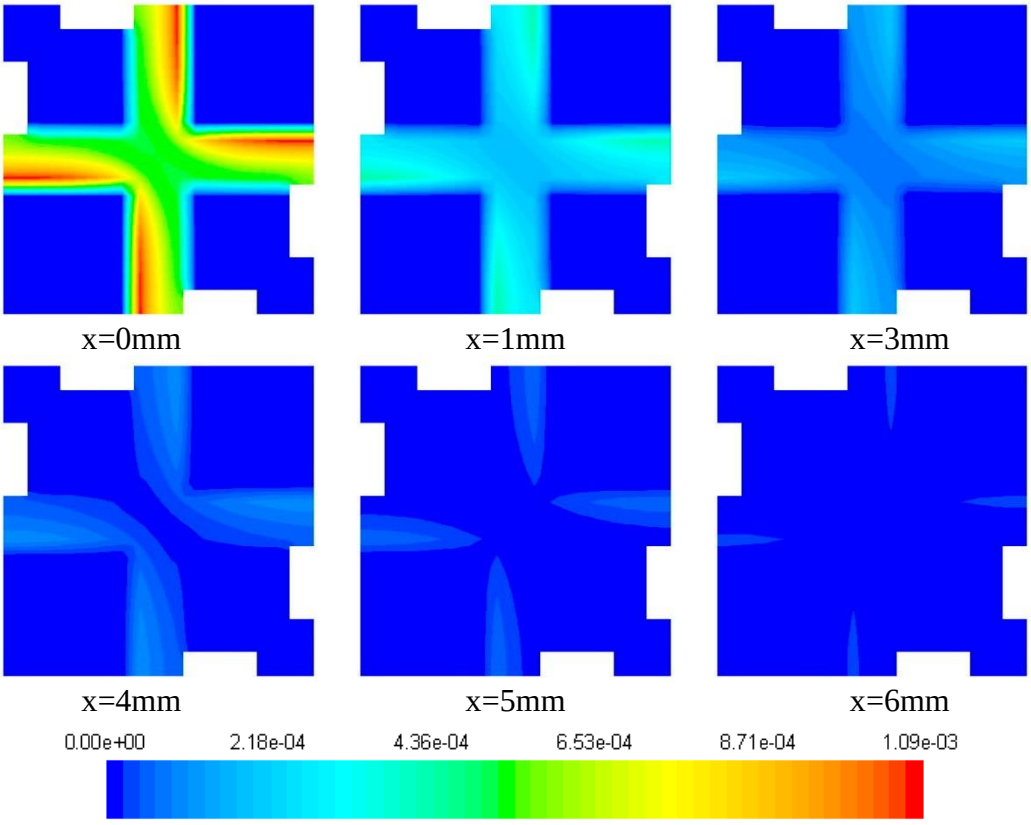

Figure 5-61: Standard SCR Reaction Rate in Porous Wall for WF-Fin

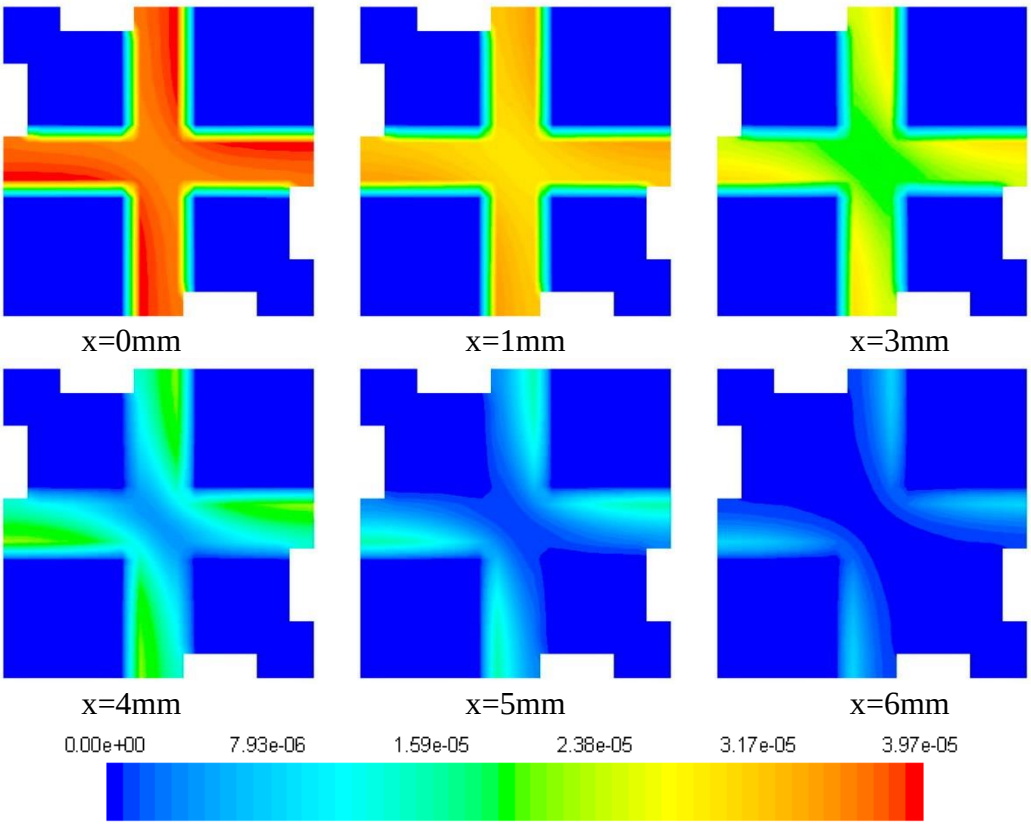

Figure 5-62: Ammonia Oxidation Rate in WF-Fin Porous Wall

5.2.7 Fins Effects

Extra fin in the outlet channel is proved to make a positive difference over the WF model, although it is only for the front part of the catalyst. In this section here, reaction rates contour on the side wall of the fins is displayed for ammonia adsorption and oxidation. In early sections, standard SCR reaction has almost identical reaction rate profile to ammonia adsorption reaction rate profile in the porous wall for both WF and WF-Fin models, for this reason, only two reactions are selected to display.

Below contours, in Figure 5-63,are overall ammonia adsorption on one of the side walls of the fins. While inlet velocity increase from 0.3m/s to 1.0m/s, peak overall ammonia adsorption has increased as well, but that high reaction rate region stays on the inlet side of the fin for all inlet velocities.

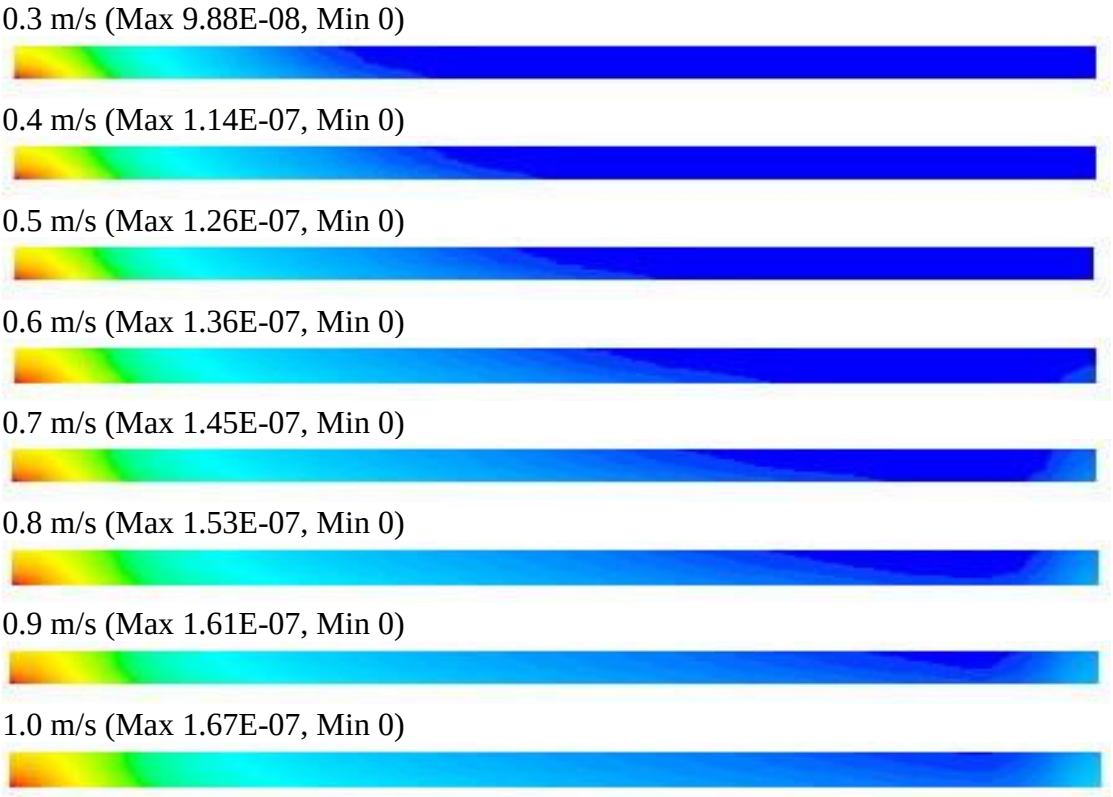

Figure 5-63: Overall NH_3 Adsorption On The Side Wall Of The Fin (300°C)

A possible reason for this situation is that the velocity is a porous wall is high on both ends of the channel, and mass flow rate also indicates nearly 95% of flow pass through the porous wall from these two regions. Velocity and mass flow rate are very low in the middle section of the channel. Therefore, it is not surprising high ammonia adsorption appears in these two regions. And due to the fast reaction rate, the majority of ammonia is absorbed and reacted within the front section of the channel under the current velocity setting. And there is chance NH_3 can reach to the middle and rear part of the fin if velocity is high enough, as indicated by NH_3(S) in the porous wall of WF model under various inlet velocity in Figure 5-10.

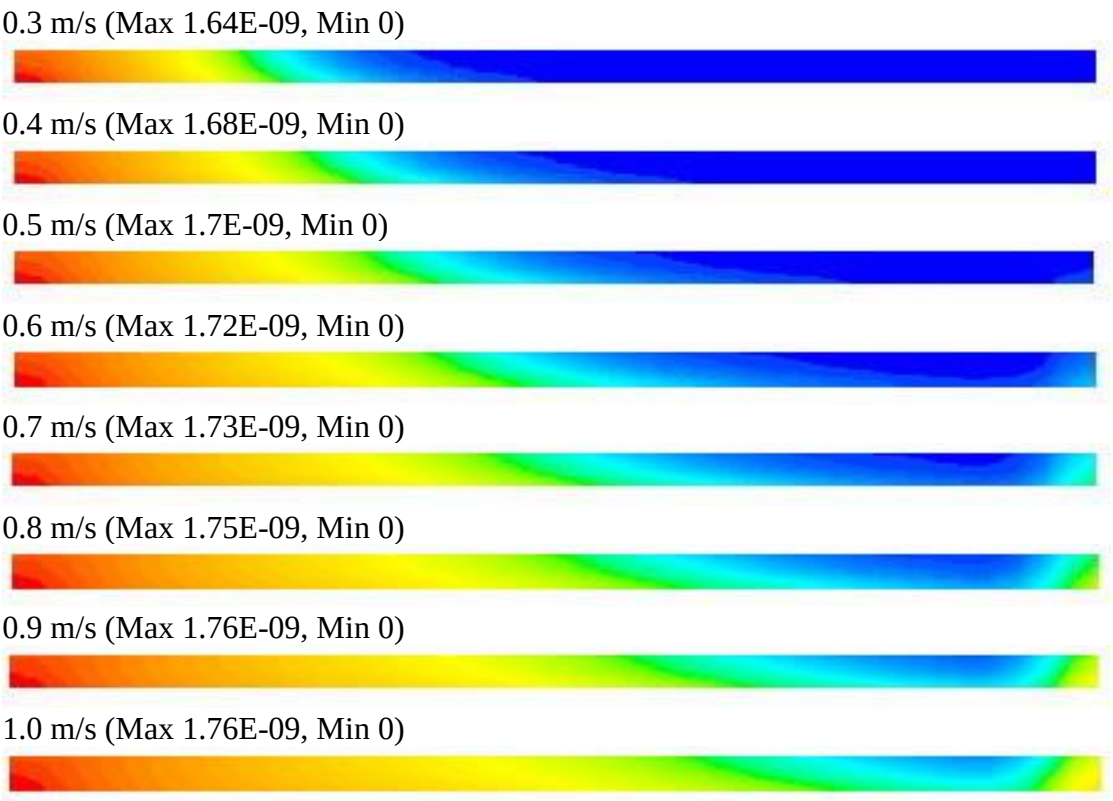

Figure 5-64: NH_3 Oxidation Rate on The Side Wall of The Fin (300°C)

In earlier result, ammonia oxidation has a negative effect on NO conversion at the high-temperature range. That effect is slightly enlarged after employing the fins in the outlet channel. This can be explained with the contour of the NH_3 oxidation rate on the fins. Roughly a quarter of the side area on the fin participates in NH_3 oxidation at 0.3m/s. and

the usage of fin surface increases to more than 80% at inlet velocity 1.0m/s. Such high usage of fin surface for NH_3 oxidation can be good and bad. The good side is high ammonia dosing can be used, excessive NH_3 can be oxidised by the rear section of the fins, but the downside is that it makes SCR reaction harder to control under high-temperature range.

Surface reactions also take place at the top of the fins, standard SCR reaction rate is shown in Figure 5-65 as an example, for the case of 300 °C and velocity is 0.3m/s for the top contour and 1.0m/s is for the bottom contour. Reaction rate varies with NH_3(S) on the surface and nearby NO concentration in the range between 2.38E-08 and 4.09E-08, the peak rate is on the far left and drops along the length toward to outlet.

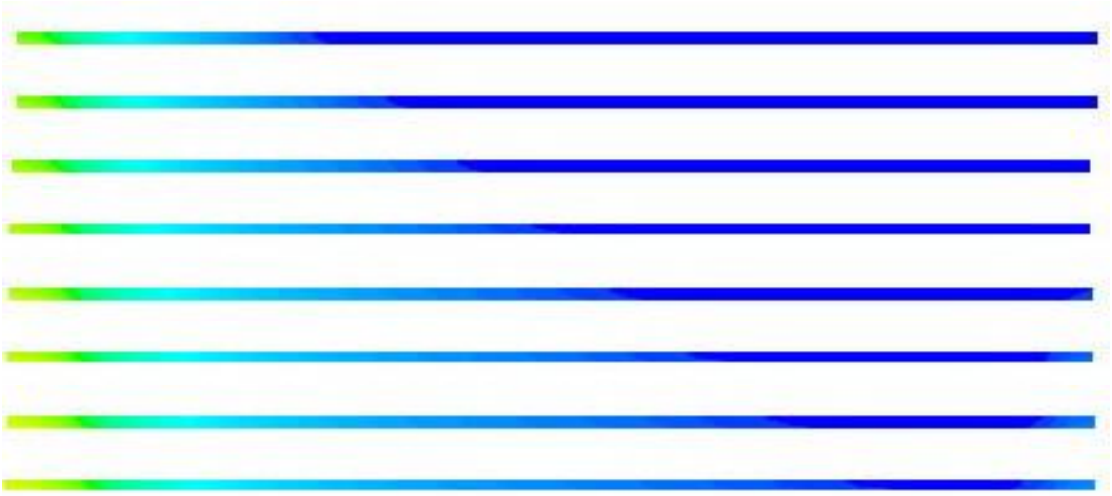

(Top to Bottom 0.3m/s – 1.0m/s)

Figure 5-65: Standard SCR Reaction Rate on The Top Surface of The Fins (300°C)

Based on these results, adding extra fins have an actual contribution to SCR reductions, especially in the front part of the channel. But the performance falls along channel length, and it falls faster than the case in the WF model. That causes WF-Fin to have similar overall performance as the WF model.

5.3 Summary

In this chapter, the results of Wall-Flow model and Wall-Flow-Fin model are presented. Inlet temperature range from 100°C up to 500°C at 50°C increment and inlet velocity is between 0.3m/s and 1.0m/s. Two inlet conditions were considered: underdose and overdose of NH_3. The results include NO, NH_3 level and reduction along the channel, the conversion at the outlet, as well as NH_3(S) on the wall surface and inside the porous media.

Based on the results, one location requires more attention. That location is the porous wall near the outlet. the NH3s level in the porous wall near the outlet. When temperature increase while the inlet velocity is fixed, for both cases, the NH_3(S) in the porous wall near the outlet is consumed first, and then it moves toward to the inlet part as temperature increase. Moreover, this area has the highest mass flow rate compared to the other part of the wall. As a result, this location has great potential to convert more NH_3 or NO.

6. Performance Comparison

In this chapter, the performance of the NO_x conversion rate under clean catalyst condition from FT, WF and WF-Fin models are compared. Several conditions are considered during the comparison, NH_3 underdose, NH_3 overdose, NO:NO_2 ratio variations and so on. Since the aim of this study is to optimise the NO_x conversion rate, the species' level on the outlet surface is used as a major indicator. Other performance factors are also compared and discussed.

6.1 Result Comparison

The first comparison case is three models are run with a mixture of 500ppm NH_3, 500ppm NO and 8% O_2 at the inlet. Temperature range from 100°C to 500°C at 100°C increment and inlet velocity is 0.15, 0.25, 0.35 and 0.45m/s.

In NH_3 conversion, as in Figure 6-1, all three models have the same performance drop due to velocity increase, especially at a temperature below 300°C. The reason is the residence time of the species is lower at higher velocity rate. The residence time is not enough to allow a complete reaction of all the reactants if the reaction rate is low. At some point, higher than 300°C in the case here, the reaction rate is fast enough to finish the reaction of all available reactants within the residence time. Therefore, the increase of inlet velocity has a great impact on the low-temperature range as the reaction rate is low, and it has less effect on the high-temperature range due to much faster reaction rates.

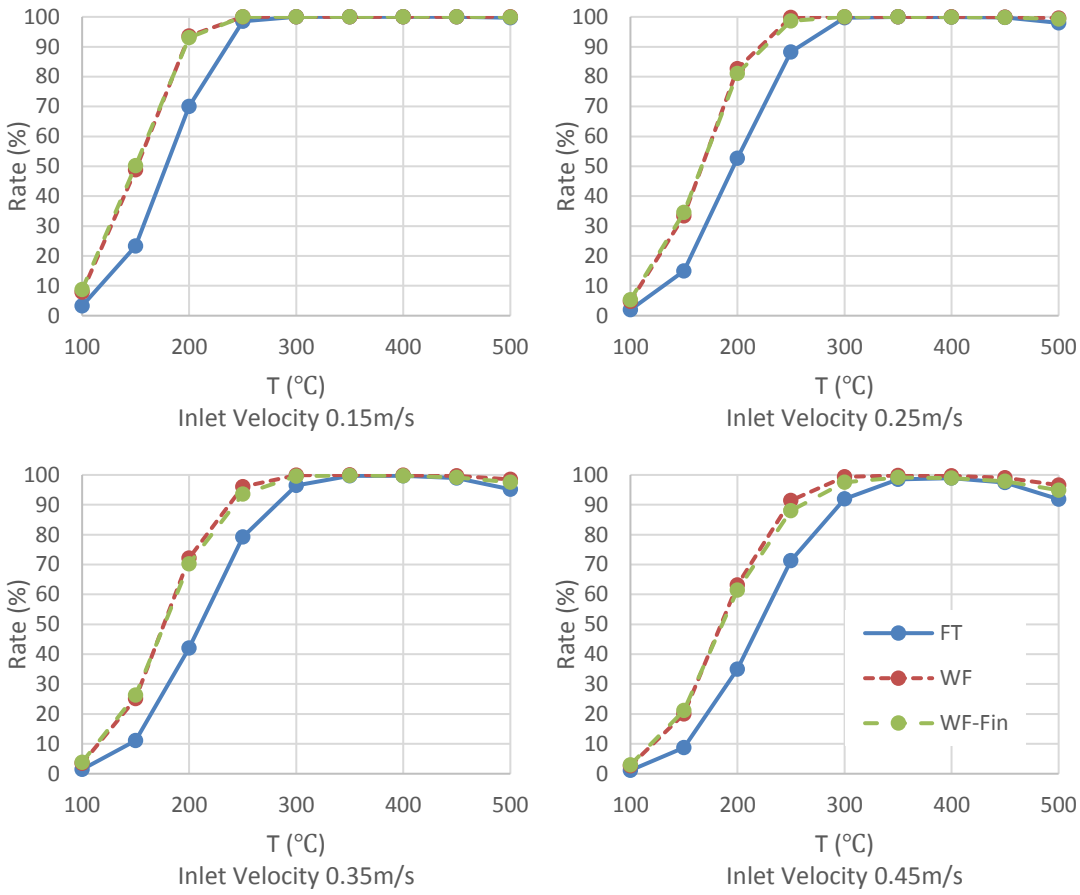

Figure 6-1: NH_3 Conversion Rate Comparison (NH_3 Insufficient Condition)

Also, all models start to have slightly drop of NH_3 conversion rate at 500°C from inlet velocity 0.25m/s and above. Along with this NH_3 drop, there is little sign of an extra decrease in NO conversion rate at velocity 0.45m/s in Figure 6-3. Decrease of NH_3 and NO conversion rate at 500°C is due to the change of flow velocity.

In regarding NO conversion, condition the rate starts dropping from 300°C. One reason is insufficient NH_3 for deNO_x reactions. The other one is that NH_3 oxidation rate is faster than SCR reactions, as in Figure 6-2, thus upstream NH_3 in the mixture is oxidized before other deNO_x reactions take place.

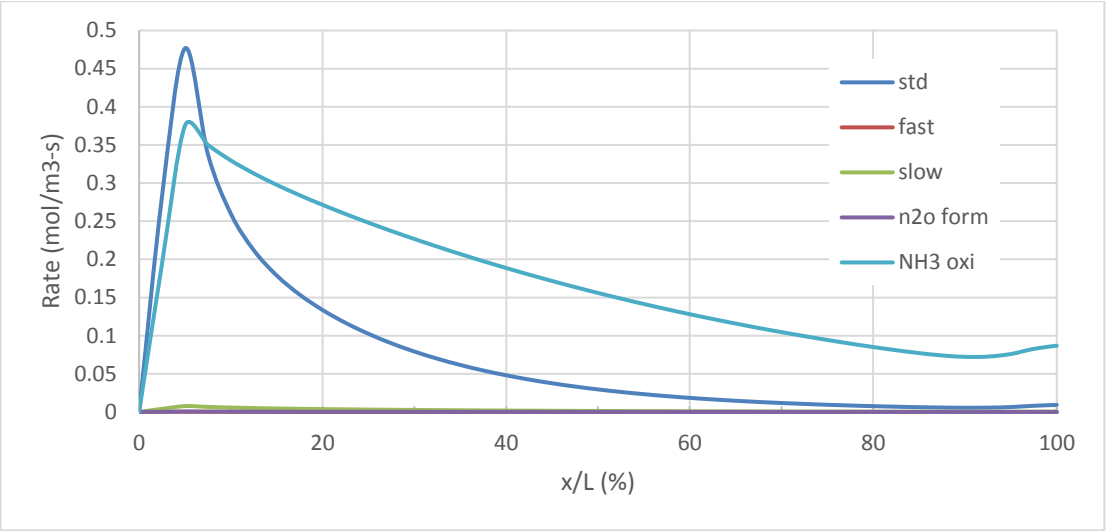

Figure 6-2: Reaction Rates in Porous Wall, WF-Fin Model (0.5m/s, 500°C)

Regarding temperature change, 250°C to 300 °C is a performance threshold for NO conversion. Below such temperature, all models have a low NO conversion rate. Unless inlet velocity rate as low as 0.3m/s or lower, it only helps at 250 °C.

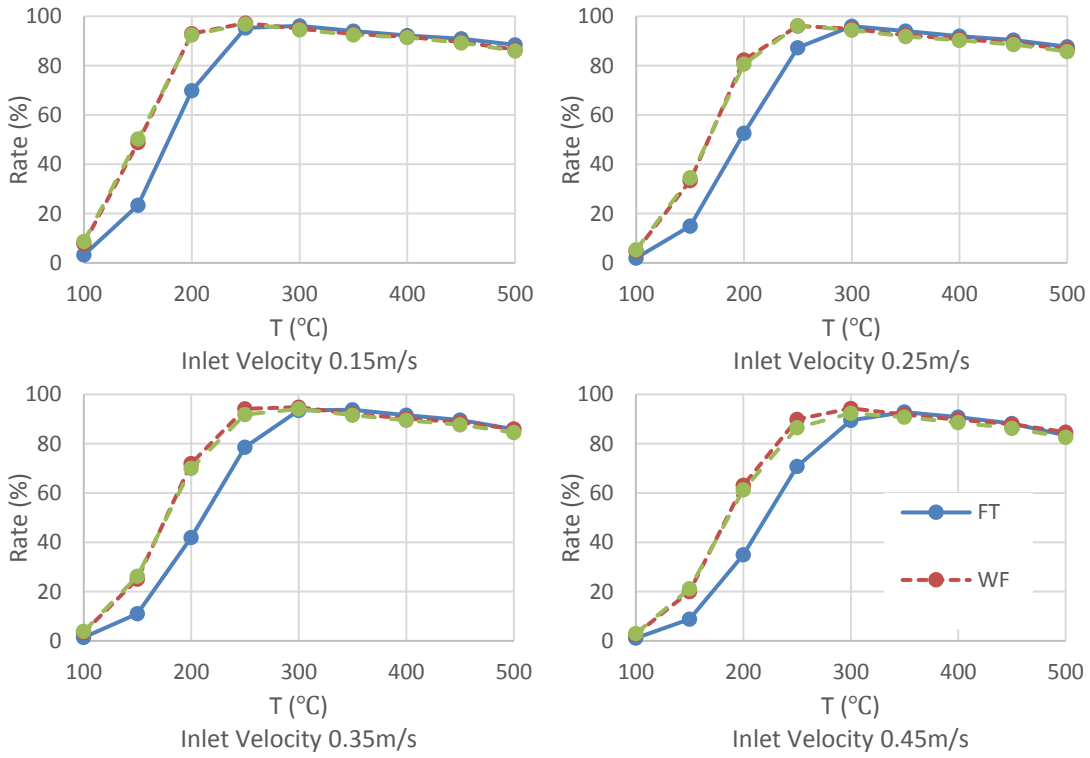

Figure 6-3: NO Conversion Rate Comparison (Insufficient NH_3 Condition)

Under the same condition, performance decline against inlet velocity change is plotted in the next figure, Figure 6-4. In this figure, v1, v2, v3 and v4 represent inlet velocity at 0.15m/s, 0.25m/s, 0.35m/s and 0.45m/s respectively. The label 'v2-v1 FT' means comparing of velocity v2 to v1 on FT model and so on. It clearly shows rising inlet velocity has a significant impact on NO conversion in the low-temperature range. Three models start at a similar level at 100°C, where velocity is increased from 0.15m/s to 0.25m/s, performance decline around 39%. However, WF and WF-Fin model have 31.6% and 31% decline rate and the FT model still has a 36% decline rate as temperature goes up to 150°C. In overall, inlet velocity has the most significant impact on FT model below 300°C. The second one is the WF model which is only around 1% worse than WF-Fin model. At 1% difference, it can be assumed they perform the same in this case.

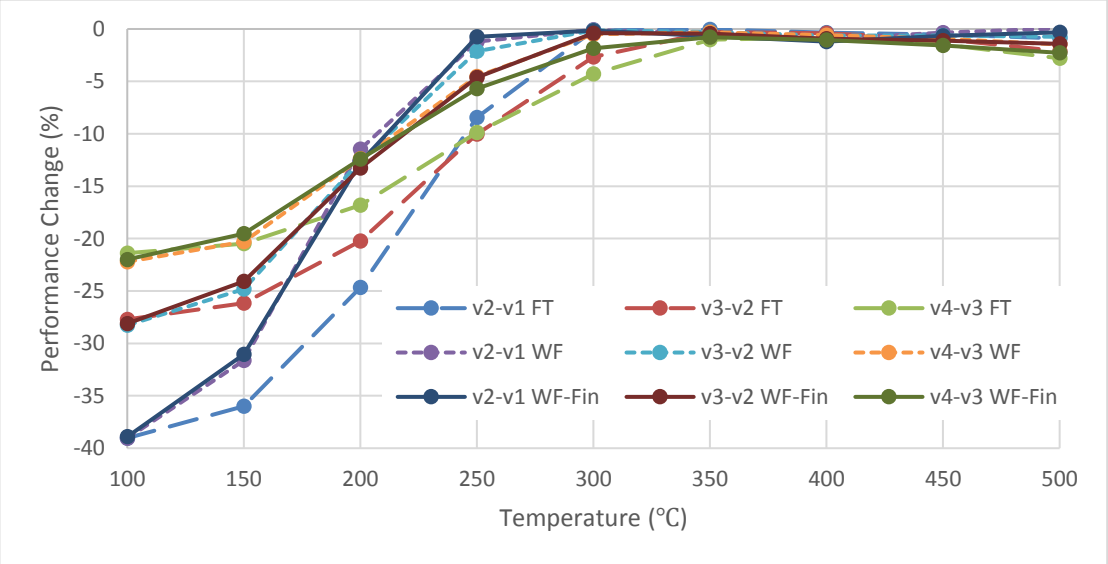

Figure 6-4: deNO Performance Decline Due to Inlet Velocity Increase

The following figure shows the improvement of the NO conversion rate when compare WF and WF-Fin model to the FT model. Both WF and WF-Fin models have remarkable improvement at low temperature, 100°C to 250°C in velocity range from 0.15m/s to 0.45m/s. However, this advantage is fading away as temperature rise. High performance

at low temperature is due to a large amount of active catalyst material in the porous wall and the structure of porous media. Catalyst material coating inside the porous wall provides an enormous amount of surface to SCR reaction, and porous wall reduces flow velocity as a fluid pass through; thus the reactants have longer resistance time on the catalyst surface.

In the high-temperature range, 350°C to 500°C, NO conversion rates of WF and WF-Fin models are about 2% lower than the FT model. It is likely that the FT model gains advantage from the flow-through structure; the higher reaction rate is achieved. Since this is under NH_3 insufficient condition, this situation is discussed in next section where high NH_3 concentration level is provided in the mixture to ensure enough NH_3 for SCR reactions, and reaction rates are plotted and compared.

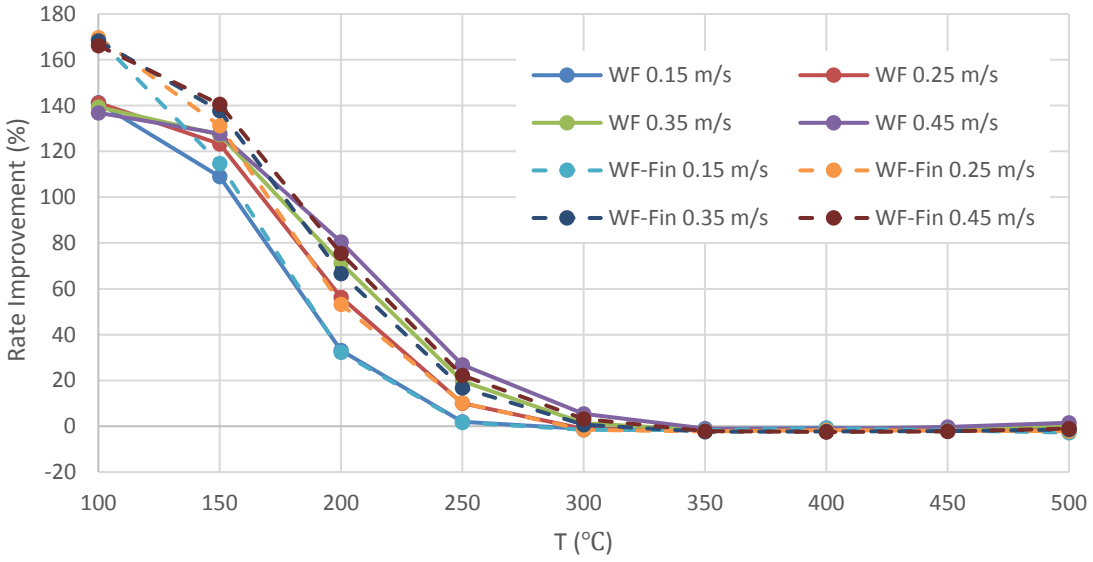

Figure 6-5: deNO Rate Improvement Comparison, WF and WF-Fin to FT

The overall performance of three models under NH_3 excess condition (1000ppm NH_3 from inlet) is compared and discussed in this section. Since inlet ammonia concentration is doubled, NO conversion performance at the high-temperature range is no longer limited

by insufficient ammonia level, so the output NO rate is more trustworthy compared to ammonia insufficient condition.

Figure 6-6 shows NO conversion rate under ammonia excess condition of all three models, inlet velocity range from 0.15m/s to 0.45m/s. It is quite clear that NO conversion rate of all three cases in the high-temperature range, 300°C to 500°C, maintenances at a very high level, 98% to 99.9%. Even with the fastest inlet velocity, NO conversion rates only fall 2.2%, 1.5% and 3% for FT, WF and WF-Fin model respectively.

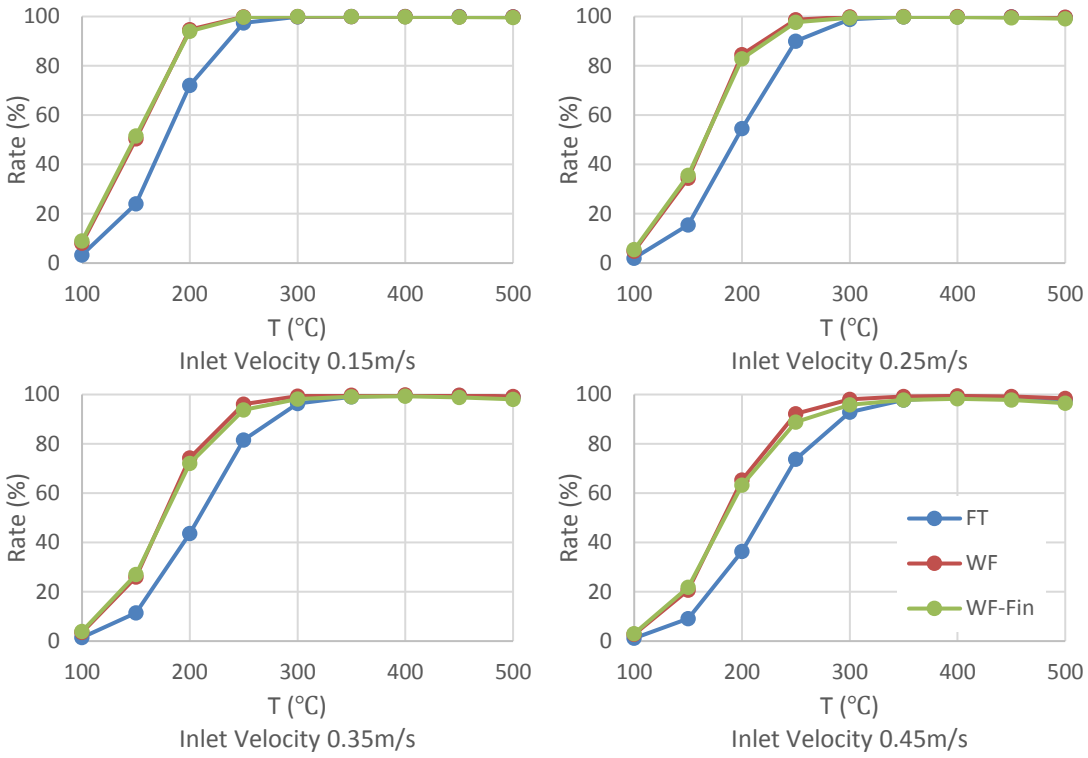

Figure 6-6: NO Conversion Rate (1000ppm NH_3 at the inlet)

Apart from the change in the high-temperature range, there is little change at 200°C to 250°C. By the average of all cases in 4 velocity rates, NO conversion rate is increased by 2.2% compared to the results of ammonia insufficient condition. In either condition, WF and WF-Fin models have very similar NO conversion rate in whole temperature range and under various inlet velocity, and both models only outperform FT model at a

temperature lower than 250°C. There is only a slight difference between them from 350°C and above.

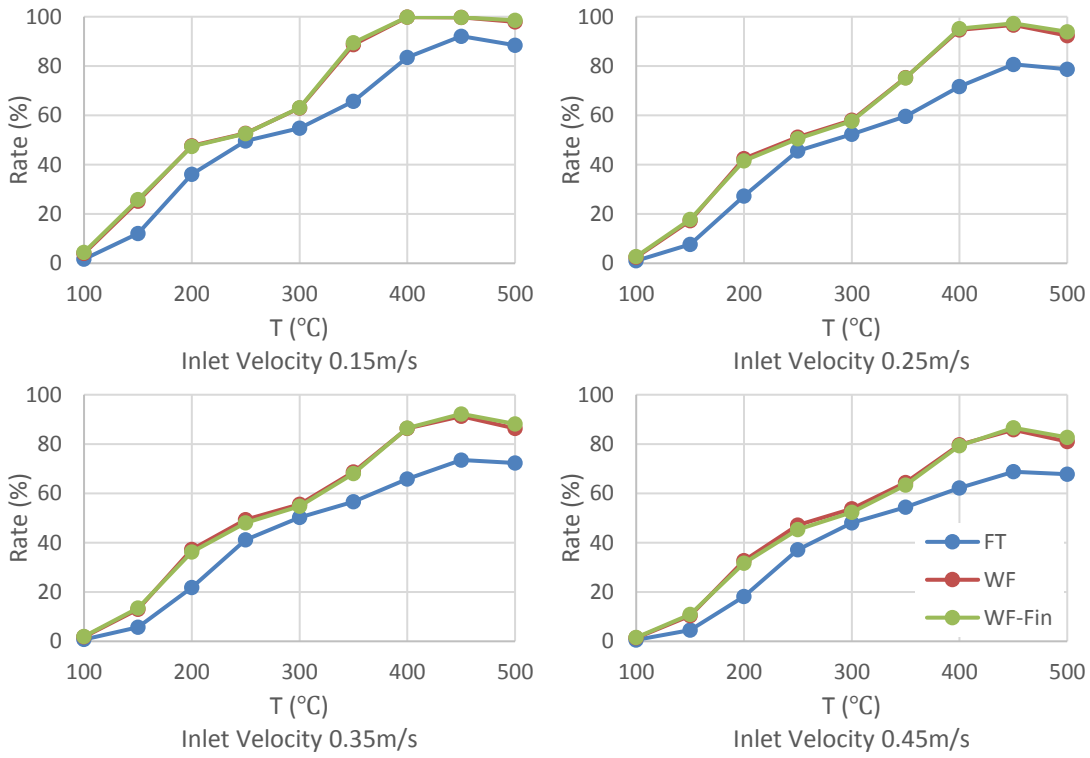

Figure 6-7: NH_3 Conversion Rate (1000ppm NH_3 at the inlet)

Since the ammonia level is much higher than the amount of needed, the ammonia conversion rate, in this case, is expected to be low. Ammonia level from the outlet is used as guidance for the capability to convert ammonia in such condition, or the actual amount of ammonia is required for complete NO conversion at high temperature.

The trend of ammonia conversion against velocity increase is the same as other cases: the rate decreases as velocity increase. In a direct comparison method, the difference of average ammonia conversion in 100°C to 250°C temperature range between velocity 0.15m/s and 0.25m/s is 4.47% for FT model, 4.07% for WF model and 4.41% for WF-Fin model. And in the temperature from 350°C to 500°C, this difference expands to 9.77%, 6.79% and 6.51% for FT, WF and WF-Fin model respectively. In short, velocity

has less effect on ammonia conversion in low temperature, 100°C to 250°C, it is a 4% drop for the first 0.1m/s velocity increase; in high-temperature range from 350°C to 500°C, it is almost 10% and 7% drop in conversion rate. However, this is compared directly by calculating the difference between the new value and the old value.

As velocity increase conversion rate drops dramatically between 400 and 500 for all cases. The effect is enlarged due to the excessive ammonia setting in the inlet mixture. as in Figure 6-1 only a few percentages

A more scientific way to quantify each of the values is shown in the next figure, Figure 6-8, the difference between the values is plotted as a percentage.

Every 0.1m/s increase in velocity is corresponding to speed increase of 66.67%, 40% and 28.5% for v2-v1 (0.15m/s to 0.25m/s), v3-v2 (0.25m/s to 0.35m/s) and v4-v3 (0.35m/s to 0.45m/s) respectively. Thus, the value of data line v2-v1 is lower than v3-v2 and v4-v3. Also, v3-v2 and v4-v3 are supposed to be closer to each other than to v2-v1.

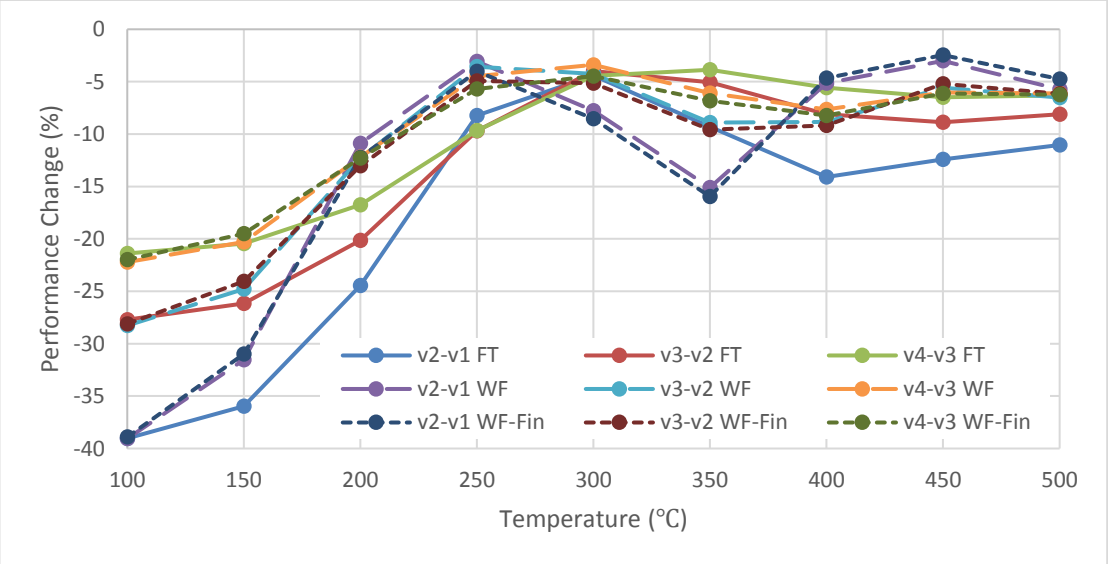

Figure 6-8: Inlet Velocity Effects on deNH3 Performance (1000ppm NH3 at the inlet)

It is more clearly in this figure that all models' performance decline nearly 40% at 100°C for the first velocity change. The performance climbs back as temperature increased, but the difference between WF (WF and WF-Fin) models and FT start to show. And at low velocity, performance recovery due to temperature increase (between 100°C and 250°C) is very fast, the gradient of this recovery becomes smaller at higher inlet velocity. At high-temperature range from 300°C, performance decline of all three models is between 5% and 10; few cases have 15% performance drop.

Despite the fact that ammonia conversion rate drops at a similar level at high temperature for all three models, WF (WF and WF-Fin) models are less affected by velocity change in almost all temperatures condition, except 350°C.

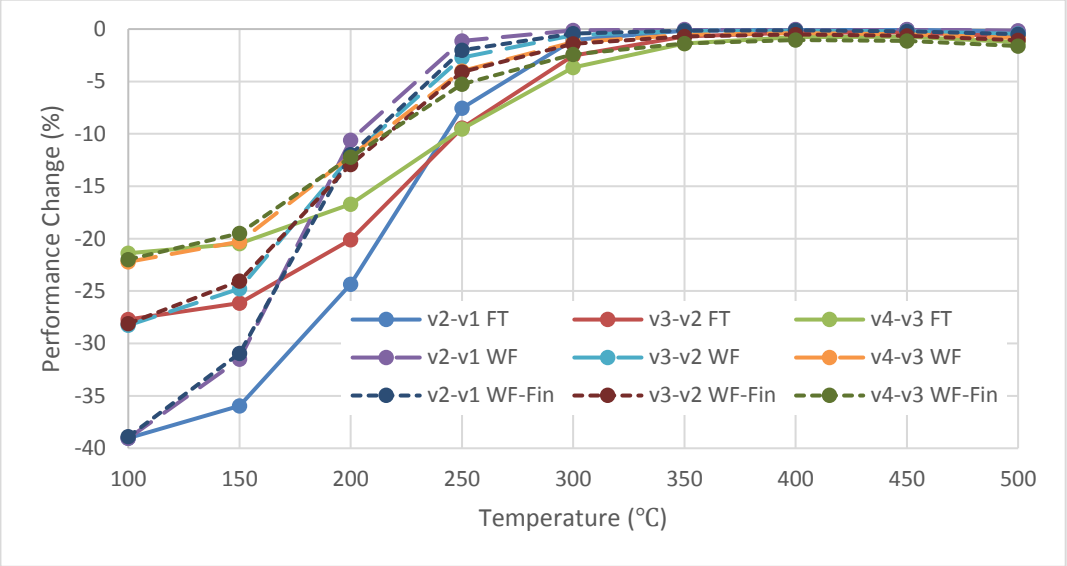

Figure 6-9: Inlet Velocity Effects on deNO (1000ppm NH3 at the inlet)

On NO conversion performance, the result is simple and clear. In all the cases of velocity change, temperature increase certainly brings up the performance, but the effectiveness is getting smaller at high velocity. And WF models (WF and WF-Fin) has a clear advantage between 150°C and 250°C, although the advantage is only a few percentages

at 150°C. In high-temperature range, from 350°C and above, performance decline is lower than 1%, this is insignificant change and can be neglected.

In terms of performance across different models, the results are plotted in Figure 6-10 and Figure 6-11, showing NO and NH_3 conversion rate respectively. The results are based on the outlet species concentration from the cases with 4 different velocities over a temperature range from 100°C to 500°C.

In NO conversion performance, both WF and WF-Fin models have an extraordinary higher conversion in low temperature, 140% and 166% of FT model at 100°C. The advantage of gas is closing as temperature rising and finally reduce to 3% at 300°C. Above 300°C, all three models have a pretty similar NO conversion rate. And between WF and WF-Fin model, WF-Fin model converts 20% more NO than WF model at 100°C and 7% more at 150°C and the difference is eventually reducing to less than 1% at 350°C.

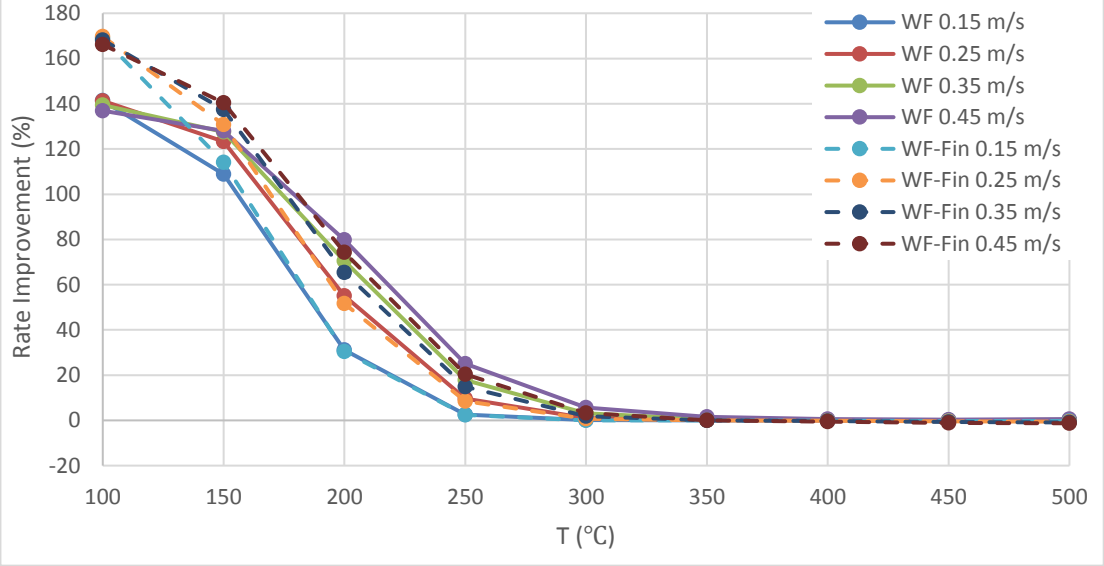

Figure 6-10: NO Conversion Rate Comparison, WF and WF-Fin to FT

There is a more or less similar situation in the comparison of ammonia conversion performance. When comparing to the FT model, both WF and WF-Fin models have a

great advantage at a low temperature up to 250°C and beyond 250°C, the advantage remains around 20%.

Average 20% improvement in NH_3 conversion between 300°C to 500°C, a possibility is 1000ppm ammonia concentration has reached the maximum ammonia conversion capability in the FT model, but this amount of species is not yet reaching the limit of WF and WF-fin model as there is almost 100% ammonia conversion rate at low velocity from 400°C to 500°C. Under such case, it proofs WF models (WF and WF-Fin) have higher ammonia conversion capability and are able to withstand more extreme ammonia overdosing during a real operation.

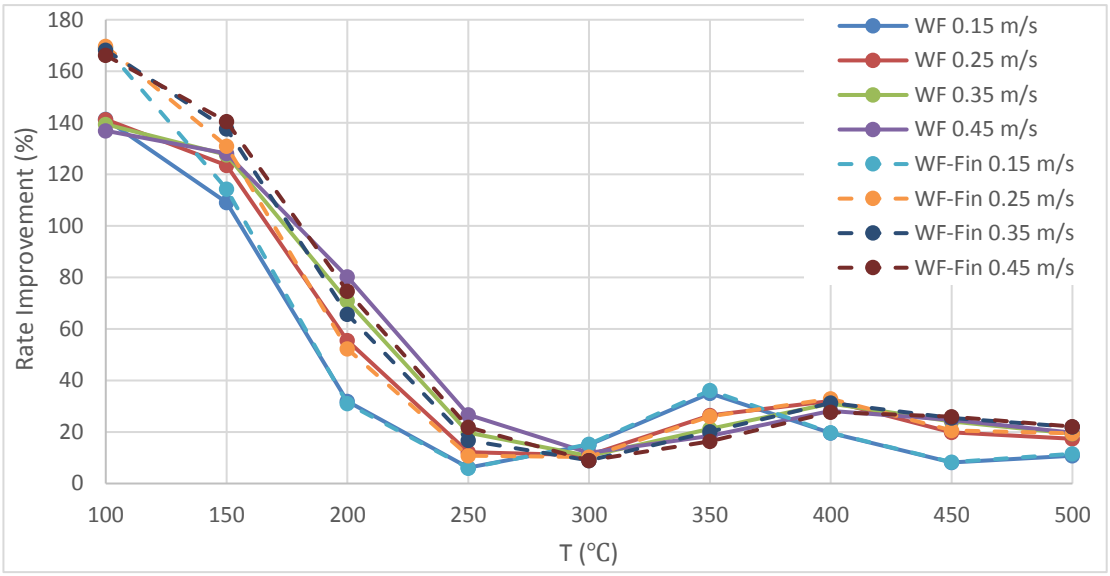

Figure 6-11: NH_3 Conversion Rate Comparison, WF and WF-Fin to FT

Figure 6-13 and Figure 6-12 are taken from the results of WF and WF-Fin under excessive ammonia supply condition. In both conversion rate figures, front section improvement is superior compare WF-Fin to WF model. And NO conversion rate reaches 99.9% in much short distance than the WF model.

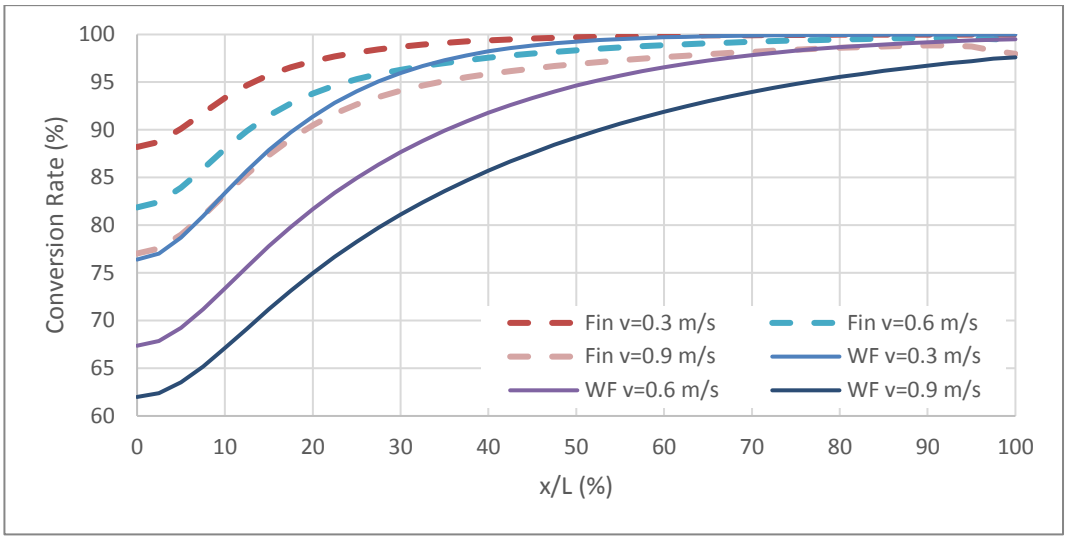

Figure 6-12: NO Conversion Rate Comparison (inlet 300°C, 1000ppm NH_3)

In NH_3 conversion rate comparison, despite the large advantage in the front section, the gas is closing as the distance increase. In the end, WF-Fin model conversion rate is only a few percents higher than WF model. The fin in the rear part of the channel is affecting the conversion process in a negative way. The second finding is the conversion rate holds back in the last 10% of the channel at low velocity, and it slightly falls at high velocity from 0.9m/s.

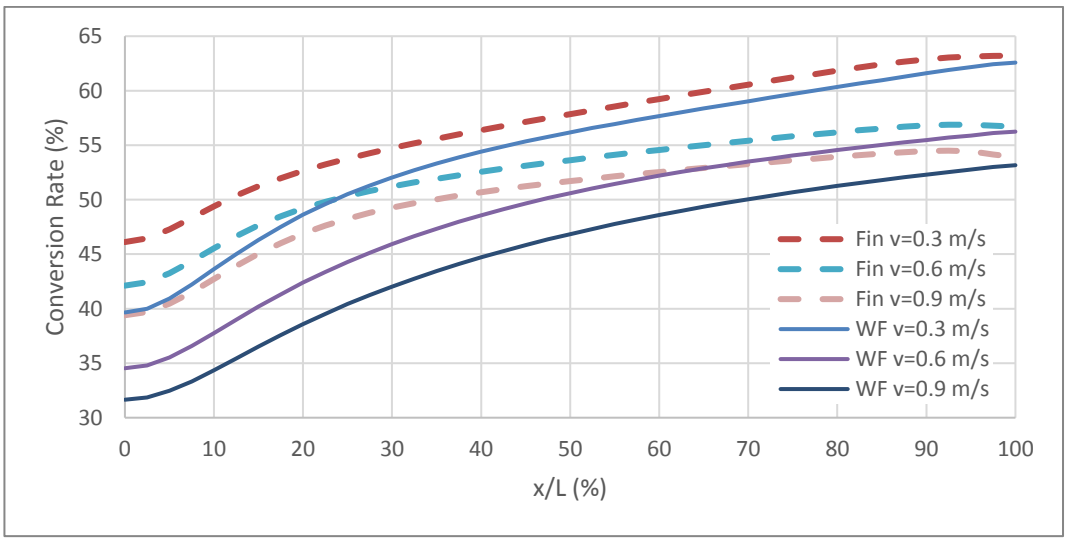

Figure 6-13: NH_3 Conversion Rate Comparison (inlet 300°C, 1000ppm NH_3)

6.2 Summary

In this chapter, a simple comparison of overall NO and NH_3 conversion rates are made between FT, WF and WF-Fin models. All cases are compared through a wide temperature range from 100°C to 500°C with inlet velocity 0.1m/s to 1.0m/s. WF type (WF and WF-Fin) catalysts have better performance in the low-temperature range for all inlet velocity settings. And for the same catalyst size, WF type catalysts have the higher capability to deal with higher NO level or NH_3 overdose situation due to the larger amount of surface catalyst site and porous wall. WF type models hold up for pretty well to velocity variations. Based on the results, adding extra fins into outlet channel improves the conversion performance in the inlet region but seem it is not contributing in the outlet section.

Further investigation might be required to explore the actual cause of the ammonia conversion rate drop in high velocity at high temperature. Nevertheless, this is a problem that can be compensated by a precisely controlled ammonia dosing strategy.

7. Conclusions and Recommendations

The purpose of this research was to investigate the deNOx performance of SCR-DPF system and also explored the possibility of performance change when adding fins into the outlet channels. After a series of simulation, here is the conclusion.

7.1 Conclusions

In this thesis, computational fluid dynamics has been used as a tool to investigate the performance of SCR reaction on wall flow type catalysts. The numerical model is developed on flow thought type catalyst and shifted to different catalyst structures. Simple calibration of reaction rate was carried out to compensate for any assumptions during modelling. The validation is through both steady and transient state; the flow field is fairly simple while the surface reaction and overall performance are one of the important factors. The validation process is comparing the species level and overall performance against other researchers' experimental work.

Upon successful validation of the flow through the model (FT-model), the results of this model are capable of predating general SCR reaction in various conditions. And then, the model is used on two wall flow type catalysts, one is normal wall flow filter like diesel particulate filter (standard WF-model), and the other one has extra fins added in the outlet channel (WF-Fin model), to investigate their performance.

For the performance of overall conversion rate, both wall flow type catalysts perform much better at low temperature owing to more surface site, slow velocity in the porous wall and extra fins (for WF-Fin model). Slow velocity allows longer resistance time, this affects conversion rate greatly as the diffusion rate, and reaction rate has more time to finish their conversion work. At high temperature, flow thought type catalyst performs

slight better because all the surface site is highly utilized. Whereas in wall flow type catalyst, the velocity field is different across the porous wall, the slowest velocity is in the middle section and a sudden increase at inlet and outlet regions. There is no clear sign that this kind of velocity has a significant impact on overall conversion rates.

If the rear part of the fin is truly the problem, a possible solution is that only apply the fin in the front section of the channel. In this way, pressure could be lower, and the conversion rate gets a boost in the front section. But this requires more investigation and results to prove.

Extra fin in the outlet channel can be a performance boost setup, but what is happening beyond the middle section needs more study.

7.2 Future Work and Recommendations

Based on the work undertaken in this research, the result shows there is potential performance improvement when adding extra fins into the outlet channel. The improvement at low temperature is great. However, there are many other cases that need to be further studied and understand.

The first one is to perform a simulation with various inlet conditions to verify if the fin added model has an advantage in all the conditions and gradually improve the model to gain better accuracy.

The second one is regarding the size of ammonia storage on the surface. As there are extra fins added into the system, that extra surface provides a large amount of ammonia storage site for NH_3 adsorption. And temperature increase during the transient states decreases the maximum capacity of ammonia storage, a large amount of NH_3 is released from the

porous due to this reason. Therefore, a high precision ammonia dosing strategy, ammonia storage prediction and control system are essential.

The next problem is the back pressure, or pressure drop, as this is one of the important factors for engine performance. Since the extra surface is added into the system, the roughness of the surface area causes extra drag to the flow. Therefore, higher pressure is expected. The trade-off points between pressure drop and deNO_x performance need to be studied.

Also, the location of the fin requires attention, located in the corner or standing in the middle of the wall in the outlet channels, as these would change the flow direction inside the porous media due to increasing resistance, and it is uncertain if this causes any performance change to deNO_x or diesel particulates filtration. Furthermore, during cold start or warm-up period, the extra fins might affect temperature change behaviour due to adding materials, and the temperature of the catalyst is important for both SCR reaction and diesel particulates regeneration.

The design of the fins is another performance factor, the size, the shape and thickness, they all play parts in the operation and affecting the final outcome. The idea is to maximise the usage of the fin to prevent wastage of the materials and keep the cost and weight low.

And finally, this type of catalyst combines diesel particulate filter and selective catalytic reduction catalyst, the performance on both sides, deNOx and diesel particulates filtration, need to be evaluated.

8. References

1. Thompson, G.J., et al., In-Use Emissions Testing of Light-Duty Diesel Vehicles in the United States, in Center for Alternative Fuels, Engines & Emissions, Dept. of Mechanical & Aerospace Engineering. 2014, West Virginia University.

2. Qi, G., Y. Wang, and R.T. Yang, Selective Catalytic Reduction of Nitric Oxide with Ammonia over ZSM-5 Based Catalysts for Diesel Engine Applications. Catalysis Letters, 2007. 121(1-2): p. 111-117.

3. Johannessen, T., et al., Improved Automotive NOx Aftertreatment System: Metal Ammine Complexes as NH3 Source for SCR Using Fe-Containing Zeolite Catalysts. Catalysis Letters, 2009. 128(1-2): p. 94-100.

4. Peace, H., B. Owen, and D.W. Raper, Identifying the contribution of different urban highway air pollution sources. The Science of the Total Environment, 2004. 334-335: p. 347-57.

5. Piumetti, M., et al., Catalysis in Diesel Engine NOx Aftertreatment: A Review. Catalysis, Structure & Reactivity, 2016. 1(4): p. 155-173.

6. Koebel, M., M. Elsener, and M. Kleemann, Urea-SCR a promising technique to reduce NOx emissions from automotive diesel engines. Catalysis Today, 2000. 59(3-4): p. 335-345.

7. Johnson, T.V., Diesel Engine Emissions and Their Control. Platinum Metals Review, 2008. 52(1): p. 23-37.

8. Naseri, M., et al., Development of SCR on Diesel Particulate Filter System for Heavy Duty Applications. SAE International, 2011. 4(1): p. 1798-1809.

9. Czerwinski, J., et al., Emission Reduction with Diesel Particle Filter with SCR Coating (SDPF). Emission Control Science and Technology, 2015. 1(2): p. 152-166.

10. Watling, T.C., M.R. Ravenscroft, and G. Avery, Development, validation and application of a model for an SCR catalyst coated diesel particulate filter. Catalysis Today, 2012. 188(1): p. 32-41.

11. Mihai, O., et al., Evaluation of an Integrated Selective Catalytic Reduction-Coated Particulate Filter. Industrial & Engineering Chemistry Research, 2015. 54(47): p. 11779-11791.

12. Conway, R., et al., Demonstration of SCR on a Diesel Particulate Filter System on a Heavy Duty Application, in SAE Technical Paper Series. 2015.

13. Benjamin, S.F. and C.A. Roberts, Methodology for modelling a combined DPF and SCR catalyst with the porous medium approach in CFD. SAE International, 2014(2014-01-2819).

14. Hamada, H. and M. Haneda, A review of selective catalytic reduction of nitrogen oxides with hydrogen and carbon monoxide. Applied Catalysis A: General, 2012. 421-422: p. 1-13.

15. Gabrielsson, P.L.T., Urea-SCR in Automotive Applications. Topics in Catalysis, 2004. 28(1-4): p. 177-184.

16. Meisami-Azad, M., et al., An Adaptive Control Strategy for Urea-SCR Aftertreatment System, in 2010 American Control Conference. 2010.

17. Fulks, G., et al., A Review of Solid Materials as Alternative Ammonia Sources for Lean NOx Reduction with SCR. SAE International, 2009(2009-01-0907).

18. Birkhold, F., et al., Modeling and simulation of the injection of urea-water-solution for automotive SCR DeNOx-systems. Applied Catalysis B: Environmental, 2007. 70(1-4): p. 119-127.

19. Helden, R.v., et al., Optimization of Urea SCR deNOx Systems for HD Diesel Engines. SAE International, 2004(2004-01-0154).

20. Birkhold, F., et al., Analysis of the Injection of Urea water solution for automotive SCR DeNOx Systems Modeling of Two phase Flow and Spray Wall Interaction. SAE International, 2006(2006-01-0643).

21. Grout, S., et al., Experimental investigation on the injection of an urea–water solution in hot air stream for the SCR application: Evaporation and spray/wall interaction. Fuel, 2012.

22. Abu-Ramadan, E., K. Saha, and X. Li, Modeling the depleting mechanism of urea-water-solution droplet for automotive selective catalytic reduction systems. AIChE Journal, 2011. 57(11): p. 3210-3225.

23. Fang, H.L. and H.F.M. DaCosta, Urea thermolysis and NOx reduction with and without SCR catalysts. Applied Catalysis B: Environmental, 2003. 46(1): p. 17-34.

24. Wang, T.J., et al., Experimental investigation on evaporation of urea-water-solution droplet for SCR applications. AIChE Journal, 2009. 55(12): p. 3267-3276.

25. Kim, J.Y., S.H. Ryu, and J.S. Ha, Numerical Prediction on the Characteristics of Spray-Induced Mixing and Thermal Decomposition of Urea Solution in SCR System, in ASME Internal Combustion Engine Division Fall Technical Conference. 2004, ASME: USA. p. 165-170.

26. Willems, F., et al., Is closed loop SCR control required to meet future emission targets. SAE International, 2007(2007-01-1574).

27. Steinbach, S., et al., Characterisation of structured hydrolysis catalysts for urea-SCR. Topics in Catalysis, 2007. 42-43(1-4): p. 99-103.

28. Hsieh, M.F., Control of Diesel Engine Urea Selective Catalytic Reduction Systems, in Mechanical Engineering. 2010, The Ohio State University.

29. Yim, S.D., et al., Decomposition of Urea into NH3 for the SCR Process. Industrial & Engineering Chemistry Research, 2004. 43(16): p. 4856-4863.

30. Yang, W., et al., Catalytic Performance of Zeolites on Urea Thermolysis and Isocyanic Acid Hydrolysis. Industrial & Engineering Chemistry Research, 2011. 50(13): p. 7990-7997.

31. Hsieh, M.F. and J. Wang, Observer-Based Estimation of Selective Catalytic Reduction (SCR) Catalyst Ammonia Storage. Journal of Automobile Engineering, 2010. 224(9): p. 1199-1211.

32. Hsieh, M.F. and J. Wang, Sliding-Mode Observer For Urea-Selective Catalytic Reduction (SCR) Mid-Catalyst Ammonia Concentration Estimation. International Journal of Automotive Technology, 2011. 12(3): p. 321-329.

33. Weisweiler, W. and F. Buchholz, Solid urea as source of ammonia for catalytic lowering of nitrogen oxide levels in diesel exhaust by the SCR process. Chem. Ing. Tech, 2001. 73(7): p. 882-887.

34. Elmøe, T.D., et al., A high-density ammonia storage/delivery system based on Mg(NH3)6Cl2 for – in vehicles. Chemical Engineering Science, 2006. 61(8): p. 2618-2625.

35. Christensen, C.H., et al., Metal ammine complexes for hydrogen storage. Journal of Materials Chemistry, 2005. 15(38): p. 4106.

36. Benjamin, S., Simulating the Performance of Automotive Catalytic Converters, in Business Briefing: Global Automotive Manufacturing & Technology. 2003, Touch Briefings: UK.

37. Liu, Z., Pulsating Flow Maldistribution in Automotive Exhaust Catalysts - Numerical Modelling and Experimental Correlation. 2003, Coventry University.

38. Sigling, R., C. Khalaf, and E. Healy, Enhance Ammonia Distribution for Maximum SCR Performance. 2003, Institute of Clean Air Companies.

39. Arrowsmith, D., A. Bott, and P. Bush, Development of a Compact Urea-SCR+CRT™ System for Heavy-Duty Diesel using a Design of Experiments Approach. SAE International, 2006(2006-01-0636).

40. Grossale, A., I. Nova, and E. Tronconi, Study of a Fe–zeolite-based system as NH3-SCR catalyst for diesel exhaust aftertreatment. Catalysis Today, 2008. 136(1-2): p. 18-27.

41. Kamasamudram, K., et al., Overview of the practically important behaviors of zeolite-based urea-SCR catalysts, using compact experimental protocol. Catalysis Today, 2010. 151(3-4): p. 212-222.

42. Jayat, F., A. Reck, and K.V.R. Babu, SCR and SCRi as After-treatment Systems for Low CO2 and Low NOx Vehicles. SAE International, 2011(2011-26-0038).

43. Grossale, A., I. Nova, and E. Tronconi, Ammonia blocking of the "Fast SCR" reactivity over a commercial Fe-zeolite catalyst for Diesel exhaust aftertreatment. Journal of Catalysis, 2009. 265(2): p. 141-147.

44. Gao, X., et al., The activity and characterization of CeO2-TiO2 catalysts prepared by the sol-gel method for selective catalytic reduction of NO with NH3. J Hazard Mater, 2010. 174(1-3): p. 734-9.

45. Krocher, O. and M. Elsener, Combination of V2O5/WO3-TiO2, Fe-ZSM5, and Cu-ZSM5 Catalysts for the Selective Catalytic Reduction of Nitric Oxide with Ammonia. Industrial & Engineering Chemistry Research, 2008. 47(22): p. 8588-8593.

46. Shan, W., et al., An environmentally-benign CeO2-TiO2 catalyst for the selective catalytic reduction of NOx with NH3 in simulated diesel exhaust. Catalysis Today, 2012. 184(1): p. 160-165.

47. Frey, A.M., et al., Fe-BEA Zeolite Catalysts for NH3-SCR of NOx. Catalysis Letters, 2009. 130(1-2): p. 1-8.

48. Kristensen, S.B., et al., High performance vanadia–anatase nanoparticle catalysts for the Selective Catalytic Reduction of NO by ammonia. Journal of Catalysis, 2011. 284(1): p. 60-67.

49. Stanciulescu, M., et al., Low-temperature selective catalytic reduction of NOx with NH3 over Mn-containing catalysts. Applied Catalysis B: Environmental, 2012.

50. Metkar, P.S., M.P. Harold, and V. Balakotaiah, Selective catalytic reduction of NOx on combined Fe- and Cu-zeolite monolithic catalysts: Sequential and dual layer configurations. Applied Catalysis B: Environmental, 2012. 111-112: p. 67-80.

51. Qi, G. and R.T. Yang, Ultra-active Fe/ZSM-5 catalyst for selective catalytic reduction of nitric oxide with ammonia. Applied Catalysis B: Environmental, 2005. 60(1-2): p. 13-22.

52. Kleemann, M., et al., Investigation of the ammonia adsorption on monolithic SCR catalysts by transient response analysis. Applied Catalysis B: Environmental, 2000. 27(4): p. 231-242.

53. Ciardelli, C., et al., SCR-DeNOx for diesel engine exhaust aftertreatment: unsteady-state kinetic study and monolith reactor modelling. Chemical Engineering Science, 2004. 59(22-23): p. 5301-5309.

54. Ciardelli, C., et al., Reactivity of NO/NO2–NH3 SCR system for diesel exhaust aftertreatment: Identification of the reaction network as a function of temperature and NO2 feed content. Applied Catalysis B: Environmental, 2007. 70(1-4): p. 80-90.

55. Hsieh, M.F. and J. Wang, An Extended Kalman Filter for NOx Sensor Ammonia Cross-Sensitivity Elimination in Selective Catalytic Reduction Applications, in American Control Conference (ACC), 2010. 2010: USA. p. 3033-3038.

56. Hsieh, M.F. and J. Wang, An Extended Kalman Filter for Ammonia Coverage Ratio and Capacity Estimations in the Application of Diesel Engine SCR Control and On-board Diagnosis, in American Control Conference (ACC), 2010. 2010: USA. p. 5874-5879.

57. Wang, D.Y., et al., Ammonia Sensor for Closed-Loop SCR Control. SAE International, 2008(2008-01-0919).

58. DEVARAKONDA, M., et al., Model-Based Control System Design in A Urea-SCR Aftertreatment System Based On NH3 Sensor Feedback. International Journal of Automotive Technology, 2009. 10(6): p. 653-662.

59. Shost, M., et al., Monitoring Feedback and Control of Urea SCR Dosing System for NOx Reduction. SAE International, 2008(2008-01-1325).

60. Chatterjee, D., et al., Numerical Simulation of Ammonia SCR-Catalytic Converters: Model Development and Application, in SAE 2005 World Congress & Exhibition. 2005.

61. Herman, A., et al., Model Based Control of SCR Dosing and OBD Strategies with Feedback from NH3 Sensors. SAE International, 2009(2009-01-0911).

62. Harder, H.-D., M. Brugger, and R. Brück, Future SCR NOX Aftertreatment Systems for Euro 6. 2011, Emitec

63. Mihai, O., M. Stenfeldt, and L. Olsson, The effect of changing the gas composition on soot oxidation over DPF and SCR-coated filters. Catalysis Today, 2018. 306: p. 243-250.

64. Kang, W., et al., PM and NOx reduction characteristics of LNT/DPF+SCR/DPF hybrid system. Energy, 2018. 143: p. 439-447.

65. Karamitros, D. and G. Koltsakis, Model-based optimization of catalyst zoning on SCR-coated particulate filters. Chemical Engineering Science, 2017. 173: p. 514-524.

66. Kang, W. and B. Choi, Effect of copper precursor on simultaneous removal of PM and NO x of a 2-way SCR/CDPF. Chemical Engineering Science, 2016. 141: p. 175-183.

67. Tronconi, E., et al., Interaction of NO x Reduction and Soot Oxidation in a DPF with Cu-Zeolite SCR Coating. Emission Control Science and Technology, 2015. 1(2): p. 134-151.

68. Sadeghi, F., et al., Investigating the effect of channel geometry on selective catalytic reduction of NOx in monolith reactors. Chemical Engineering Research and Design, 2017. 118: p. 21-30.

69. Mladenov, N., et al., Modeling of transport and chemistry in channel flows of automotive catalytic converters. Chemical Engineering Science, 2010. 65(2): p. 812-826.

70. Olsson, L., H. Sjövall, and R.J. Blint, A kinetic model for ammonia selective catalytic reduction over Cu-ZSM-5. Applied Catalysis B: Environmental, 2008. 81(3-4): p. 203-217.

71. Lietti, L., et al., Dynamics of the SCR-DeNOx Reaction by the Transient-Response Method. AIChE Journal, 1997. 43(10): p. 2559 - 2570.

72. Winkler, C., et al., Modeling of SCR DeNOx Catalyst - Looking at the Impact of Substrate Attributes. SAE International, 2003. 2003-01-0845.

73. Chen, J., et al., Mathematical modeling of monolith catalysts and reactors for gas phase reactions. Applied Catalysis A: General, 2008. 345(1): p. 1-11.

74. ANSYS, I., ANSYS Fluent Theory Guide. 2016.

75. Patankar, S., Numerical Heat Transfer and Fluid Flow. 1980.

76. ANSYS, I., ANSYS Fluent Users Guide. 2018: ANSYS, Inc.

77. Liu, Y., J. Zhao, and J.-M. Lee, Conventional and New Materials for Selective Catalytic Reduction (SCR) of NOx. ChemCatChem, 2018. 10(7): p. 1499-1511.

78. Vuong, T.H., et al., Efficient VOx/Ce1–xTixO2 Catalysts for Low-Temperature NH3-SCR: Reaction Mechanism and Active Sites Assessed by in Situ/Operando Spectroscopy. ACS Catalysis, 2017. 7(3): p. 1693-1705.